Scientific Research Publishing

Open Journal of Applied Sciences, 2025, 15(10), 3146-3236
https://www.scirp.org/journal/ojapps
ISSN Online: 2165-3925
ISSN Print: 2165-3917

Five New Observables of UAP: Empirical Evidence of Dark Operational Warp Propulsion Systems

Chad Wanless, Dave Palachik

Centre for the Scientific Study of Atmospheric Anomalies, Ontario, Canada
Email: Chad@CSSAA.org, Dave@CSSAA.org

How to cite this paper: Wanless, C. and Palachik, D. (2025) Five New Observables of UAP: Empirical Evidence of Dark Operational Warp Propulsion Systems. *Open Journal of Applied Sciences*, **15**, 3146-3236
https://doi.org/10.4236/ojapps.2025.1510207

Received: July 14, 2025
Accepted: October 18, 2025
Published: October 22, 2025

Abstract

This paper presents empirical evidence suggesting that some Unidentified Aerial Phenomena (UAP) employ a form of spatial warp propulsion. In astronomy, the prefix *dark* is applied to discoveries where indirect evidence reveals otherwise invisible phenomena—such as gravitational lensing attributed to dark matter or cosmic acceleration attributed to dark energy. In an analogous way, this study identifies five consistent visual observables in UAP data: gravitational lensing, leading-edge vapor cones, oscillatory motion blur, pronounced disc tilt in low-speed flight, and "saucer-like" skipping trajectories during horizontal maneuvers. Together, these signatures align with Alcubierre-type warp field models and elastic spacetime formulations. While the underlying mechanism and engineering remain unknown, the data suggest that UAP display the same pattern of "visible evidence of an invisible cause" that has historically justified the classification of *dark* phenomena in physics. Building on preliminary observations first presented in the book *Hidden in Plain Sight*, *Evidence of Exotic UFO Propulsion*, this paper formalizes and expands those concepts within a rigorous, peer-reviewed framework. New video case studies, photographic evidence, and field-based theoretical interpretations are presented for each observable. The analysis is collaborative and interdisciplinary, bridging principles of general relativity and aerodynamics with phenomenological insights from UAP sightings. By consolidating these five new observables and examining their physical implications, the study provides a foundation for identifying potential warp-field propulsion signatures in future UAP reports, aimed at an audience spanning physics, aviation, and phenomenology. While this paper does not claim to determine the composition, origin, or engineering of UAP systems, it demonstrates that their effects can be measured. Just as science accepts dark matter and dark energy through their observable consequences, even without knowing their fundamental nature, we argue that UAP display the same pattern of "visible evidence of an

invisible cause." The five new observables documented here constitute empirical evidence of a *dark operational warp drive*: a phenomenon apparent through its measurable signatures, even if its mechanism remains beyond current understanding. The interpretations presented here rely exclusively on established astronomy-based physics, including gravitational lensing and the Alcubierre warp metric, to explain UAP observables. The term dark is employed in the same sense used in astronomy—designating a phenomenon that is invisible in itself but made detectable through secondary, observable effects.

Keywords

Unidentified Aerial Phenomena (UAP), Unidentified Flying Objects (UFO), Alcubierre Warp Drive, Warp-Field Propulsion, Spacetime Curvature, Gravitational Lensing, Leading-Edge Vapor Cone, Oscillatory Motion Blur, Disc Tilt, Gravity Counterbalancing, Skipping-Saucer Motion, Advanced Propulsion Systems, Exotic Aerospace Technology, Spacetime Distortion, Frame-by-Frame Video Analysis, Radar Return Anomalies, Infrared Imaging, General Relativity, Aerodynamics, Historical UFO Case Studies, Rex Heflin Photographs, Aguadilla UAP Video, Perth UAP Sighting, Ridoy UAP Footage, Laser Pointer Lensing Test, Multi-Camera UAP Imaging, Field Research Methodology, Exotic Field Propulsion Signatures, Physics-Based UFO analysis

1. Introduction—Five New Observables

This paper presents empirical evidence that Unidentified Aerial Phenomena (UAP) appear to employ a form of spatial warp system as their primary means of propulsion. In the history of astronomy, the prefix dark has been applied to phenomena revealed indirectly gravitational lensing betraying the unseen mass of dark matter, or the measurements of supernovae implying the influence of dark energy. In each case, visible evidence pointed to invisible forces, compelling acceptance of their existence long before their underlying mechanisms were understood.

In an analogous manner, UAP exhibit five recurring observables that suggest the presence of a warp field: gravitational lensing of background objects, leading-edge vapor cones consistent with localized spacetime compression, both fast and slow warp field oscillations, pronounced disc tilt in low-speed flight, and "saucer-like" skipping trajectories. This constellation of clues indicates an operational, though unseen, spatial warp propulsion system.

The method employed in this study is designed with a clear boundary. We do not attempt to identify the composition, origin, or fundamental mechanism that produces spacetime warping. Instead, we focus on what can be measured directly: the effects of spacetime curvature as revealed through visual, thermal, and radar signatures. In this sense, our approach parallels the way science treats dark matter and dark energy—as real phenomena known through their effects, even while

their underlying causes remain unresolved. Just as science cannot specify what dark matter is made of, but can say with confidence what it does, this paper argues that UAP evidence demonstrates the operation of a dark warp propulsion system, observable through its consistent interactions with light, air, and radar.

While the ultimate source of warp generation is unknown, this paper does address partial engineering questions by examining how warp effects might be controlled. Building on Alcubierre-type metrics and the elastic warp models we have developed, we explore how nested or asymmetric warp nacelles could account for tilted disc flight, oscillation, and sudden directional changes. In this sense, the analysis speaks to possible methods of flight control, while leaving the deeper question of how the warp effect itself is produced to future research.

The question then arises: across more than eighty years of recorded history, did independent witnesses—including 48 crew members of the Brazilian Navy research vessel during the 1958 Trindade event—and multiple sensor systems somehow fabricate a body of photographs, videos, and radar returns that by coincidence replicate the empirical predictions of warp-field theory? Or are these records consistent because they reflect the visible trace of an otherwise hidden technology—what might properly be termed a dark operational warp drive?

Recent acknowledgments by the U.S. Department of Defense that some UAP remain unexplained despite investigation underscore the need for systematic, physics-based study. For decades, visual clues have appeared in the record, yet their significance was seldom recognized. This paper formalizes and expands upon these overlooked features, presenting five new visual observables proposed to indicate warp-drive propulsion and correlating them with historical and modern UAP cases.

This publication also constitutes the second formal release of results from the Skywatcher.ai field research team and from the peer-reviewed Tedesco Brothers radar gravitational-lensing experiments, together representing a third line of convergent evidence within the emerging Dark Warp Propulsion research framework.

In science, mathematics has often preceded observation—Einstein's equations predicting gravitational lensing, Dirac's formulation revealing antimatter, or Pauli's conservation laws requiring the neutrino decades before detection. In the same way, the elastic spatial contraction model developed here predicts vapor cone formation, and a little-known recording, the Ridoy video discussed in this paper, provides the corresponding observational match.

Just as gravitational lensing was accepted with a single photograph in 1919, when Eddington confirmed Einstein's prediction of starlight deflection, repeated UAP observations now retroactively match theoretical warp-field forecasts. The five observables documented here form a consistent and falsifiable pattern, aligning with Alcubierre-type metrics and the elastic warp models we have developed. As with dark matter, dark energy, and gravity itself, persistent observation and theoretical coherence justify treating these warp-field effects as real phenomena worthy of scientific investigation—even in the absence of a complete engineering

blueprint.

Without a physical specimen—which may or may not exist in restricted classified facilities, this may be the closest civilian science can come to defining what they are, and if these same signatures appeared in a non-controversial domain such as astronomy, they would be considered enough to establish reality.

Scope and Disclaimers

This study applies astronomy-based methods and physics—such as gravitational lensing and relativistic warp metrics—to the analysis of UAP, interpreting them through the same evidentiary framework used for phenomena like dark matter and dark energy. The term dark is used strictly in this astronomical scientific sense: to describe something invisible that can be detected indirectly through measurable effects. The authors emphasize that no classified information was used in the research or preparation of this paper. The views expressed are solely those of the authors and do not represent the positions of their employers or affiliated institutions.

1.1. The New Observables

Building upon Luis Elizondo's original Five Observables (as described in Imminent and further expanded in our 2025 book Hidden in Plain Sight), we propose five additional visual observables indicative of field-based propulsion systems as predicted by Alcubierre-type warp metrics.

While Elizondo's framework emphasizes performance characteristics, our proposed set focuses on environmental interactions—how UAPs appear to distort light, air, and radar in ways which match predicted localized spacetime curvature. These effects, once dismissed as anomalies or artifacts, now form a repeatable and physically grounded pattern across diverse cases.

The five new observables include:

1) gravitational lensing,

2) leading-edge vapor cones,

3) tilted disc flight,

4) oscillation blur, and

5) saucer-like skipping motion.

Each is introduced in Section 3 with theoretical background and representative examples. Together, they offer a testable framework for identifying warp-field interactions across visual, thermal, and radar domains.

1.2. Clarification of Scope

This paper is not about how to construct an Alcubierre warp drive. While we reference the original spacetime metric, recent elastic warp models, and the documented formation of micro warp bubbles, our goal is not to describe the mechanics of propulsion or field generation. Rather, this study focuses on detection: identifying consistent visual and radar-based signatures that align with the presence of localized spacetime warping. These include phenomena such as gravitational

lensing, leading-edge vapor cones, zigzagging flight paths, and radar anomalies.

We recognize that a critical engineering step remains—transforming micro-scale warp effects into functional, macro-scale propulsion systems. That leap is not within the scope of this paper, nor is it ours to make. It is a leap for another paper, and likely, for other researchers. Our aim here is to present a scientifically grounded framework for recognizing and classifying real-world data that may already be capturing the effects of such advanced field-based propulsion in operation.

We view this paper as a contribution similar in nature to the early scientific efforts that first postulated the existence of atmospheric sprites, dark matter, and dark energy—phenomena that were initially inferred through limited or indirect observations before being confirmed by larger datasets or direct detection. Sprites, for example, were debated for years based on just 18 recorded events before broader acceptance emerged. In the same spirit, this paper presents observational evidence matching predicted theoretical Alcubierre-type warp field effects, while openly acknowledging that further field testing is required. To that end, we offer proposed field methodologies aimed at independently validating—or falsifying—the presence of these effects through structured, replicable experiments.

1.3. Historical and Mathematical Parallels in Scientific Discovery

The methodology employed in this paper—integrating video analysis, photographic evidence, and mathematical modeling to detect anomalies inconsistent with conventional physics—follows a well-established pattern in scientific discovery. Many phenomena now central to physics and astronomy were first inferred through indirect signals or theoretical predictions long before direct confirmation.

One example is the neutrino. In 1930, Wolfgang Pauli postulated its existence to preserve conservation laws in beta decay, though no instrument of the time could detect it. For more than two decades the neutrino remained a "particle of faith," until Cowan and Reines confirmed it experimentally in 1956. What began as a mathematical necessity ultimately reshaped particle physics.

Gravitational lensing provides another precedent. Predicted by Einstein in 1915, it was famously confirmed in 1919 during a solar eclipse, when Eddington's team photographed the deflection of starlight around the Sun. That single plate was sufficient to transform physics and validate general relativity. By comparison, this paper examines eight photographic cases, nine video sequences, and one eyewitness account spanning decades that exhibit gravitational lensing consistent with Alcubierre-type curvature effects—including background deformation, disc edge distortion, and radar echo anomalies.

The discovery of the cosmic microwave background radiation (CMB) offers a third example. In 1965, Arno Penzias and Robert Wilson detected persistent noise in a radio telescope. After systematically excluding all known sources of interference, they realized it was the predicted afterglow of the Big Bang—indirect evidence precisely aligned with theoretical expectations.

In each case—the neutrino, gravitational lensing, and the CMB—scientific breakthroughs emerged from anomalous patterns reinforced by mathematical

predictions. These precedents legitimize the approach taken here: identifying repeatable distortions in UAP imagery and modeling their behavior through general relativity and fluid dynamics. Just as neutrino theory preserved conservation laws and lensing revealed unseen mass, the anomalies documented here may reflect a deeper physical mechanism not yet recognized by conventional models.

Taken together, these examples show that science often advances by recognizing patterns in anomalies long before direct mechanisms are understood. What distinguishes the present study is that the five new UAP observables align not with one or two such precedents, but with all of the major methodologies by which physics has historically validated transformative discoveries. These include: independent confirmation by separate research groups (dark energy); exceeding the 5σ statistical threshold (particle physics); mathematical prediction sustained for decades before eventual experimental validation (neutrino); visible evidence of an invisible cause (dark matter); and the immediate revelation of a novel scientific effect through a single photographic plate, directly aligned with theory (gravitational lensing). To our knowledge, no prior discovery has simultaneously aligned with all five of these historical standards. That convergence places the present evidence in a unique position within the history of science. If this were a non-controversial subject, such convergence would already have secured recognition without question.

1.4. Mathematical Proof of Existence in Science

Throughout the history of physics and astronomy, mathematics has often revealed the existence of phenomena long before direct observation or engineering explanation was available. In these cases, theoretical equations made precise predictions that could not be ignored once observational data aligned with them.

Examples include:

- **Gravitational lensing (1915-1919):** Einstein's field equations predicted that light passing near the Sun would be deflected by 1.75 arcseconds. Eddington's eclipse expedition confirmed this with a single photographic plate, mathematically proving spacetime curvature.
- **Antimatter (1928-1932):** Dirac's relativistic electron equation contained negative-energy solutions, implying a mirror particle with opposite charge. The positron was discovered four years later, exactly as predicted.
- **Electromagnetic waves (1865-1888):** Maxwell's equations mathematically unified electricity and magnetism, requiring that oscillations propagate as waves at the speed of light. Hertz later detected these waves, confirming radio physics.
- **Neutrinos (1930-1956):** Pauli introduced the neutrino mathematically to preserve conservation laws in beta decay. For decades it was "real" only in the equations until Cowan and Reines detected it experimentally.
- **Cosmic expansion and background radiation (1920s-1965):** Friedmann's solutions to Einstein's equations required an expanding universe, later verified

by Hubble. Big Bang theory then predicted residual microwave radiation, confirmed by Penzias and Wilson as the CMB.

These precedents illustrate a recurring scientific principle: mathematical coherence plus observational consistency is sufficient to establish the existence of a phenomenon—even in the absence of a complete physical model.

The same reasoning applies here. The scatter-plot model of spatial contraction, see Section 2.3, predicts the formation of leading-edge vapor cones at specific field boundaries. Independent video evidence—such as the Ridoy recording—exhibits vapor cones at exactly these predicted locations. Just as lensing validated general relativity, and as negative-energy solutions validated antimatter, the alignment between theoretical warp-field predictions and empirical observation constitutes a legitimate mathematical proof of existence.

2. Methods

This study employs a multi-modal investigative approach integrating photographic analysis, frame-by-frame video decomposition, radar return modeling, and comparative geometry. Source data includes publicly released military UAP footage, stabilized civilian video, historical photographs, and screen-stabilized infrared overlays.

2.1. Video and Photographic Evidence Review

Videos and photographs were selected for analysis based on the presence of motion anomaly, structured blur, radial light distortion, or observable atmospheric interaction. Each candidate clip was stabilized either manually or using AI-enhanced frame correction and then dissected to detect lensing patterns, oscillation signatures, and environmental deformations.

2.2. Radar Signal Interpretation

Radar echo anomalies—including double returns, long-delay echoes, and range shadowing—were evaluated as indirect indicators of spacetime manipulation. These data were cross-referenced with known radar jamming profiles and environmental propagation conditions to rule out standard interference explanations.

2.3. Theoretical Framework and Geometric Distortion Modeling

The theoretical basis for the five proposed visual observables draws upon Alcubierre's 1994 model for faster-than-light spacetime manipulation, as well as field deformation theory and elastic response analysis derived from general relativity. In the Alcubierre metric, a warp bubble is defined by regions of spacetime contraction in front of or above a craft and expansion behind or below it. This allows the craft to "ride" a curvature wave without violating local relativistic speed limits.

The Alcubierre shape function describes the curvature of spacetime around the warp bubble as a function of radial distance:

Equation (1). Alcubierre Metric Shape Function:

$$f(r)=\left(\tanh\left(\sigma\left(r+R\right)\right)-\tanh\left(\sigma\left(r-R\right)\right)\right)\Big/\left(2\tanh\left(\sigma R\right)\right) \tag{1}$$

where r_s is the radial coordinate from the bubble center, R is the warp bubble radius, and σ is the steepness parameter.

Figure 1 shows how Alcubierre's shape function generates the classic lens-shaped warp field geometry.

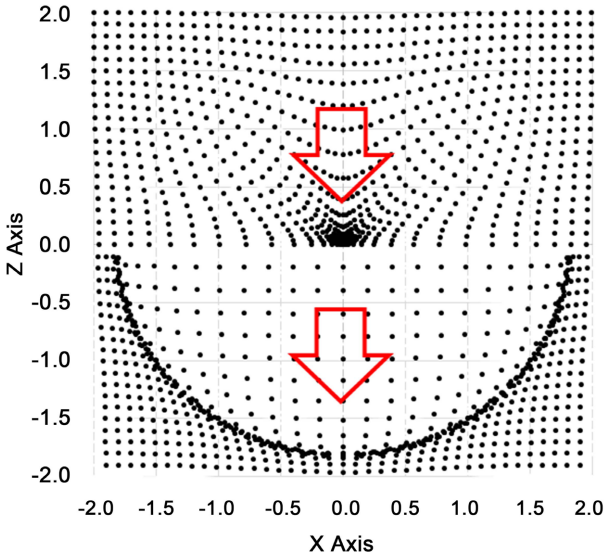

Figure 1. Scatter plot representation of the Alcubierre warp bubble geometry showing spatial contraction above/ahead and expansion below/behind the object.

To correct and refine this shape, an elastic response deformation formula is applied.

To calculate the warp bubble with an elastic deformation, the physical displacement formula used to create Figure 1 was updated as follows:

- r is the original physical distance between two points (center of the grid and the grid point to be calculated) without warping.
- Δs is the physical displacement or change in the actual distance due to warping. Here the elastic formula is applied using $f(r) \times$ absolute(z).
- Δx is the resulting x-coordinate's new calculated offset position.
- Δz is the resulting z-coordinate's new calculated offset position.

The transformation Equations (2) used to generate the scatter plot are:

$$\begin{aligned}\Delta s &= r\times f(r)\times|z|\\ \Delta x &= x+\Delta s\times(x/r)\\ \Delta z &= z+\Delta s\times(z/r)\end{aligned} \tag{2}$$

Figure 2 below shows the resulting elastic curvature expressed using the default margin of 50% and a scalar value of 3.0. Adjusting these two parameters affects the steepness and spread of spatial curvature.

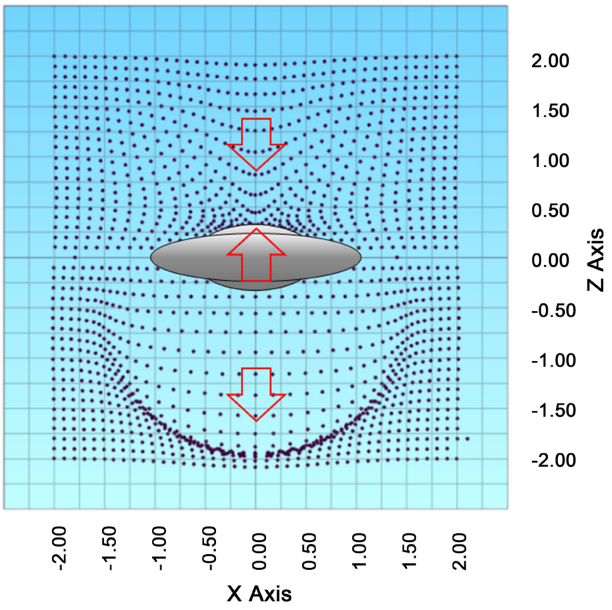

Figure 2. Alcubierre warp bubble corrected using elastic spatial deformation formula.

This accounts for the damped, non-linear distortion of local spacetime as a function of amplitude, frequency, and damping factor, resulting in smoother transitions at the boundaries of the warp bubble. Note, three arrows have been added to show the gravitational acceleration in upper and lower hemispheres is downward (to counter Earth's gravity) and a narrow section along the dividing line shows an upward pointing spatial curve indicating a narrow area in which a vehicle and its occupants can safely exist and would experience upward gravitational acceleration. The resulting shape of the vehicle, when maximizing internal storage, passenger, science, and engineering spaces, is disc shaped. This correlation reflects a fundamental engineering principle: "form follows function" — Luis Elizondo, Imminent

The warp bubble shape can be described as both round and as a wine decanter. The warp bubble is spherical in shape, yet, within it, the upper and lower hemispheres are contracted or expanded into a smaller internal wine decanter shape. **Figure 3** below shows spatial compression and expansion values using a color-coded scatter plot. This scatter plot becomes important when describing vapor cones later in Section 4.

A key implication of spacetime warping is how light behaves near the field boundaries. **Figure 4** shows the prediction of how, and observed in some cases, light paths curve around gravitational fields, which can visually momentarily deform background objects causing, in some cases, a UAP to appear to be enclosed in a clear sphere.

Figure 5 presents a rendering of how light could be distorted by a warp-bubble enveloping a cubically shaped UAP. Notice how the background landscape dips unnaturally downwards along a curved profile, how the clouds appear to bulge

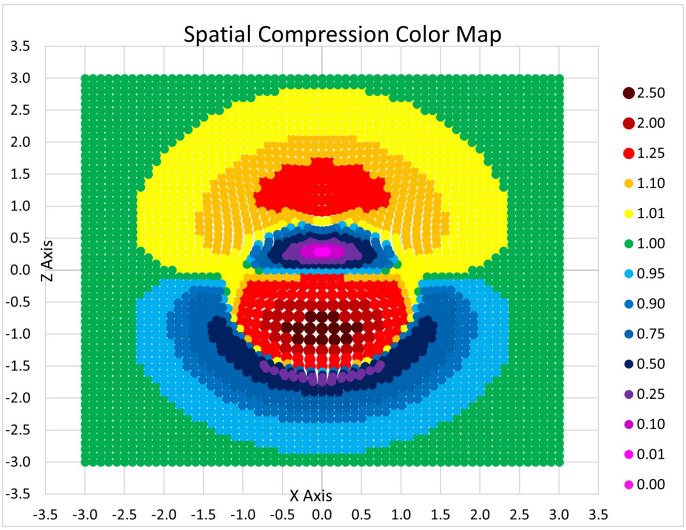

Figure 3. Spatial compression scatter plot.

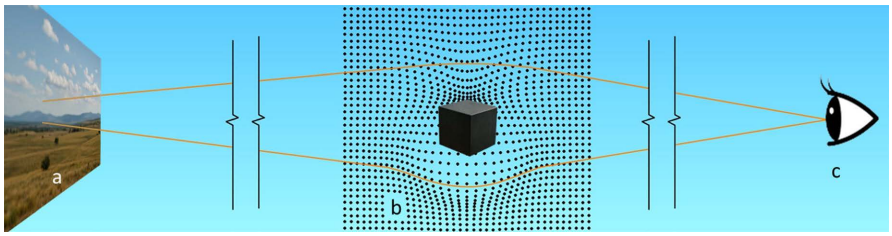

Figure 4. Light path trajectory plot showing light from the landscape (a) curving around a cube-shaped UAP (b), traveling along altered trajectories the observer (c) causing the object to appear enclosed in a clear sphere.

outward and upward, and how the entire scene seems compressed around the region marking the outer boundary of the warp bubble, forming an almost circular outline. To a first-time observer, these optical effects could easily be mistaken for a clear sphere enclosing the dark cube-shaped object. The cube shape for this UAP was chosen specifically to reconstruct the visual features described by Ryan Graves in his July 26, 2023 testimony before the U.S. House Oversight Subcommittee on National Security, the Border, and Foreign Affairs [1].

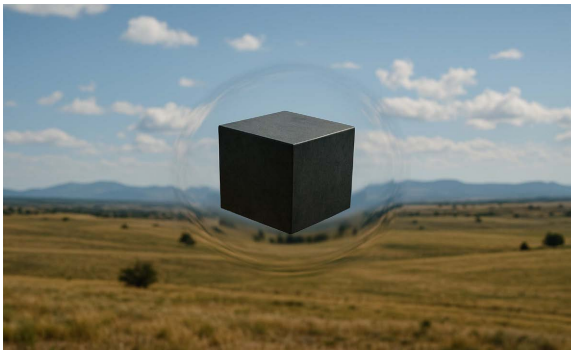

Figure 5. Rendering simulating background deformation around a dark cube-shaped UAP due to localized spacetime contraction and compression.

Additionally, research described in Hidden in Plain Sight [2] introduced the concept of nested micro-warp nacelles.

In the July 31, 2021 published paper titled "Worldline numerics applied to custom Casimir geometry generates unanticipated intersection with Alcubierre warp metric". The paper describes how they accidentally and unintentionally discovered how to create micro-warp bubbles when studying the Casimir effect. The authors postulated that if these micro warp bubbles were daisy chained together on a microchip, that perhaps the sum total would increase the size of an overall warp bubble to make the warp field usable."

Figure 6 below shows that when taking the authors' next step suggestion, Alcubierre's shape formula does indicate nesting micro warp bubbles next to each other does create a larger combined warp field. Taking the next logical step of combining them into a cone shape nesting creates a larger and steep warp field, thus providing throttle control.

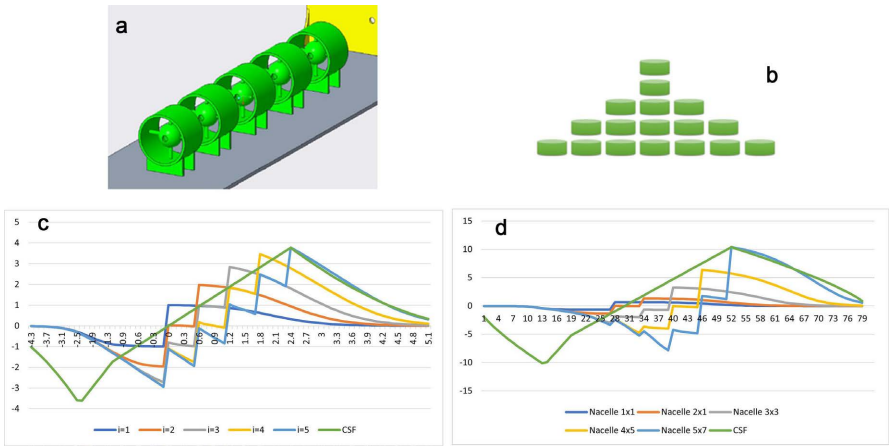

Figure 6. Collage showing micro-warp nacelles nested into larger formations. Left: linear array forming extended propulsion. Right: cone array forming a wider/steeper bubble used for throttle control.

Figure 6(c) and Figure 6(d) show that adding multiple nested warp nacelles produces a sawtooth pattern in the rising linear onset of the accumulated shape function. Because this discontinuous pattern cannot be used directly in the elastic formula, we developed a Compound Shape Function (CSF) to represent the combined output. The CSF provides a smooth analytic surrogate that averages out the sawtooth fluctuations while preserving the overall rise, cusp peak, and smooth landing of the nested configuration. Full details of the CSF are provided in Appendix A.

2.4. Flight Control Study

The following section develops an engineering framework for flight control based on Alcubierre-type warp dynamics. While treated as a working hypothesis, we regard this model as the most consistent with current evidence: gravitational

lensing, leading-edge vapor cones, oscillatory blur, and tilted disc flight repeatedly align with the predicted behavior of localized spacetime curvature. On that basis, we explore how such a warp-field system could be directed and stabilized, treating it as a testable foundation for UAP propulsion. The goal is not to claim certainty about the underlying mechanism, but to show that the convergence of theory and observation makes warp-field physics the most viable framework for modeling flight control.

In particular, we present nested and asymmetric nacelle configurations as engineering analogues for how directional control could be achieved in practice. Historical photographs and some videos depict recurring structural features such as extruding conical protrusions (noted in two case study photographs) and triadic undercarriage hemispheres often interpreted as landing pods or suspected nacelle housings (a semi-common motif outside the case studies). Our flight control study focuses on the plausibility of these configurations. The observed morphologies correspond closely with the theoretical requirements described herein for both lift and directional control within the nested nacelle framework, offering independent visual support for the proposed flight-control architecture.

Ultimately, this work was undertaken to advance understanding of gravitational lensing effects and characteristic flight behaviors documented in photographs and videos across multiple decades of observation. By application of Occam's razor, the repeated alignment of independent photos and videos with the theoretical framework developed here suggests that the simplest explanation is also the most direct: the observed phenomena match the theory because they operate in the manner described.

Nested Warp Nacelle Configuration

To control flight direction, the concept of nested asymmetric warp bubbles is introduced. By offsetting warp field strengths around the craft, allowing the craft to maneuver with precision in any direction, without relying on aerodynamic lift or propulsion nozzles. This is achieved by nesting smaller warp nacelles within and offset from the center of a larger nacelle.

Figure 7 presents two scatter plots showing how a disc-shaped craft employes nested warp nacelles to generate symmetric and asymmetric warp fields for controlled flight. The left panel (a) shows all lower nacelles operating at equal partial capacity. The central upper-deck nacelle—a cone-shaped array of micro-warp units—paired with at least three lower-deck nacelles (two shown in elevation), forming a vertically stacked warp configuration. Panel (b) provides the plan view with section-cut arrows, illustrating how the lower nacelles are offset laterally to shape the overall field geometry.

The right panel (c) shows the lower left nacelle turned off and the lower right nacelle rotated 45 degrees and turned up in strength. This asymmetric arrangement enables the formation of a composite warp bubble that is directionally skewed—creating spatial curvature biased to the one side of the craft. The upper spatial compression is located above left and the lower spatial expansion is located

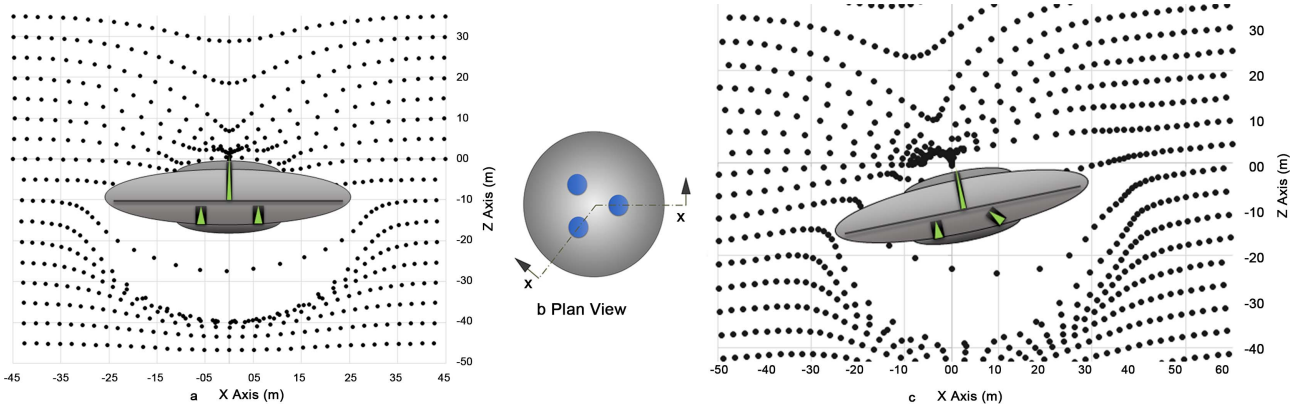

Figure 7. Scatter plots illustrating nested macro flight control warp nacelles in symmetric (a), plan view with section-cut arrows (b), and asymmetric (c) configurations. In the asymmetric case (c), gravitational lensing may cause external observers to perceive the craft as more tilted or distorted than its actual orientation.

lower right. The plot demonstrates that offsetting, rotating and modulating the strength one or more lower nacelles shapes and increases the warp field strength locally, resulting in a steeper gradient and theoretical directional control. The configuration shown is designed to counteract Earth's gravity, while allowing the craft to simultaneously travel horizontally across the Earth's sky.

Note: Gravitational lensing produced by the spatial warp configuration shown in Figure 7(c) is expected to cause external observers to perceive the craft as more tilted than it actually is, with apparent stretching, skewing, or even curvature. For real-world photographic examples, see Section 2.5 and Case Studies 4.2.1 and 4.5.1.

Theoretically, this nested configuration allows the pilot(s) to dynamically modulate the shape and intensity of the warp bubble by varying the individual nacelle outputs. This enables gravitational lift, pitch control, and propulsion without reliance on aerodynamic surfaces or conventional thrust mechanisms. In simplified terms, the control dynamics during slow horizontal flight inside of Earth's gravity resemble those of a helicopter—where localized field output adjustments function analogously to collective and cyclic pitch inputs.

The characteristic shape of the nested warp nacelles—and the resulting curvature of the warp bubble—has direct implications for vehicle design. The disc shape, frequently reported in UAP sightings, may be a functional expression of this underlying propulsion geometry. Its wide, low-profile structure offers stability for the surrounding curvature, maximizes internal symmetry, and facilitates fine-tuned asymmetric control at low altitudes. In this context, form follows function—not due to aerodynamic necessity, but as a result of relativistic field dynamics. It may be no coincidence that medium-sized UAPs are consistently observed as disc-shaped, particularly in cases involving tilted low-speed flight as discussed in Section 3.3.

Taken together with the preceding figures, this dual-view analysis reinforces the theoretical and visual foundation for the five proposed visual observables and provides a replicable framework for modeling how structured spacetime curvature

may govern UAP flight dynamics and environmental interaction.

Radially Aligned Warp Nacelle Configuration

An advanced variation of the nested micro-warp nacelle architecture involves a radial alignment between the inner and outer lower-deck nacelles. In this arrangement, each outer warp nacelle is positioned directly in line with a corresponding inner nacelle, extending radially from the center of the disc. When all nacelles in this system are oriented in the same vector direction and activated simultaneously, they produce a coherently reinforced warp field along that radial axis.

Unlike the cone-nested configurations discussed earlier—which modulate curvature vertically to enable lift and balance—this radial design steepens the spatial gradient along the horizontal axis. Figure 8 shows the result as a disc-encompassing, laterally extended warp cone with significantly sharper curvature across the plane of motion. This generates rapid inertial decoupling and sudden translational acceleration along the disc's flight axis, enabling abrupt horizontal displacement.

This configuration directly fulfills Luis Elizondo's first observable: "rapid acceleration"—a defining signature of advanced UAP behavior. It offers a plausible physical mechanism for the abrupt lateral disappearance captured in the final Rex Heflin photograph and may also account for the sharp departure recorded in the Ridoy video.

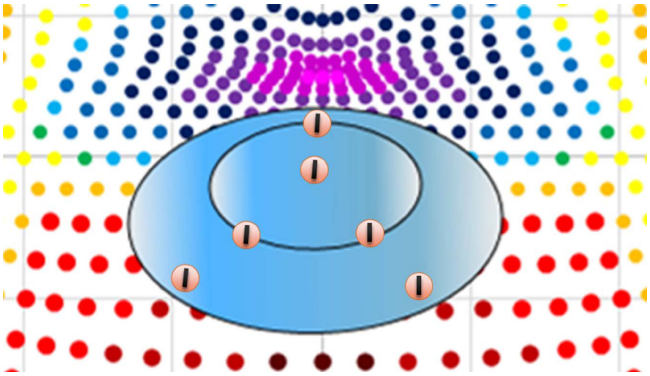

Figure 8. A disc-shaped craft showing radially aligned inner and outer warp nacelles overlaid on the color-coded spatial compression plot from Figure 3.

This configuration reinforces the horizontal compression band just ahead of the disc, forming a steep, laterally oriented warp cone. The resulting field geometry supports hyper-acceleration without inertia, matching Elizondo's first observable: extreme acceleration without aerodynamic explanation.

2.5. Gravitational Lensing: The Basis

Gravitational lensing is the deflection of light caused by spacetime curvature around a massive body or energy-dense region. In the weak-field limit of general relativity, the total deflection angle α for light passing at an impact parameter b from a lens of mass M is given by:

$$\alpha \approx \frac{4GM}{c^2 b} \tag{3}$$

where:

G—Gravitational constant (6.674×10^{-11} $m^3 \cdot kg^{-1} \cdot s^{-2}$)

M—Effective lensing mass (or equivalent mass–energy of the warp field)

c—Speed of light (2.998×10^8 m/s)

b—Closest approach distance between the light ray and the lens center

This equation, derived from the Schwarzschild metric, successfully predicts the deflection of starlight observed during the 1919 Eddington solar eclipse expedition, which measured $\alpha \approx 1.75$ arcseconds for light grazing the Sun's surface.

Application to UAP Observations:

If UAP-associated warp fields produce a local spacetime curvature equivalent to a lensing mass M_{eff}, then light from background objects passing near the craft would be bent by a measurable angle α. The apparent displacement Δx on an image sensor can be estimated as:

$$\Delta x \approx D \cdot \tan(\alpha) \approx D \cdot \left(4GM_{eff} / c^2 b\right) \tag{4}$$

where D is the distance from the observer to the background object. For example, with M_{eff} chosen to produce a deflection of only 0.01˚, a background edge at D = 2 km could appear shifted by ~35 cm, corresponding to several pixels in high-definition video—within the measurable range for stabilized, frame-by-frame analysis.

Implication:

Including this formalism allows observed pixel-scale distortions to be inverted to estimate M_{eff} (or equivalent field strength), providing a quantifiable link between imagery and underlying physics.

To extend the mathematical discussion of gravitational lensing, we developed a series of ray-trace models illustrating how different warp-field configurations alter the apparent geometry of UAP structures. Each model applies the scatter-plot geometry from **Figure 7(c)** to representative disc forms, showing how asymmetric contraction and expansion across field quadrants bend light paths and displace structural features as perceived by an observer. These examples provide a visual framework for understanding how warp-induced lensing produces the skewed, tilted, or displaced profiles documented in historical photographs.

Gravitational Lensing Ray-Trace – Plan Cut Through Dome Apex

The following ray-trace model, created in AutoCAD, represents a plan cut of a typical "sombrero hat" type UAP. The section is taken through the peak of the dome in elevation. For reference, the elevation scatter plot from **Figure 7(c)** has been overlaid on the UAP elevation drawing. In this configuration, the lower-right nested warp nacelle is angled at 45˚, shifting the region of maximum spatial contraction to the upper-left quadrant above the craft.

This asymmetric contraction produces a leftward curvature of light paths emerging from the dome apex. Rays that would normally travel straight to the observer bend leftward, while those originating farther to the right are also re-

fracted toward the same vantage point. As a result, the apparent peak of the dome is displaced rightward relative to its true geometric center.

Figure 9 shows how the effect is strongest at higher elevations, gradually diminishing toward the disc midline, and becomes negligible at the bottom center of the UAP's dome. To an external observer, the dome therefore appears stretched and skewed to the right. In the diagram, the original dome profile is shown in dashed line (phantom), while the lensed profile perceived by the observer is shown in solid black.

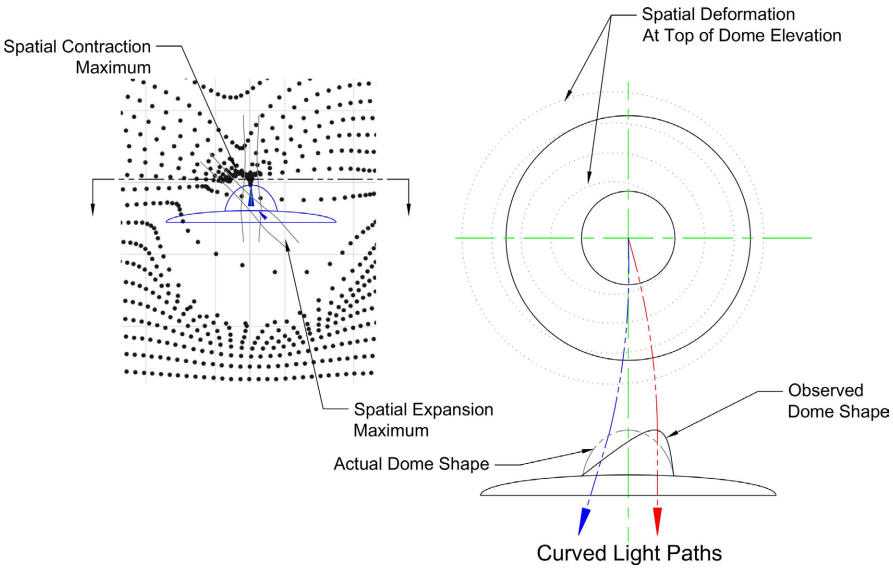

Figure 9. Gravitational Lensing study of sombrero hat UAP, plan cut taken at peak of dome.

This observed dome shift matches the photos from the Hopeh, China and George Stock events, see case study 4.2.1. Note, this observed offset will equally affect protrusions as seen in the Trent and Rouen Photos.

Gravitational Lensing Ray-Trace – Plan and Section Cuts Through Disc

This ray-trace model applied to a Trent/Rouen-style "pie plate" UAP with an extruding conical structure combines both plan and elevation section cuts, allowing the light paths to be traced to a distant vantage point. The analysis revealed several consistent distortions:

- Disc asymmetry: The leading edge (left) appears taller to the observer, while the trailing edge (right) appears shorter.
- Corner stretching: In plan view, both upper corners of the disc are displaced toward the trailing edge. The upper left corner is stretched only slightly, appearing shallower, while the upper right corner is stretched more strongly, appearing steeper.
- Cone displacement: The extruding conical structure is shifted rightward and also leans farther to the right.
- Overall proportions: The final ray-trace (Figure 10, lower right) shows that

the disc appears slightly tilted left, with the lower ring measuring taller on the right than the left, giving a slight pinched appearance. The apparent diameter is stretched by ~23% compared to the actual geometry, with the right-hand side displaced farther from the disc centerline than the left.

- Curvature Disc Warp: The lower disc trailing edge appears higher than the leading edge, with a non-linear transition between them. If the visible offset distance appears large enough, a pronounced curvature in the lower disc, may appear causing the disc to appear warped and asymmetrical. This may appear as a visible step (Figure 10 lower right and Hopeh China UAP, case study 4.2.1), or the UAP is titled toward or away from the viewer/camera, the lower disc edge may appear as a long stretched out continuous skewed curve (Heflin photos #1 and #3, case study 4.5.1). The larger the difference between the left and right heights, the larger the disc warp may appear.

Figure 10 presents how these distortions reproduce the skewed geometry visible in the Trent and Rouen photographs (see case study 4.2.1) providing a clear ray-trace demonstration of how warp-induced lensing alters both dome placement, sloping angles and disc proportions.

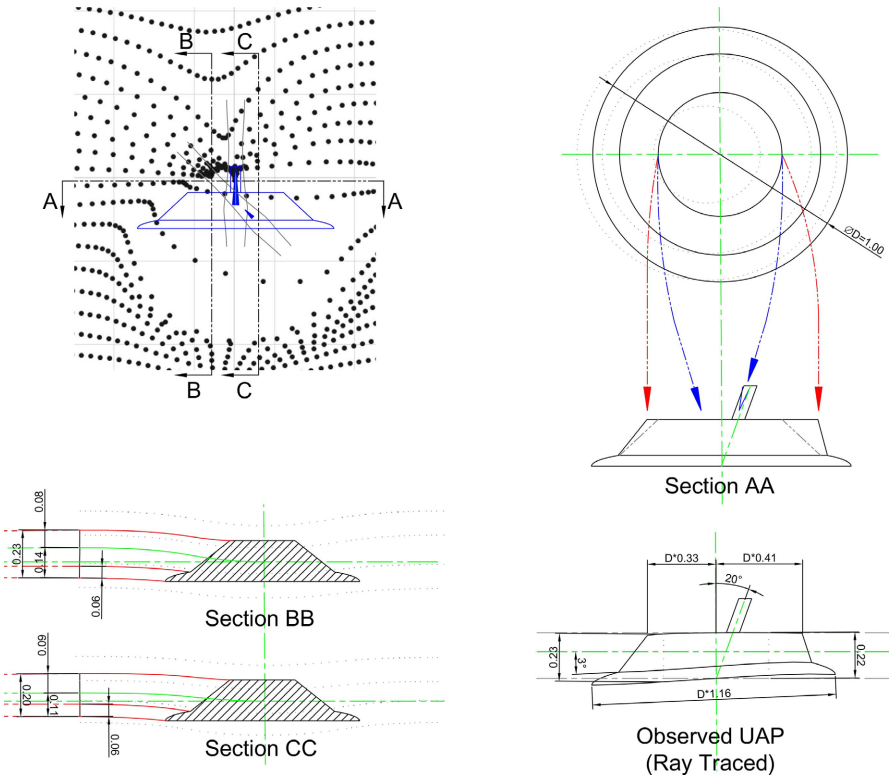

Figure 10. Gravitational Lensing study of Trent/Rouen UAP, plan and sections.

Gravitational Lensing Ray-Trace – Disc Observed from Above

Figure 11 presents a single vantage point above the craft to replicate the dome displacement seen in the Ridoy video. While the dome appears shifted rearward toward the trailing edge, the ray-trace shows that this effect results not from the

dome itself moving, but from differential compression of the far side of the disc. The disc edge behind the dome is optically displaced forward, creating the illusion that the dome sits farther back than its true position. Both disc and dome appear compressed to the observer, but the disc exhibits a greater degree of front-to-back compression, making the dome seem recessed into the structure. This provides a lensing-based explanation for the apparent dome displacement in the Ridoy video, see case study 4.4.2.

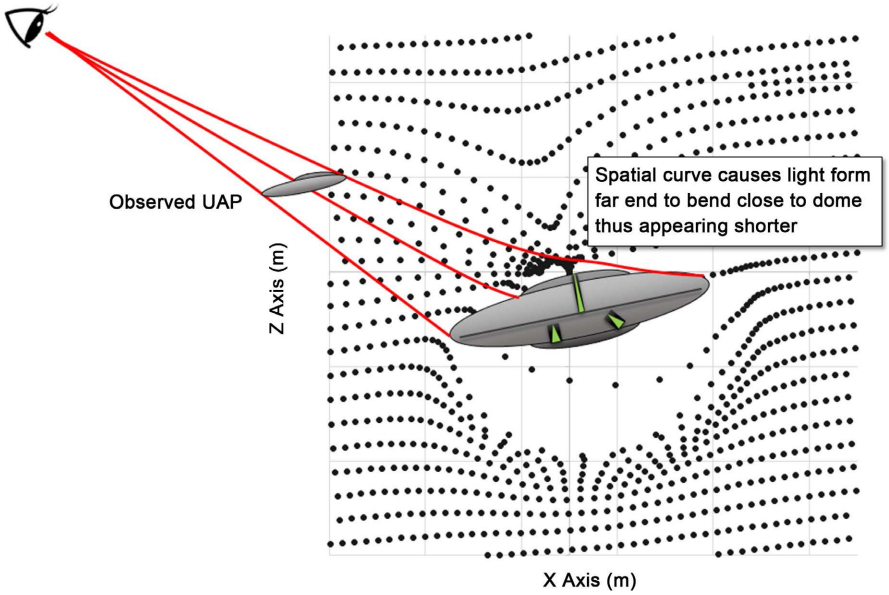

Figure 11. Gravitational Lensing study of Ridoy, disc observed from above.

Explanation/Counter-Explanation Section

Some skeptics may argue that historical disc distortions are the result of camera flaws, motion blur, or deliberate hoax models. However, this interpretation does not account for the precise and consistent deformation patterns observed across decades of independent photographs and recent videos. The ray-trace studies in Figures 9-11 show that specific anomalies—such as dome displacement, asymmetric edge stretching, disc warping and visually shortened trailing structures—are not random. They emerge naturally from the predicted behavior of light in nested, asymmetric warp fields.

Consider what a hoaxer or accidental artifact would need to reproduce by coincidence: offset domes that lean opposite to tilt vectors, edges compressed in exact quadrants, and trailing ends optically shrunk in ways consistent with warp-induced contraction. These features appear repeatedly in imagery captured long before gravitational lensing or warp metrics were part of public discourse. The cumulative weight of multiple one-to-one correlations between ray-trace predictions and archival imagery makes coincidence or fabrication increasingly implausible.

In this sense, the skepticism itself becomes less parsimonious than the warp-

field hypothesis. Rather than requiring decades of unrelated photographers to have accidentally mimicked warp-lensing geometry, the simplest explanation is that these distortions reflect a real physical mechanism. By showing how theoretical lensing translates directly into observed anomalies, the ray-trace models presented here undercut the notion that "it could just be this or that," and establish warp-field effects as the most coherent explanation for the photographic record.

By the principle of Occam's razor, the most straightforward explanation is also the most compelling: the photographs and videos align with warp-field predictions not by accident, but because UAP are operating exactly in the manner described.

2.6. Inertial Decoupling and Occupant Acceleration Effects

A key implication of field-based propulsion—particularly in models derived from Alcubierre-type metrics—is the concept of inertial decoupling. In traditional propulsion systems, acceleration is transmitted directly through the vehicle's structure to its occupants, producing inertial forces that can be physically harmful or even fatal at high G-loads. By contrast, warp field propulsion modifies the geometry of spacetime around the craft itself.

In such configurations, the vehicle does not move through space in the conventional sense. Instead, the spacetime volume containing the craft is translated relative to the surrounding environment, while the internal spacetime remains nearly flat. As a result, both the craft and its occupants are uniformly accelerated by the surrounding spacetime curvature, rather than by applied mechanical force.

One can think of this as the entire craft—and everything inside it—"falling" forward or upward together. Because the internal environment moves with the warp field, occupants would be unaware of any acceleration unless observing changes outside a window.

This uniform motion through curved spacetime creates a condition of inertial decoupling, wherein the occupants experience no classical G-forces—even during maneuvers that appear externally as sudden or extreme. The warp bubble effectively isolates internal matter from external inertial gradients, preserving a stable, non-accelerating experience within the craft.

2.7. Dimensional Overlay Methodology

To quantify structural deformations of UAP imagery, collages of selected historical photographs and video stills (see Section 4) were imported into AutoCAD and dimensioned using a standardized overlay procedure. The objective was not to determine absolute size in meters, but to present reproducible ratios of geometric proportions and angular deviations visible within each collage.

The procedure followed three steps:

1) Disc Diameter Reference (D). For each collage, the maximum disc diameter in pixels was dimensioned and labeled D = xxx px. This served as the primary reference scale.

2) Normalized Ratios. All secondary dimensions—such as disc thickness, dome displacement, or cone offsets—were expressed as ratios of the disc diameter. For example, a disc thickness measuring 12% of the diameter is shown directly as D × 0.12. Ratios are listed to two decimal places.

3) Angles. Angular deviations, such as dome tilt or protrusion offset, were measured directly in AutoCAD and displayed rounded to the nearest whole degree.

4) Dimensions are displayed directly on the collages, ensuring that the visual overlays themselves serve as the data presentation. This approach reduces redundancy and keeps the methodology transparent without the need for a separate results table.

3. Five New Visual Observables: Proposed Warp Propulsion Signatures

The original five observables—established by defense agencies such as AATIP—are kinematic and performance-based traits observed at the platform scale. These include behaviors such as sudden acceleration, trans-medium travel, and lift without control surfaces. They focus on how the object moves and interacts with physical forces in its environment.

In contrast, the five new observables introduced in Section 1.1 of this paper are visual in nature and serve as diagnostic warp-field signatures. Rather than measuring dynamic motion, they document how light, air, and spacetime are affected near the craft. These visual distortions provide insight into the mechanism of propulsion itself, and are often observable in stabilized video, frame-by-frame analysis, infrared imagery, or high-quality still photographs.

Crucially, the new observables are complementary—not redundant—to the original five. Together, they offer a more complete classification system: one that considers both flight dynamics and the environmental effects produced by field-based propulsion.

3.1. Gravitational Lensing and Radar Echo Distortion

Some UAPs exhibit visual distortions in the surrounding environment—bending light or radar signals—suggestive of localized gravitational lensing. This distortion is consistent with predictions from general relativity regarding massive objects in space or dense energy fields. Such lensing may present as ripples, halo effects, blurring, or background displacement near the craft's outline. The visual appearance of the craft themselves will also appear deformed. This observable supports the hypothesis that certain UAPs generate intense spacetime curvature, theoretically as part of a warp-drive. Unlike stealth, this effect alters the visual field around the object itself, indicating external manipulation of spacetime.

Gravitational lensing associated with UAPs appears in three distinct subcategories:

a) Lensing of background space—manifesting as displacement, warping, or

compression of environmental features behind or beyond the craft.

b) Lensing deformation of the UAP structure itself—manifesting as asymmetric disc shapes, displaced domes, warped perimeters, or uneven edge compression. Historical photographic evidence—including the Heflin, Trent, Trindade, Hopeh China, and McMinnville cases—exhibit these features, suggesting a stable lensing boundary aligned with the outer shell of the warp field.

c) Anomalous radar echoes—where signal anomalies—such as long-delay echoes, multipath returns, or radar target duplication—occur due to the bending or refraction of radar pulses across a curved spacetime gradient. These effects are as predicted by Alcubierre-style warp field geometries and are only observed in correlation with confirmed UAP presence (via visual, infrared, or radar modalities).

3.2. Leading-Edge Vapor Cones

Several UAP videos show vapor clouds forming above or ahead of the craft at both subsonic and hypersonic speeds—anomalous under classical aerodynamics. These are interpreted as adiabatic vapor formations caused by spatial compression ahead of the craft: ambient air entering the compressed region of a warp bubble undergoes rapid decompression, cooling enough to condense into mist. The resulting vapor halos align with the magenta-colored compression zones as seen in Figure 3's Alcubierre-model scatter plot, and may appear symmetric, transient, and field-bound, or manifest as short-lived trailing clouds. Notable examples include the Aguadilla thermal video, the Skywatcher.ai still frames, and the Perth UAP recording.

Field-Induced Vapor Via Spatial Compression

In warp-field models derived from Alcubierre-type metrics, regions of space surrounding a craft may appear compressed to an external observer while being internally expanded. This geometry—conceptually similar to the "bigger-on-the-inside" effect popularized by science fiction constructs like the TARDIS in Doctor Who—has unique thermodynamic implications.

When ambient air enters such a region, it is not physically compressed by force or motion. Instead, the air passively finds itself suddenly occupying a larger internal volume than the previous surrounding coordinate space.

Figure 12 illustrates using a smaller scale: what appears externally as 1.0 cubic foot of space may internally contain 1.05 to 1.10 cubic feet of proper volume. This relativistic spatial compression/expansion difference causes the air to decompress adiabatically, reducing its temperature without requiring velocity or mechanical input. In humid atmospheric conditions, such decompression can bring the air temperature down to the local dew point—typically requiring a drop of just 1.5 to 2.0 K.

The result is localized condensation forming a visible vapor cloud near the field boundary—often appearing ahead of or above the moving UAP. Unlike traditional vapor cones formed by aerodynamic compression at transonic speeds, this phenomenon occurs without shockwaves or supersonic motion.

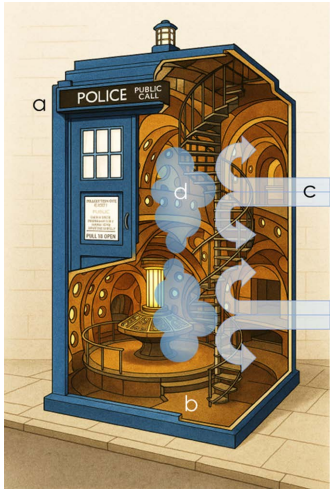

Figure 12. What appears externally as 200 ft^3 of space (a) may internally contain 10,000 ft^3 of proper volume (b). When a 200 ft^3 pocket of air (c) enters this region, it undergoes rapid adiabatic decompression, causing moisture entrained in the air to condense into visible vapor.

This proposed mechanism corresponds directly with the spatial gradient patterns modeled in **Figure 3**, where the upper magenta boundary denotes spatial compression coupled with internal volumetric expansion. Such geometries provide a plausible physical explanation for the persistent leading-edge condensation observed in both subsonic and hypersonic UAP cases, matches predicted warp-field curvature effects.

3.3. Tilted Disc Flight, Low-Velocity Gravity-Counterbalancing

A commonly reported, but underappreciated flight mode involves disc-shaped craft hovering or gliding slowly while tilted at an angle. Unlike helicopters or drones that require active balancing, these UAPs remain stable and often exhibit no audible propulsion or heat signatures. The tilted orientation may reflect asymmetric gravitational field interaction—theoretically enabling controlled forward acceleration while simultaneously countering Earth's gravity. Its repeat appearance in credible reports from the 1940s to the present suggests an intentional, engineered mode of subluminal atmospheric operation.

As described in Section 2.4, this asymmetric balance may be achieved using smaller, nested warp nacelles (see **Figure 7**)—compact field generators embedded around or beneath the primary disc structure. By selectively activating or phasing these localized nacelles, the UAP can distort spacetime unevenly across its structure. This provides not only lift, but also rotational and translational control, enabling pitch, yaw, and roll without physical control surfaces. Movement is directed by shaping the field envelope rather than applying mechanical thrust.

3.4. Warp Field Oscillation

Warp field oscillation is defined as observable structural or background distor-

tions that occur when a UAP dynamically reconfigures its warp bubble, producing transient visual signatures in photographs or video. In practical terms, oscillation can be understood as the act of photographically or video graphically capturing a UAP in the process of changing its warp field. Such field adjustments may occur for several reasons related to flight control, as discussed below.

In imagery, this does not resemble ordinary motion artifacts. Instead of directional smearing, vibration streaks, or camera shake, the object may appear duplicated, ghosted, blurred, or intermittently displaced—while the background often remains sharp and undistorted. In other cases, background features themselves momentarily deform or shift in isolated frames, further suggesting field-induced distortion. Collectively, these effects are interpreted as signatures of warp field oscillation resulting from active modulation of surrounding spacetime curvature.

Two modes of oscillation are apparent in the record:

- *Fast Oscillation*. This mode manifests as edge duplication, ghosting, or flickering of the craft, sometimes accompanied by momentary background displacement in single frames. The effect is best illustrated in Rex Heflin's third Polaroid (1965), where a sharply defined disc is accompanied by a secondary offset outline (see Section 4.2). The anomaly cannot be explained by motion blur or double exposure—the Polaroid Model 101 mechanically precludes such errors. Crucially, surrounding elements such as power lines and foliage remain crisply rendered, localizing the distortion to the UAP itself. Fast oscillation suggests high-frequency cycling of the warp field, possibly as part of inertial recalibration or temporary sensor transparency through the bubble.
- *Slow Oscillation*. This mode appears as a gradual displacement of structural features over multiple seconds, such as a dome drifting off-center and then returning to alignment. Unlike fast oscillation, which produces transient duplications, slow oscillation reflects a progressive adjustment of the warp field as it rebalances. A notable example is found in the 2023 Ridoy video, where the dome's slow migration coincides with a saucer-like skipping maneuver (see Section 4.11). This implies a controlled modulation of field asymmetry rather than an abrupt on-off cycling.

Together, these observations indicate that oscillation is not incidental but may be a deliberate and flight-critical feature of warp-based propulsion. Fast oscillation could provide momentary inertial or sensory recalibration, while slow oscillation may reflect gradual field realignment during directional changes. Both modes reinforce the interpretation that observed distortions arise from dynamic spacetime modulation intrinsic to UAP propulsion systems.

3.5. Saucer-Like Skipping Motion

Some UAPs display a punctuated, arc-like trajectory—resembling a skipping stone—rather than smooth, continuous, or ballistic motion. This irregular flight pattern may result from manual compensation for inertial drift or spatial disorientation within a warped spacetime field.

If the UAP's warp field is not oscillating, gravitational lensing may distort the pilot's view of the external environment, shifting or compressing the perceived position of the horizon and nearby landmarks. This is analogous to driving while wearing someone else's prescription glasses—where spatial relationships appear altered or unstable. Compounding this, each change in heading or pitch may further modify the appearance of the outside world, complicating orientation. Without reliable visual references, manual course corrections may be required, leading to a visible zigzag or hop-like trajectory—particularly during low-altitude and high-speed maneuvers.

This effect is notably documented in the 2023 Ridoy video and the 2025 KFOR news footage, both of which show discontinuous lateral motion inconsistent with aerodynamic flight. It is also consistent with Kenneth Arnold's 1947 original account, which described a series of "saucer-like skipping" movements across the sky—long before such behavior could be framed in relativistic terms.

3.6. Why the Observables Rule out Other Propulsion Theories

Numerous alternative propulsion theories have been proposed to explain UAP behavior—including magnetohydrodynamic drives, high-intensity magnetic fields, electrostatic lifters, ion propulsion, plasma sheaths, and other exotic electromagnetic mechanisms. While these models may account for limited aspects of observed UAP performance, they fail to explain the unique combination of visual and environmental signatures described in this paper. The five new observables—when taken together—effectively rule out these alternative mechanisms.

- *Gravitational lensing*, as seen in photographic and video evidence, cannot be produced by magnetic or electrostatic effects. Lensing requires spacetime curvature resulting from intense energy density or field manipulation consistent with general relativity.
- *Vapor clouds at subsonic speeds*, particularly the symmetric oval-shaped formations seen above UAPs, do not resemble shockwave patterns or ion discharge phenomena. Instead, they are consistent with adiabatic decompression resulting from spatial expansion Alcubierre-style warp fields.
- *Tilted disc flight without propulsion signature*, contradicts all known aerodynamic, electromagnetic, or plasma-based lift systems. Traditional high-voltage propulsion or MHD systems would still require some form of jetwash, corona discharge, or acoustic disturbance—all of which are absent in credible visual cases.
- *Warp Field Oscillation*, which results in flickering, phase-shifted, or duplicated imagery of the object without background distortion, cannot be recreated through camera motion or plasma fields. This effect is uniquely matches predicted field-based position modulation or phased warp field oscillation.
- *Skipping motion*, involving rhythmic hops with no aerodynamic lift or momentum loss, cannot be explained by plasma or electrostatic propulsion. The motion suggests discrete bursts of spatial displacement or field correction be-

havior—not continuous thrust.

The combination of these observables indicates not just unknown technology, but an entirely different framework of propulsion—one based on the manipulation of spacetime itself. This also helps explain one of the original core observables: sudden acceleration and rapid course changes. Conventional propulsion systems would expose occupants to extreme inertial forces that should be fatal. Only localized gravitational acceleration—where spacetime itself moves the craft rather than forces acting upon it—would allow such maneuvers without crushing occupants under their own inertia. This aligns directly with theoretical models such as the Alcubierre theory and supports emerging Department of Defense (DoD) research suggesting that UAP may be exploiting spacetime curvature to achieve their extraordinary maneuvers.

As Luis Elizondo noted in Imminent, the behavior of these objects points toward technologies "that appear to bend spacetime itself." These observables do not merely support that conclusion—they provide the visual signatures that make it testable.

4. Case Studies: Observables in Historical and Modern UAP Evidence

The previous section outlined five new visual observables that may indicate the presence of localized spacetime manipulation. In this section, each observable is examined in its own dedicated sub-section (Sections 4.1 through 4.5), with multiple photographic, video, and radar-based case studies presented under each category. These examples are evaluated in the context of their associated visual signatures, allowing for systematic comparison, cross-referencing, and pattern recognition.

This structure enables both historical and modern UAP incidents to be reinterpreted through the lens of warp-field theory—revealing consistencies across time periods, geographic locations, and recording media. The five proposed visual observables—gravitational lensing (1a, 1b, 1c), leading-edge vapor cones (2), warp field oscillation (3), gravity-counterbalancing tilted flight (4), and saucer-like skipping motion (5)—are supported by multiple, independently sourced observations spanning over six decades. These include photographic evidence (e.g., Rex Heflin), video footage (e.g., Aguadilla, Skywatcher.ai, Perth), military radar logs (e.g., the Tic Tac incident), infrared overlays, and corroborating eyewitness testimony from both civilian and military sources.

4.1. Summary of Confirmed Visual Observables

As summarized in Table 1, each observable now meets or exceeds the scientific threshold for initial confirmation—defined as three or more independent and repeatable occurrences. This comparative matrix represents a significant step toward establishing a coherent, physics-based framework for evaluating UAP behavior using conventional scientific methodology.

Table 1. Chronological UAP event log with visual observables.

Event	Year	Event Description	1a	1b	1c	2	3	4	5	-
			gravitational lensing							
			background objects	UAP itself	radar returns	vapor cones	oscillation	tilted flight	skipping motion	Totals
1	1941	Hopeh China Photo		1				1		2
2	1947	Kenneth Arnold Sighting							1	1
3	1947	William Rhodes Photos		1			1	1		3
4	1950	Paul Trent/McMinnville		1				1		2
5	1952	George Stock, Passaic, New Jersey		1				1		2
6	1957	Rouen, France Photo		1				1		2
7	1958	Trindade Island Navy		1				1		2
8	1965	Rex Heflin Photos		1		1	1	1		4
9	2004	US Navy Tic Tac Video and Radar Data			1					1
10	2013	Aguadilla UAP Video	1			1				2
11	2013	Dark Cube Inside Round Sphere	2							2
12	2021	Sky Watching event YouTube	1							1
13	2021	Saturn over Columbia Video	1				1			2
14	2022-2024	Tedesco Brothers Radar Recordings/IR Photos			14					14
15	2023	Ridoy Disc Video	1	1		1	1	1	1	6
16	2023	Tear-drop FOIA Eyewitness Sketch	1							1
17	2023	Perth UAP Video		1		1			1	3
18	2024	CSSAA Sky Watching Event	1							1
19	2024	Skywatcher.ai Video				3				3
20	2025	KFOR Oklahoma News Video							1	1
New Observable Totals			8	9	15	7	4	8	4	55

Notes: *Visual still frame analyses from Hidden in Plain Sight (Wanless, 2025) are included where individual observables were identified, even when not treated as full case studies in this paper. **The Tedesco brothers have confirmed in private correspondence that they have recorded a total of 14 radar echo events in which a UAP was confirmed using a visual or IR camera. ***Skywatcher.ai has indicated in interviews that they have multiple recordings of leading-edge vapor cones, but to date, have only released one video publicly indicating three possible separate videos.

Although the five new observables were introduced independently, real-world evidence rarely presents them in isolation. Many case studies exhibit multiple visual signatures simultaneously—such as gravitational lensing paired with vapor cone formation, or tilted flight coinciding with warp field oscillation. In this section, each case study is organized under the observable it most prominently demonstrates.

The observable indicating tilted flight is present in a significant percentage of historical photographs, both with and without other new observables. For this reason, cases involving tilted flight are placed under the category of the other primary observable they exhibit, rather than in a standalone category.

To reduce the risk of retroactive mimicry, all photographic case studies analyzed here are drawn from sources captured prior to 1970—well before gravitational lensing or warp field dynamics were publicly recognized. This temporal cutoff serves as a control against cultural contamination, increasing confidence that recurring visual anomalies stem from consistent physical mechanisms rather than imitation.

Image and Video Processing Methods

For this study, image and video processing was limited to basic adjustments intended solely to improve clarity without altering the underlying content. Photographs and still frames from videos were isolated and cropped using Adobe Photoshop. Adjustments were restricted to brightness, contrast, and saturation. No additional cleaning, denoising, or artifact-removal methods were applied, as such techniques could be claimed to introduce false positives.

Video analysis was conducted using the Camtasia software platform, which allowed frame-by-frame review of footage. Examination videos created for this paper—linked within the relevant case studies—were assembled using Camtasia. For example, the Ridoy video was both manually stabilized in Camtasia and automatically motion stabilized using Adobe software prior to inclusion in the compilation examination video.

Certain examination sequences also included manually stabilized segments, where individual frames were manually aligned to ensure background appears as stationary. This approach, clearly noted in the videos, was used to reveal how the background changed or momentarily deformed as the UAP passed in front of it. These manual stabilizations were performed frame-by-frame without introducing new image data or altering the original visual content.

All original, unaltered image and video files have been linked within this paper and are available for independent inspection.

4.2. Background Gravitational Lensing Case Studies

Case studies in this category present clear examples where background distortions were observed in photographs, videos, or documented by trained U.S. Air Force or Navy fighter pilots. These examples suggest lensing effects which appear to match predicted spacetime curvature in the vicinity of the UAP.

4.2.1. Laser Pointer Skywatch Events Suggestive of Gravitational Lensing

Two independent skywatching events have captured UAP-related anomalies using high-power laser pointers, offering preliminary evidence of localized spacetime distortion consistent with gravitational lensing. In both cases, the laser beams—used to safely indicate aerial objects—exhibited momentary horizontal deformation when passed behind or near the UAP, suggestive of lensing-induced beam deflection.

Laser pointers are commonly used during skywatch events to indicate the position of a UAP to others in the observation group. The standard procedure involves circling the object with a high-powered laser rather than aiming directly at it, minimizing the risk of inadvertently targeting aircraft. When the laser beam passes behind the UAP, it may silhouette the object—providing not only spatial reference, but also a potential opportunity to observe gravitational lensing effects, as demonstrated in Figure 13 below.

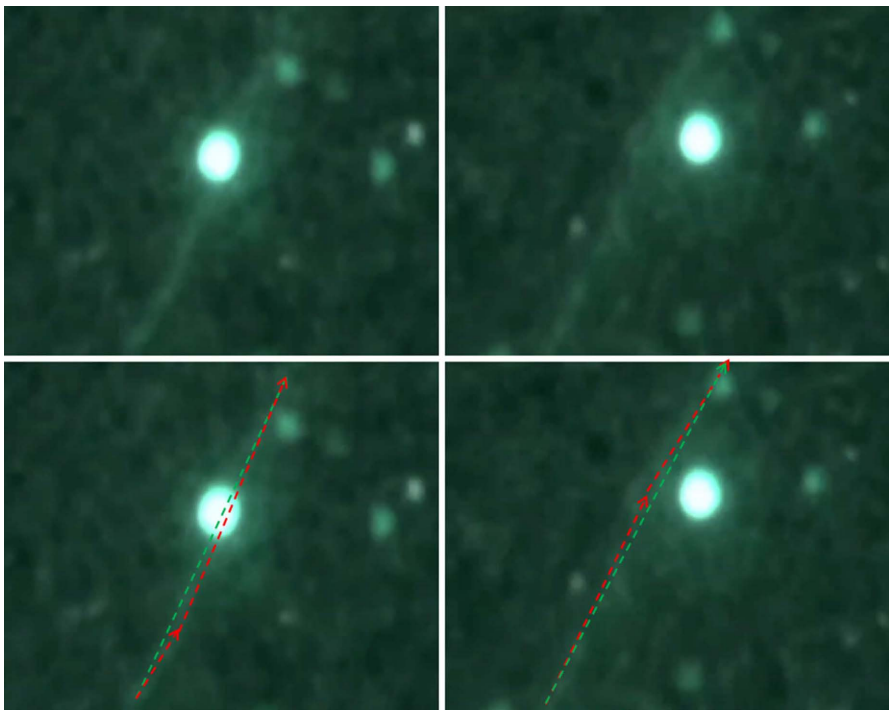

Figure 13. Two still frames from a skywatch event where a laser pointer captured momentary gravitational lensing [3].

Figure 14 shows a second field event (July 2024) near Capilla del Monte, Argentina, researchers Rob Freeman and Mark McNabb with the Centre for the Scientific Study of Atmospheric Anomalies (CSSAA) conducted nighttime skywatching with a multi-camera setup directed away from urban light pollution.

Figure 15 shows an overlay analysis in which the laser beam is seen apparently curving downward and then around the object—a behavior inconsistent with linear propagation through a uniform medium. These deformations were brief

Figure 14. CSSAA video two still Frames showing laser beam Behind UAP.

and appeared only during rapid laser motion, indicating a small but localized field effect. The left still frame from Figure 14, recreated in the ray-trace model of Figure 15, shows light that originally followed a steeper trajectory curving upward beneath the UAP through its lower warp hemisphere before being redirected toward the camera's position.

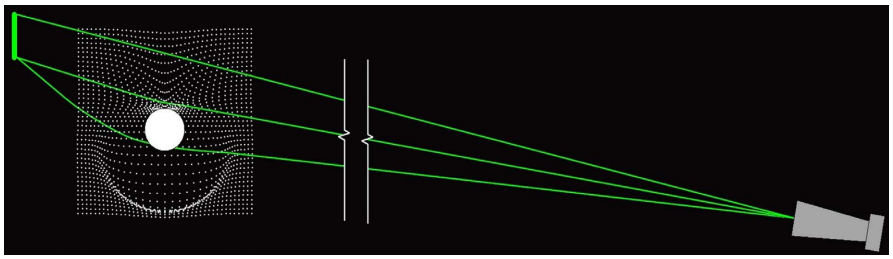

Figure 15. Laser beam lensing captured in first frame.

In both skywatch cases, enhanced contrast imaging supports the hypothesis that the observed laser deformations may result from a localized gravitational lensing effect produced by a potential spatial warp field.

Consideration of Alternative Explanations

While alternative explanations—such as particulate scattering, atmospheric refraction, or camera-induced artifacts—cannot be entirely excluded, they do not fully account for the symmetric, directional curvature of the beams observed relative to the UAP positions. The repeatable geometric relationship between laser deformation and object location in both cases suggests the presence of a structured, non-random lensing effect, making this a compelling candidate for further study.

These two skywatch field events provide a foundational dataset for future field replication studies, particularly under controlled observational protocols outlined in Section 5.

4.2.2. Air Force Sketch–Teardrop FOIA Eyewitness Sketch

On January 26, 2023, an Air Force pilot flying over the Gulf of Mexico near Florida encountered an unidentified aerial object described as a dark, capsule-like structure with a reddish-orange glow and visible atmospheric distortion. Figure 16 shows the pilot's detailed sketch—obtained through FOIA and publicly released in 2024—depicts a structured craft with a "segmented gunmetal gray dome, a self-illuminating base," and "blurry, distorted air" beneath the object. This optical anomaly is visually matches predicted gravitational lensing or heat mirage-like effects, which aligns with New Observable #1 in this paper.

Radar contact was initially acquired but reportedly failed as the pilot approached within ~4000 feet. The pilot report later attributed the radar malfunction to a blown fuse. While the failure was technical in origin, its timing—occurring at the moment of close-range UAP proximity—mirrors a broader pattern of sensor anomalies reported during UAP encounters.

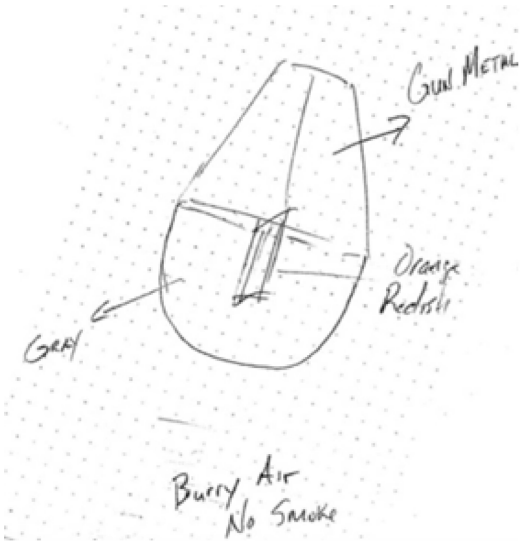

Figure 16. Eyewitness sketch submitted to the U.S. Air Force showing a disc-shaped UAP and blurred roadway directly beneath [4]. This intentional distortion suggests perceived gravitational lensing or visual compression matches predicted warp field boundary effects.

Explanation/Counter-Explanation

AARO later suggested the object was likely a self-illuminating balloon, possibly from a commercial or research provider. However, no manufacturer was named, and no tracking logs or telemetry data were presented. This omission is critical: if a balloon manufacturer were responsible, traceable data or corporate acknowledgment would be expected under FAA and commercial standards. Furthermore, no known class of balloon matches the specific physical or optical description in the sketch.

To evaluate the plausibility of this explanation, Table 2 compares known self-illuminating balloon types to the observed object characteristics.

Table 2. Comparison to known self-illuminating balloons.

Balloon Type	Manufacturer/ Examples	Illumination Method	Typical Use	Altitude/Size Range	Match with 2023 Sketch?
LED-Lit Party Balloons	*illooms*®, GlobalSources, etc.	Internal battery-powered LED	Consumer events, parties	Small (1 - 2 ft); low altitude	No, too small; not aerodynamic; not tracked
Glow-in-the-Dark Coated Balloons	*Noxton*, generic	Phosphorescent paint	Nighttime decoration	Small; ground level only	No, passive glow; not visible at high altitude
Large Industrial Lighting Balloons	*Airstar*, *PowerMoon*®	High-lumen lighting system	Film, construction, emergency sites	Stationary, on tripods, no helium used	No, tethered; not aerial vehicles, heavier than air
High-Altitude Balloons (e.g. Stratollites)	*World View*, *Near Space Corp*	Passive reflectivity or solar power	Research, comms	Very high altitude; tracked	Not self-illuminating; shape mismatch
Toy/Reflective Foil Balloons	*Anagram*, *Qualatex*	Reflective only (not lit)	General public	Ground level to a few hundred ft	No internal lighting; shape mismatch

The object's described structure, luminosity, radar behavior, and optical distortion do not match any known category of balloon. Additionally, The Air Force's and AARO's refusal to release the video—despite being able to redact classified details—raises further questions. If the footage were merely a balloon, redaction would have been sufficient. The withholding suggests that the video may reveal observable characteristics inconsistent with mundane explanations.

Crucially, no known balloon technology—whether illuminated or reflective—is capable of distorting the visual background beneath and surrounding the object. The pilot's sketch explicitly depicts blurred, wavy distortion below the craft, affecting not only the air near its surface but the terrain and environment behind it. This phenomenon is inconsistent with heat shimmer or thermal bloom, which would localize near the balloon envelope. Instead, the visual distortion is spatially offset and symmetric—a signature more consistent with gravitational lensing caused by localized spacetime curvature.

Note: Although the video has never been released, the accompanying report—submitted internally through Air Force channels—describes a loss of radar lock coinciding with close-range approach to the object. This detail was not crafted for public effect, nor intended for UAP researchers. It was part of an operational debrief, written under military chain of command. As such, the content can be treated as a sincere and technical description of sensor behavior, made by a trained observer reporting to superiors—not as speculation or folklore. While the video would provide empirical confirmation, the pilot's written account remains a credible and valuable source (The Black Vault, FOIA Release, April 2024).

Skeptical interpretations may argue that the radar failure was due to internal

aircraft issues rather than any external interference. In this case, the pilot report later attributed the radar malfunction to a blown fuse. However, the failure occurred at the precise moment the pilot approached a structured, self-illuminating object exhibiting visible distortion effects—mirroring patterns seen in other UAP incidents where electronic or radar anomalies coincide with visual proximity. While the cause of radar disruption is mechanically understood, its timing remains notable. Moreover, the pilot would still be fully capable of identifying when radar lock has been acquired and subsequently lost. The value of the report lies not in proving cause, but in establishing repeatable patterns of radar instability and visual anomalies in close proximity to UAPs.

4.2.3. The Cube-in-Sphere UAP Geometry and Implicit Containment Lensing

It is important to recognize that the U.S. Department of Defense has publicly confirmed that Unidentified Aerial Phenomena (UAP) are real, physical objects observed through multiple sensor modalities—including visual, radar, and infrared—and that the U.S. government does not currently know, or will not admit to what they are [5]. This admission shifts the baseline for scientific analysis: pilot accounts of UAP should no longer be treated as speculative or mistaken anecdotes. Rather, they should be presumed to reflect real encounters with unknown aerial objects. The question is no longer if something was seen—but what was seen.

With that in mind, both the Navy cube-in-sphere incident and the Air Force vent event offer rare but valuable examples of pilot-reported encounters consistent with gravitational or spatial lensing. Crucially, both reports were made through official military channels, with no expectation of public release or media attention. The motivation behind both was clear: "flight safety", not publicity.

In the Navy case, as reported by former F/A-18 pilot Ryan Graves, two jets were flying in formation—each with a front-seat pilot and a back-seat weapons systems officer. All four aircrew members observed a UAP described as a "black or dark gray cube suspended inside a translucent sphere" (see **Figure 5**). The object passed directly "between the two aircraft", physically splitting their formation before departing on a stable trajectory. The event was reported immediately up the chain of command as a flight safety violation.

Similarly, in the Air Force "teardrop FOIA eyewitness sketch," the pilot observed a disc-shaped object that appeared to momentarily warp the cloud structure behind it. The event coincided with a loss of radar lock, initially believed to be a technical fault—until it was determined that fuse had blown, suggesting possible interference consistent with localized spatial distortion. Like the Navy report, this incident was submitted internally, not intended for public release.

Some skeptics may argue that "*even trained pilots can be wrong*." While technically true, this objection lacks specificity. It ignores the fact that modern fighter pilots are trained to recognize, interpret, and respond to every known aerial phenomenon detectable by sight, radar, or infrared. Their training encompasses not

only conventional aircraft but also drones, missiles, weather anomalies, and electronic warfare countermeasures. Many hold engineering degrees—often in aerospace or mechanical disciplines—and are deeply familiar with the physics of flight, sensor behavior, and radar anomalies. When such pilots report an object they cannot explain, the strength of that report lies in their inability to do so.

In scientific terms, the significance of a UAP sighting is inversely proportional to the pilot's failure to identify it. The better trained the observer, the more meaningful their admission of uncertainty becomes. And when four aircrew members in two jets witness the same novel, geometrically precise object in real time—one that physically interacts with their formation—the likelihood of collective misperception becomes vanishingly small.

Neither of these incidents was intended for public release. Neither was driven by notoriety, social pressure, or media influence. Both were submitted through official military reporting protocols as aviation hazards. These circumstances make them especially valuable for scientific analysis, because they are largely free from cultural contamination, hoax risk, or motivated reasoning.

4.3. Gravitational Lensing Causing Distortions of UAP Structures

These cases show compelling evidence where gravitational lensing appears to directly alter the visual appearance of the UAP's structure, producing distortions or shape warping in still imagery or video footage.

Pre-1970's Gravitational Lensing and Tilted Flight Case Studies

Tilted disc flight—where a UAP maintains a stable, non-horizontal orientation while hovering or gliding—is one of the most visually distinctive and aerodynamically anomalous behaviors documented in UAP sightings over the past 80 years. These objects appear to hover or cruise at a visible pitch or roll angle without any apparent aerodynamic control surfaces, propulsion exhaust, or downwash. The consistency of this tilt across multiple sightings, geographic regions, and camera types suggests not aerodynamic balancing, but rather a form of controlled, asymmetric gravitational field generation—a key indicator of directed spacetime curvature.

As with all pre-1970 photographic cases in this study, the inclusion of this image was guided by a key methodological filter: restricting analysis to historical data predating public awareness of gravitational lensing and warp-field theory. This helps ensure that any recurring distortions—such as disc curvature and asymmetric dome or cone protrusion skews—arose naturally, not through later attempts to replicate earlier visual clues.

To illustrate this behavior, **Figure 17** presents a composite of six historic UAP photographs and one modern UAP video, each capturing a disc in clearly tilted flight and often exhibiting signs of gravitational lensing and momentary structural deformation:

a) Hopeh, China Photo (1942): Daylight capture of a disc in titled flight to the right over the city of Hopey, China, showing clear and defined skewing defor-

mation of the disc's left side and tilting of the dome towards the trailing edge at an angle of 16 degrees. Note, the leaning dome centerline measures as coincident and aligned with center of the disc.

b) Paul Trent Photo (1950, Oregon): Iconic canted disc with a shallow dome and protruding conical feature in tilted flight. The image displays visibly deformed edge curvature where sloping upper curvature of the left side of the disc appears steeper than right side of the disc, and a pronounced horizontal displacement and leaning tilt of the conical tip at 7 degrees. Note, the leaning cone centerline measures as coincident and aligned with center of the disc.

c) Rouen, France Photo (1954): Similar to the Trent photo, this canted disc shows a shallow dome and conical protrusion with visible edge distortion and lateral displacement, the disc is different enough from the Trent photo to indicate the same "make and model" but is not a duplication of the Trent photo. Note, a deviation was found in that the leaning cone centerline measures as coincident and is misaligned with center of the disc.

d) George Stock Photo #1 (1952, Passaic, New Jersey): The disc photographed in tilted flight to the left. The left edge measures significantly thicker than the right, and the dome is both offset and leaning rightward at an angle of 20 degrees. Note, the leaning dome centerline measures as coincident and aligned with center of the disc.

e, f) George Stock Photo #2 and #3 (1952): For comparison, these photos show the disc appears in tilted flight towards or away from the camera. The measures shown that the dome leans by 2 or 3 degrees and to one side and the centerline measures as coincident and aligned with center of the disc.

g, h) Trindade Island Photos #1 and #2 (1958): Two-frame sequence showing a Saturn-shaped disc bank in leftward tilted flight as it traveled west over the island. The central upper bulge measures as being skewed to left, with a steeper left slope than the right slope. The lower bulge measures as the opposite. The lower dome is skewed to the right and steeper on the right than the left. This consistent with a warp field oriented perpendicular to the camera.

i, j) Trindade Island Photos #3 and #4 (1958): Two additional frames show the same Saturn-shaped disc traveling eastward, showing titled flight to the right. The disc is measured as symmetrical in these frames, yet both equally measure taller. This suggests a symmetrical warp field—meaning the lower nested warp nacelles are roughly equivalent in power output, possibly due to the active descent in trajectory.

Several of the images include the spatial grid from **Figure 7** overlaid to illustrate how spatial deformation affects the gravitational lensing appearance of each UAP. Photos a and b reveals clear deformation of both the leading (right for a and left b) and trailing (left for a and right for b) edges of the disc, while the central dome appears offset and bent toward the trailing edge—consistent with asymmetric compression. Shown for comparison, photo c shows the same disc tilted away from the camera, appearing largely symmetrical. This indicates that the direction

of a tilted warp bubble directly impacts whether or not an outside observer will notice if the UAP structure is deformed.

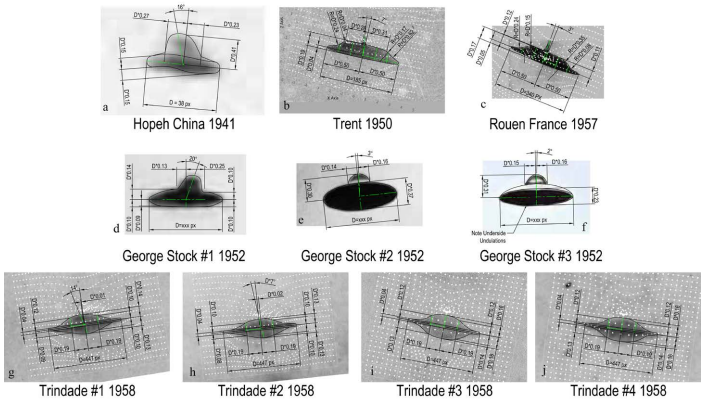

Figure 17. Collage of photos from ten dimensioned photos from five UAP events between the 1940's through the 1960's.

Photos d and e, the converging upper spatial contraction causes the upper cone—likely an extended central warp nacelle—to appear bent toward the left, opposite the tilt vector.

The four Trindade event photos shows two sets of photos where UAP structural deformation is clearly visible, photos f and g, as the UAP travels westward (leftward motion). However, in photos h and i, the same disc appears more symmetrical while descending in the opposite direction—eastward (rightward motion). These alternating patterns suggest that apparent disc asymmetry is strongly dependent on orientation within the spatial gradient, consistent with the optical effects of a dynamic, asymmetric warp field.

In each case, the disc's tilt defies conventional aerodynamic behavior. There is no indication of airframe control surfaces, thrust vectoring, or active balancing mechanisms. Instead, the visible structural changes in each UAP's appearance suggests the use of asymmetric warp field configurations to achieve both lift and vectoring control. This interpretation is reinforced by the application of spatial warp scatter plot overlays to several of the images (Trent, Rouen, Trindade), which reveal that the observed surface distortions align with predicted Alcubierre-type warp boundaries.

As such, these images do not only reflect New Observable #3: Tilted Disc Flight, but also strongly exhibit New Observable #1B: Gravitational Lensing of the UAP structure. This includes:

- Compressed or smeared trailing edges—where one side of the disc's rear appears optically thinned or blurred.
- Height expansion at the leading edge—resulting in a vertically stretched profile consistent with light distortion near the warp boundary.
- Apparent dome or conical feature misalignment—including lateral displacement and tilt toward the trailing edge of the disc.

- Asymmetric shaping and edge curvature—indicating structural deformation consistent with external field lensing.

These distortions appear consistently across analog photographs taken decades before the Alcubierre metric was proposed, making post-processing artifacts, camera flaws, or hoax explanations less plausible. Their recurrence across time, culture, and continent suggests that the tilted disc flight configuration is not incidental—but intentional, theoretically resulting from the use of nested or offset warp nacelles that produce controlled, asymmetric lift vectors.

Explanation, Counter-Explanation

Some skeptics argue that historical disc photographs may be the result of hoaxes or misidentified mundane objects such as hubcaps, pie plates, or thrown models. However, this interpretation fails to account for the precise and consistent deformation patterns observed across decades of sightings—many of which predate modern gravitational lensing theory, l*et al.*one Alcubierre-type warp drive models.

In particular, three recurring geometric features stand out:

1) The disc is visibly tilted in flight, without visible propulsion or control surfaces.

2) The dome or central protrusion is leaning or displaced toward one side—not centered when the disc is tilted and viewed edge-on and becomes centered when tilted or traveling towards or away from the observer.

3) Peripheral elements such as cones or fins are curved or bent, often offset asymmetrically toward the opposite side of the disc's lean.

These features—consistently present in independent sightings from 1942 through the present—match modern simulations of asymmetrically nested warp nacelles (see **Figure 7**). Yet such subtle deformation patterns would be extremely difficult to hoax accidentally, particularly using physical models or darkroom tricks in the 1940s-60s.

Consider what a hoaxer would have had to know in order to match these patterns by coincidence:

1) How did they know to tilt the disc not just off-axis, but with the dome displaced opposite the tilt vector, consistent with gravitational asymmetry in an Alcubierre-type warp field?

2) How did they know to bend the peripheral domes, cones or protrusions away from the tilt direction, mimicking the spatial gradient distortion predicted by field asymmetry?

3) How did they know to introduce gravitational lensing-like deformation along one edge, especially in cases like the Trent, Stock, and Rouen photos—years before gravitational lensing was part of any public or photographic discourse?

These coincidental alignments would require not just technical skill, but advanced theoretical foresight. And yet, in nearly every case, the photographs display these same patterns—regardless of geographic location, camera type, or witness background.

The most parsimonious explanation is not that hoaxers across continents somehow stumbled into visual matches for warp geometry decades before such theories existed. It is that these visual features are real, and arise from a consistent, underlying physical mechanism—namely, asymmetric spatial curvature associated with field-based propulsion.

As with gravitational lensing in astronomy, once the theory became available, earlier unexplained anomalies suddenly made sense. In the same way, warp field predictions retroactively explain the geometry, tilt, and deformation patterns in these historic photographs—offering not just an explanation, but a unifying framework for decades of observational data.

Finally, the 1942 Hopeh photograph deserves special consideration. Taken five years before the modern UFO era and more than half a century before the Alcubierre warp metric was proposed, it cannot reasonably be attributed to cultural influence or theoretical mimicry. Yet the image exhibits structural distortions that correspond in a one-to-one correlation with the ray-trace predictions shown in Figure 9 and Figure 10. Importantly, while a handful of earlier photographs exist, this appears to be the first UAP image to show clear and measurable evidence of gravitational lensing—structural deformations consistent with localized spacetime curvature. This temporal alignment presents a significant challenge to any counter-explanation involving hoax. The sighting occurred in 1941—six years before the term "flying saucer" was popularized by Kenneth Arnold's 1947 report, often cited as the beginning of the modern UFO era. This raises a critical question: how could a hoaxer in 1941 have produced a model with precise deformations and light distortions that were neither described nor theoretically modeled until decades later? By the principle of Occam's razor, the most parsimonious conclusion is that the distortions are genuine signatures of localized spacetime curvature. While such an interpretation is undeniably uncomfortable—implying the operation of non-human technology well before modern discourse on warp theory—it remains the explanation most consistent with both the photographic record and theoretical modeling.

4.4. Gravitational Lensing Affecting Radar Returns

In these examples, gravitational lensing is inferred from anomalies in radar performance—such as unexpected return patterns, range delays, or apparent target displacement—that coincide with visual UAP observations.

Radar anomalies observed during UAP encounters provide some of the strongest empirical indicators of field-based propulsion. Three independent cases— and the 2004 Tic Tac incident and the Tedesco brothers' 2022-2024 radar experiments. Each where included here because the UAP(s) were recorded on radar. The Tic Tac and Tedesco events demonstrate repeatable signal splitting and delay effects consistent with Alcubierre-type warp field distortions.

4.4.1. Matched-Return Anomalies: The 2004 Tic Tac Event

During the now-famous USS Nimitz encounter, F/A-18 fire-control radars dis-

played the anomalous "99.9 RNG 99" error—indicating the radar received two matched pulses at incompatible return times. Three primary explanations are consistent with this observation:

1) Warp-Induced Signal Splitting: Figure 18 illustrates how the outgoing radar pulse is split as it interacts with compressed and expanded spacetime regions around the UAP, returning early and late echoes with identical coding.

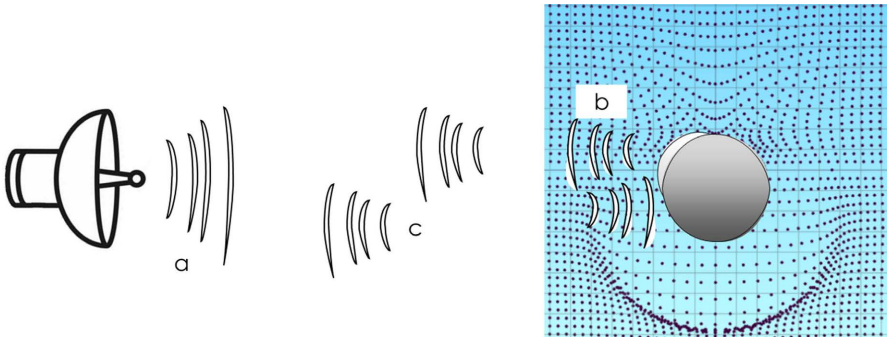

Figure 18. Radar beam interacting with a warp bubble geometry. The pulse splits as it travels through regions of spatial compression and expansion, producing two time-separated returns from the same target.

2) Warp-Induced Propagation Delay: Figure 19 illustrates how radar pulses may loop or stall within a localized gravitational field, causing return delays inconsistent with flat-spacetime propagation.

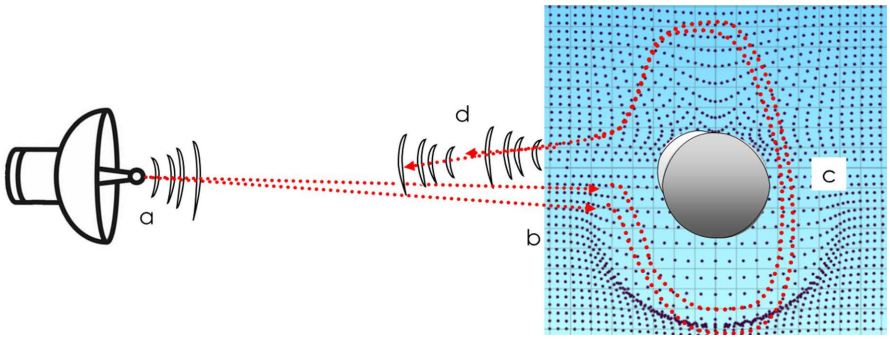

Figure 19. Radar pulse interaction with a warp bubble: signal splitting and temporal spreading due to spacetime curvature.

3) Intentional ECM (Electronic Countermeasures): The UAP may have rebroadcast the radar pulse after receiving it, requiring anticipatory knowledge of waveform structure—an advanced capability.

The January 2004 incident revealed persistent anomalies across multiple sensors. Figure 20 shows two still frames where the AN/APG-73 radar's "99.9 RNG 99" code indicates multiple matched-filter returns at incompatible delays—a signature inconsistent with calibration drift or noise. The system, designed for combat reliability, includes built-in diagnostics to flag timing or phase errors. No such faults were recorded.

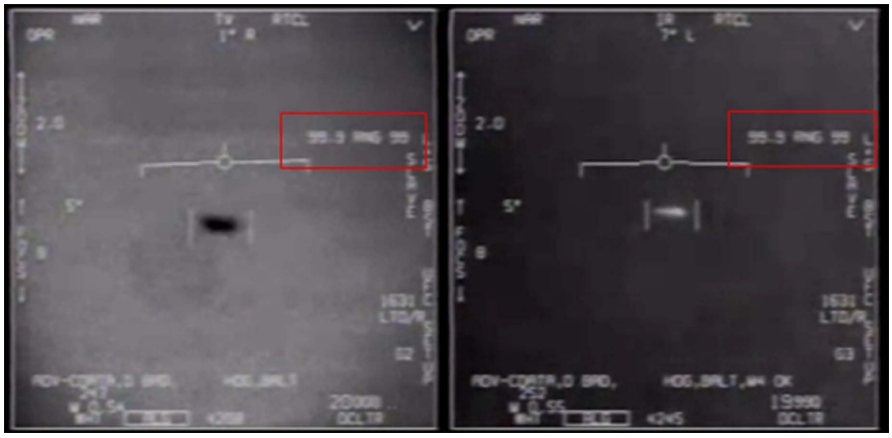

Figure 20. Still frame of the F/A-18 radar display during the Tic Tac encounter, showing "99.9 RNG 99" matched return code.

4.4.2. Long-Delay Echoes: The Tedesco Experiments

Additional support comes from the peer-reviewed research of John and Gerald Tedesco, who recorded long-delay echoes (LDEs) using marine X-band radar during UAP tracking experiments. Their dataset uniquely combines radar anomalies with direct visual and infrared confirmation of UAP presence.

These distortions occurred only when UAPs hovered faintly, seen in Figure 21, in the line of sight between radar and offshore surface vessels. Plan-view radar displays showed boats elongated or duplicated, with echoes arriving multiple seconds after pulse emission. In verified cases, apparent vessel length doubled or more without physical changes. The anomalous radar returns disappeared as soon as the UAPs were no longer present.

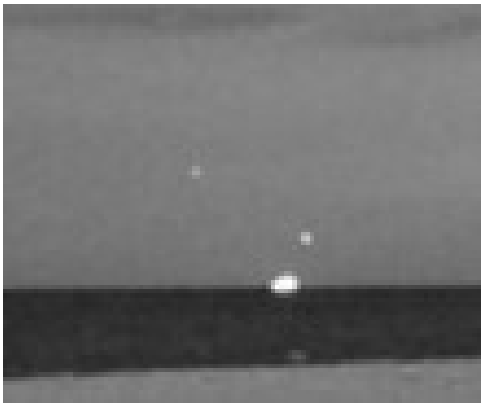

Figure 21. IR image from Tedesco bothers' paper (Figure 21) showing two objects between a medium size vessel and the IR Camera.

This effect is consistent with gravitational lensing caused by Alcubierre-type warp fields. Figure 22 illustrates how radar pulses passing through the warp's geometry may be bent back toward the dish via altered geodesics, producing duplicate or delayed returns as seen in Figure 23. Item a is the actual boat and item b is the duplicate.

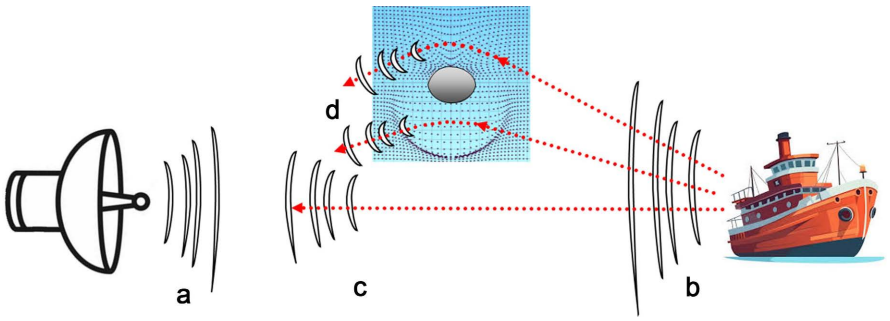

Figure 22. Elevation diagram showing radar signal interacting with a warp bubble. The outgoing radar pulse (a) is bent by the gravitational lensing field (b), creating early and delayed returns to the dish (c), causing duplication or stretching of radar targets.

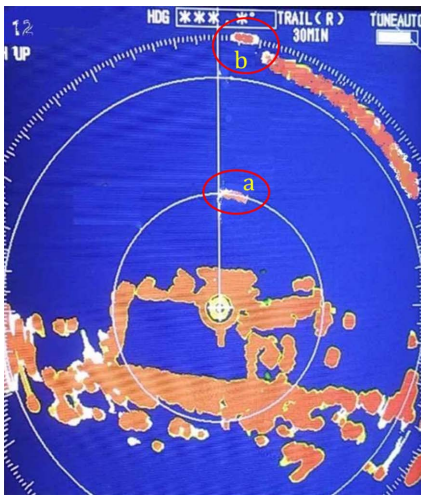

Figure 23. Map view from X-Scan radar PPI showing a boat at the first distance mark (a) and again at the distance extremities (b).

Hypothesis 1 – *Long-Path Storage via Warp Bubble Geometry*

Although delays of 1 - 2 seconds are unusually long for radar systems, such durations become plausible when radar pulses follow closed-loop geodesics within warped spacetime. Models such as Müller & Weiskopf (2011) show that light-like paths can become trapped temporarily inside spacetime distortions.

Figure 24 illustrates how the radar signals may thus orbit within a gravitational cavity and re-emerge after prolonged internal reflection. This hypothesis eliminates the need for a 300,000 km delay path and instead attributes LDEs to spacetime curvature itself.

The Tedesco team recorded 14 such LDE events. In six selected examples, echoed returns stretched across multiple antenna sweeps, forming radar trails indicative of multiple reflection angles within a curved warp boundary.

Hypothesis 2 – *Intentional Radar Jamming*

An alternative hypothesis is intentional jamming: the UAP may capture and retransmit radar signals with precise delays—similar to Range-Gate Pull-Off (RGPO) techniques used in military electronic warfare.

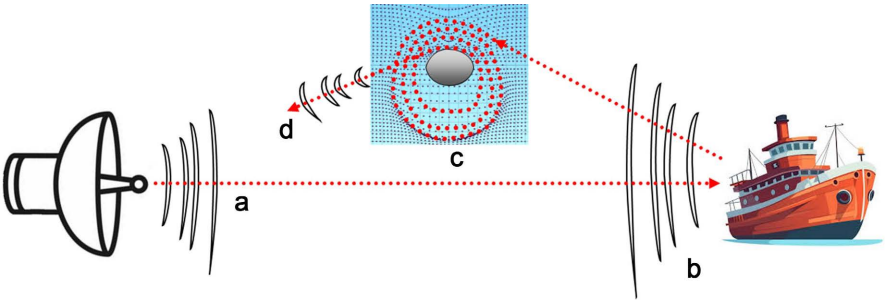

Figure 24. Elevation diagram showing radar ping reflecting off a surface vessel, then circulating through a warp bubble before delayed return.

Figure 25 shows a screen capture of radar returns by a known a marine buoys, equipped with radar transponders, respond to radar pings with immediate sharp echoes. This figure was included to show the Tedesco brothers has undertaken appropriate calibration steps. This predictable behavior forms a baseline for distinguishing jamming from legitimate returns.

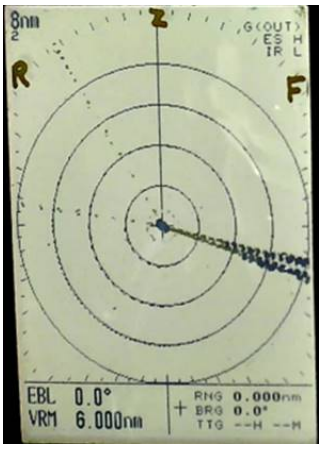

Figure 25. Radar plan-view of radar transponder return of known buoy at sea, recorded for calibration purposes (see Tedesco paper **Figure 4**).

By contrast, Figure 26 shows a collage of several UAP-associated LDEs occurred 1 - 3 seconds after pulse transmission, arriving across multiple antenna revolutions and disappearing as the UAP left the scene.

These delays cannot be explained by passive reflections or radar system lag. The likely options are:

- Signal capture and intentional re-transmission (akin to range gate pull-off (RGPO) jamming), or
- Radar signals looping inside a local spacetime distortion before returning, as predicted by warp field models.

In either case, these echoes differ fundamentally from those of known marine transponders—both in timing and behavior.

Explanations vs. Counter-Explanations

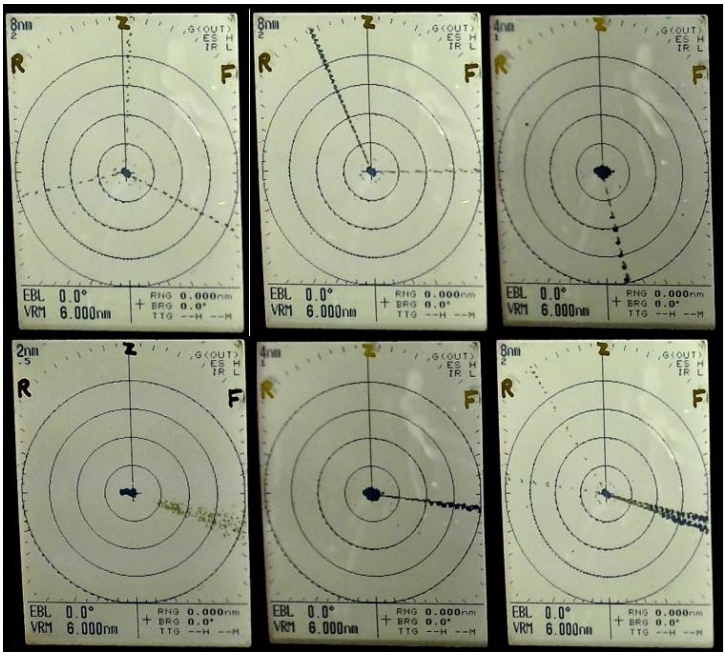

Figure 26. Collage of radar screenshots showing elongation of vessels during UAP presence—each case visually confirmed by night-vision optics.

This explanations vs. counter-explanations section has been separated to include arguments for both events as they pertain to both events.

Calibration Argument:

Some skeptics have argued that radar anomalies such as the "99.9 RNG 99" code observed in the 2004 Tic Tac case might be attributable to calibration issues. This is either a misunderstanding of what calibration does, or it plays upon the intended audience's misunderstanding. Calibration does not determine whether a phenomenon exists—it simply narrows the range of uncertainty in measuring it. By calling upon calibration as a debunking tool, the speaker is attempting to deflect the significance of the event by raising a misunderstood non-issue as if it were a valid objection.

Consider the following analogy. Suppose two telescopes are used to observe a comet's tail. One is precisely calibrated, the other less so. Both record the tail. The calibrated telescope may measure its length as 9980 - 10,020 km, while the uncalibrated one may report 9500 - 10,500 km. The degree of precision differs, but the comet's existence is not in question; it is plainly present in both instruments.

The same reasoning applies to UAP data. A vapor cone or a radar return either appears, or it does not. Calibration affects measurement accuracy, not the existence of the phenomenon. In the Tic Tac case, the "99.9 RNG 99" code has been confirmed in declassified defense documentation to indicate multiple identical, valid ID-coded radar returns. It cannot be explained away as calibration drift, particularly given that the AN/APG-73 radar system performs continuous self-tests, fault detection, and phase alignment checks. No calibration errors were logged during the incident; had they occurred, a different and distinct set of error codes

would have been generated.

Thus, invoking calibration to dismiss the anomaly conflates measurement precision with the existence of the signal itself. The radar data, corroborated by simultaneous FLIR and visual tracking, constitutes evidence of a genuine, physical phenomenon.

Countering Atmospheric Ducting and Sensor Error Claims:

Some have proposed that the long-delay radar echoes observed in the Tedesco experiments may be due to atmospheric ducting or intermittent sensor malfunction. However, these explanations are inconsistent with the time-locked behavior of the anomalies. In each of the fourteen events, the radar distortions appeared only while a UAP was visually present, and ceased immediately upon its departure. This temporal precision contradicts the known behavior of atmospheric ducting, which typically produces persistent or slowly shifting returns independent of visual stimuli, and sensor faults, which do not self-resolve in response to transient external objects. As Gerald Tedesco emphasized:

"*These weren't static ghosts or sea clutter—they only occurred when a UAP was seen hovering just above and in front of the vessel. The moment the UAP left, the distortion vanished.*"

—Gerald Tedesco, SCIRP Open Journal (2024)

This high degree of correlation across multiple instruments and sensor types strongly favors a localized and structured cause—such as radar interaction with a spatial distortion, or intentional radar jamming—over environmental or mechanical noise.

4.5. Leading Edge Vapor Cone Case Studies

Case studies here demonstrate evidence of leading-edge vapor cones consistent with predicted compression zones in warp field models. In many instances, these cases also exhibit one or more additional new observables described in Section 3.

4.5.1. Aguadilla UAP (2013)

Captured on April 25, 2013, by a Customs and Border Protection aircraft near Aguadilla, Puerto Rico remains one of the most scientifically significant UAP cases. Released by the Scientific Coalition for UAP Studies (SCU) [6], it features a thermally hot object exhibiting consistent shape, flight, and environmental effects. Video still frames analyzed by the paper are taken from two sources: the FOIA video [7] and the video originally studied by the SCU [8].

Unlike optical footage, the FLIR camera captured invisible phenomena including transient cold zones and gravitational lensing. The UAP appeared hot, ruling out reflective materials such as Mylar or latex balloons, which are cold or transparent in infrared. Notably, the object split into two over water—eliminating sky lanterns as a plausible explanation.

Leading-edge vapor cones (New Observable #2) appear as cold, shifting clouds above the UAP, consistent with adiabatic decompression from spatial compression—suggesting a warp bubble boundary. These clouds form at subsonic speeds,

defying classical aerodynamics.

Figure 27 shows a collage of still images from the infrared footage (color-coded for clarity and to emphasize the temperatures, red for hot and blue for cold) reveal frame-by-frame cold field formations appearing above-left, above-center, and above-right at various times.

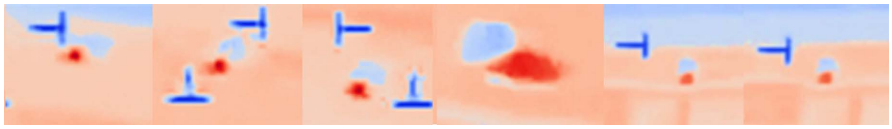

Figure 27. Enhanced collage of thermal video frames showing cold cloud formations above the UAP.

These transient clouds are consistent with adiabatic decompression caused by spatial compression in the warp bubble's upper hemisphere (see Figure 3). Their persistence, dynamic shape, and directional alignment with the UAP suggest leading-edge vapor cones (New Observable #2) forming at subsonic speeds—a behavior inconsistent with any known atmospheric or mechanical craft

Thermodynamic Threshold for Vapor Formation

To evaluate the plausibility of a field-induced condensation cloud, we consider the ambient conditions recorded during the 2013 Aguadilla UAP event: temperatures of ~25˚C - 26˚C, high humidity (estimated above 80%), and subsonic flight speed (~100 mph or 45 m/s). Under these conditions, the dew point would be approximately 23˚C. A drop of just 1.7 K is therefore sufficient to trigger visible condensation in moist air.

In the warp-field model, this temperature drop results from adiabatic decompression caused by spatial compression within the field geometry (see Section 3.2). If a 1 cubic foot parcel of air enters a region of space that externally appears to be 1.0 cubic foot—but internally contains 1.05 - 1.10 cubic feet of proper volume—the air will passively expand without external work. Applying the adiabatic expansion equation:

$$T^2 = T^1 \cdot \left(\frac{p^2}{p^1} \right)^{\left(\frac{\gamma - 1}{\gamma}\right)} \tag{5}$$

with $\gamma = 1.4$ for air, a pressure drop of just 2% - 3% (equivalent to a 5% - 10% spatial expansion) yields a final temperature:

$$T^2 \approx 298 \cdot (0.975)^{0.286} \approx 296.3 \text{ K} \tag{6}$$

This result confirms that a ~1.7 K cooling is physically plausible, even in the absence of motion or aerodynamic shock. The resulting condensation cloud aligns with the leading-edge structure observed in infrared footage—supporting the interpretation that spatial expansion within the warp field boundary is sufficient to induce vapor cone formation at subsonic speeds.

Leading Edge Vapor Correlation

Most still frames that show leading-edge vapor cones reveal the cloud drifting slightly behind the point of initial formation. This behavior is expected: even conventional aircraft produce vapor trails that persist momentarily as the condensed cloud is swept away by airflow. The Aguadilla UAP video demonstrates the same transient sweeping of vapor clouds. However, certain still frames indicate that the vapor cloud is not being displaced by wind and can be directly compared to the spatial compression scatter plot in Figure 3.

The two frames illustrate distinct warp-field configurations. In Figure 28, the vapor cloud appears angled at ~45˚, suggesting that the UAP is both counteracting Earth's gravity and generating additional forward acceleration by strengthening and tilting the field forward. In Figure 29, the vapor cloud is broader and located directly above the UAP, consistent with a configuration that counteracts gravity while maintaining existing forward momentum.

Figure 28. Aguadilla UAP still frame from the FOIA release at 1:16:14, showing a leading-edge vapor cone angled at ~45˚ compared with a modified Figure 3 spatial compression scatter plot. An ellipse was drawn by visual best-fit to highlight correspondence between the UAP shape and predicted field contours.

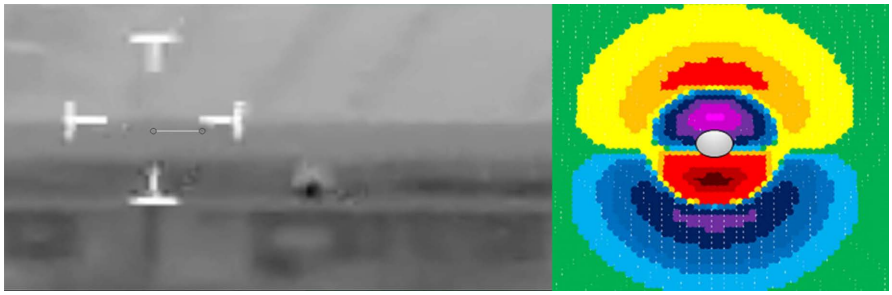

Figure 29. Aguadilla UAP still frame from the FOIA release at 1:25:13, showing a leading-edge vapor cone centered directly above the UAP compared with a modified Figure 3 spatial compression scatter plot. An ellipse was drawn by visual best-fit to highlight correspondence between the UAP shape and predicted field contours.

Both figures show strong alignment with the Figure 3 spatial compression model: Figure 29 exhibits a 1:1 correlation, while Figure 28 shows a close match that could be refined toward 1:1 with additional analysis of the warp-field configuration.

Gravitational Lensing and IR Distortion

Gravitational lensing (New Observable #1) is evident as the UAP passes in front of infrastructure, visibly distorting rooftops and airport tarmac lines. This supports real-time spacetime curvature, visually analogous to gravitational lensing simulations of black holes.

Figure 30 is a collage of still frames showing how as the UAP passes in front of building's roof line, the roof line momentarily bends downwards under the UAP.

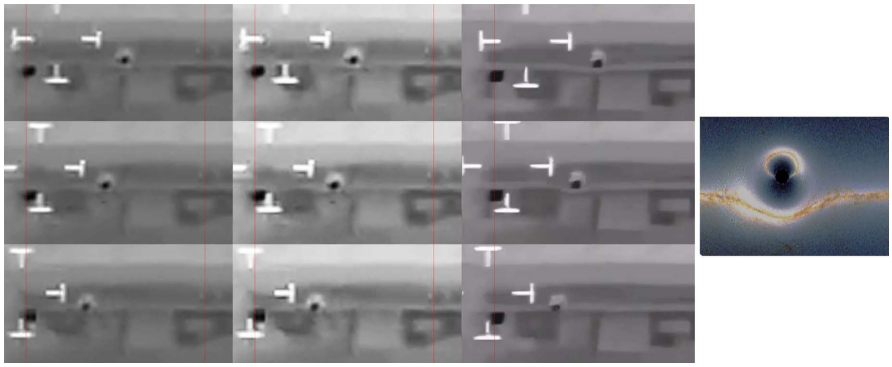

Figure 30. Video still collage showing background deformation due to gravitational lensing. FOIA-released stills (left), SCU released video (middle), and denoised computer-enhanced versions (right). Far Right shows a simulation black hole gravitational lensing simulation [9].

Figure 31 is a collage of still frames showing the tarmac lines bending and reappearing behind the UAP. These effects—independently noted by SCU, physicist Kevin Knuth [10], and others [11], and formally analyzed by this author in a two-part MUFON Journal article [12]—cannot be dismissed as video artifacts (see also Wanless [13] for video detailing visual breakdown).

Figure 31. Video still frames showing tarmac line deformation. First row; FOIA released video, second row; SCU released video.

The object also demonstrates positive lift without control surfaces (Original Observable #5). Its consistent thermal signature, lack of exhaust, and close-

ground flight reinforce the interpretation of asymmetric gravitational field control.

In total, this case demonstrates:

- Gravitational lensing (New #1)
- Leading-edge vapor cones (New #2)

Explanation, Counter-Explanation

A common counter-explanation suggests that the cold "halo" seen around the Aguadilla UAP is a known IR artifact caused by zoom level. Figure 32 still frames a, b and c, show an example cold halo visible around a commercial aircraft footage when zoomed out, which disappears when zoomed in. Indeed, in the Aguadilla video, a similar effect occurs at magnification 165 (early frames d and e), halos appear around the UAP and all other hot objects. When the camera zoomed in (to magnification 635), these halos vanished. Instead frame f shows no halo and frame g instead shows a trailing vapor cone in which the cloud is dragged to the right by the wind velocity.

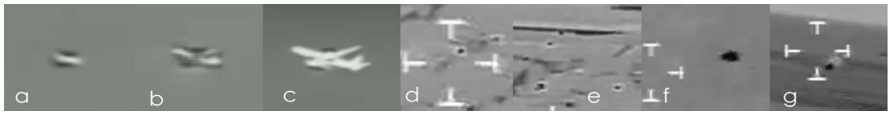

Figure 32. IR stills showing commercial aircraft with halo fading under magnification (a)-(c); Aguadilla UAP and nearby hot objects with halos at low zoom (d)-(e); and the UAP at high zoom without halo (f), but showing trailing asymmetric vapor cloud (g).

Notably, unlike standard halo artifacts, when the camera is zoomed in, the Aguadilla UAP displays localized, directional cold regions—not full symmetric halos. As seen above in image (g) of the tailing vapor cone. When viewed against a dark background, the vapor-like cold zones consistently form above, to the left, or right of the object, not evenly around it. This asymmetry, especially its persistence through motion and zoom changes, supports the interpretation of a field-induced condensation cloud, not a lensing artifact.

Review of AARO Balloon Hypothesis

AARO's 2024 conclusion—that the object was "likely a pair of balloons or sky lanterns"—ignores these diagnostic features. Figure 33 is a collage of comparative infrared footage which shows that:

- Latex balloons are nearly invisible in IR at close range.
- Mylar balloons reflect ambient cold sky and are mirrorlike.
- Sky lanterns have soft heat signatures but lack cold vapor fields.

None exhibit the hot, lensing, or atmospheric interaction features seen in the Aguadilla case.

AARO's 2024 assessment—that the object was likely a pair of balloons or sky lanterns—does not account for the thermal, lensing, and vapor cone features documented in the infrared footage. Notably, their report does not reference comparative IR profiles of known balloon types, which are available in both academic and public domain sources. This omission may reflect a tendency toward hypothesis-

driven interpretation rather than data-driven evaluation. A more thorough comparative analysis, grounded in physics, would be required to substantiate the balloon hypothesis.

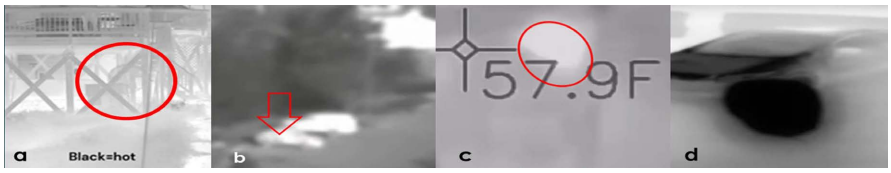

Figure 33. contrasts the Aguadilla UAP with known IR footage of a latex [14] balloon up close (a), a latex balloon at distance [15] (b), a mylar [16] balloon (c) and a sky lantern [17] (d). The absence of vapor cone and lensing effects in those control samples underscores the uniqueness of the Aguadilla footage.

4.5.2. Ridoy Video (2023)

In early 2023, TikTok user md_ridoy_ahmed145 posted a video [18] (note TikTok user account has since been removed by user) showing a disc-shaped UAP approaching a commercial airliner mid-flight. Upon enhancement, the footage reveals a rare combination of four of the five new visual observables: gravitational lensing (types 1a and 1b), a leading-edge vapor cone (type 2), tilted flight (type 3) and saucer-like skipping motion (type 5). This case is examined in detail with stabilized and contrast-enhanced stills in a companion video analysis by Wanless [19], which highlights the sequence of shape deformations and warp-consistent observables.

Gravitational Lensing

Localized distortions of background terrain—visible as pixel blurring and vertical shifts—indicate background gravitational lensing (New Observable #1a), while initial momentary deformations of the disc and slow observed relocation of the dome over time reveal gravitational lensing of the UAP itself (New Observable #1b), and slow oscillation (New Observable #4). After turning toward the camera, the disc appears in tilted flight (New Observable #3), consistent with gravity-counterbalanced asymmetric orientation. The disc also follows an erratic, zigzagging trajectory inconsistent with aerodynamic flight, exemplifying saucer-like skipping motion (New Observable #5). As the disc sharply accelerates away, a clear elliptical vapor cone forms at the leading edge, aligning with the magenta compression zone predicted by warp field models (New Observable #2).

Figure 34 shows a collage of still frames showing how the disc is deformed over time.

Figure 34. Collage of sequential still frames from the Ridoy video showing progressive shape deformation of the disc-shaped UAP, including dome displacement (lower left dome appears off-center to the right). These changes support New Observable #1b: gravitational lensing of the UAP structure, and New Observable #3: tilted flight configuration.

Figure 35 shows a collage of still frames showing how the background is deformed on a frame by frame basis.

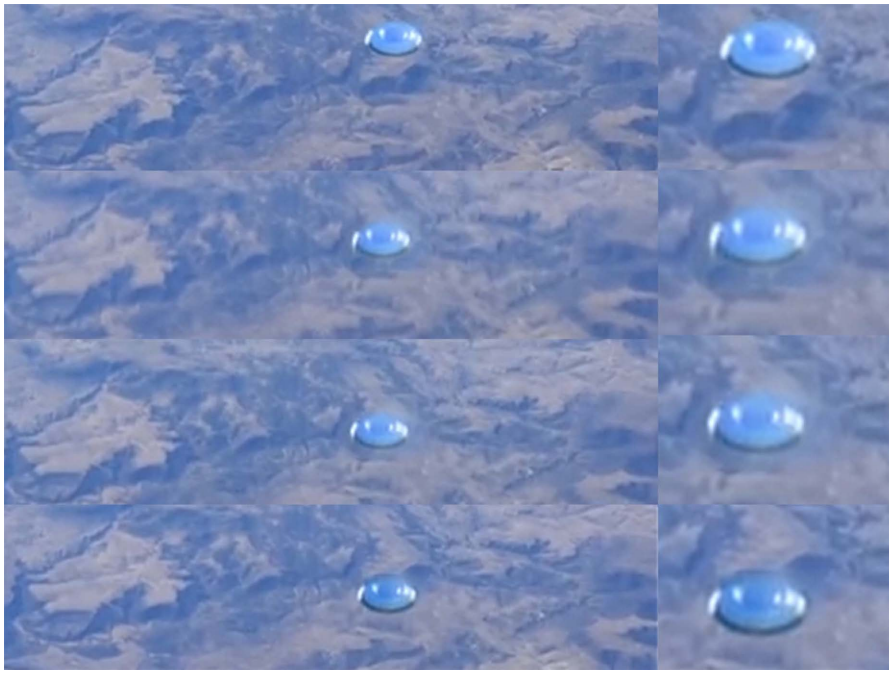

Figure 35. Collage of Ridoy video stills showing background warping, vapor cone formation, and directional shifts consistent with warp-field observables. The final still frame shows the disc rapidly departing, with a clearly visible leading-edge vapor cloud in front of the UAP in the center-right and lower-right still frames.

Forensic Reconstruction of Dome Displacement

To determine whether the dome displacement seen in the Ridoy video could be explained by a simple CGI hoax or by ordinary camera perspective, we generated a pair of control models in Autodesk 3ds Max. The purpose was twofold: first, to compare a symmetrical baseline model against the video stills in order to test whether a straightforward CGI render could replicate the observed geometry; and second, to measure the degree of dome displacement and evaluate whether the deformation reflected lateral (side-to-side) offset, fore–aft compression, or a combination of both.

The control renders were produced in pairs. The left model retained a perfectly symmetrical disc with a dome centered in plan view. The right model was progressively modified—widening the disc laterally, altering fore–aft proportions, relocating the dome, and in one case resizing it—until alignment with the still frames was achieved. Plan-view screen captures were also created to document how the dome had to be shifted and rescaled relative to the disc outline to reproduce the appearance in the video.

Analysis of three frames, corresponding to time stamps 4:11 s, 7:00 s, and 11:14 s, yielded the following pattern:

- Frame 4:11 s — The dome appears displaced halfway to the right of center,

with a slight rearward offset relative to the disc.

- Frame 7:00 s — The dome is displaced fully to the right margin and required both lateral shift and strong rearward compression to align with the still frame. In addition, the dome itself had to be compressed fore–aft to reproduce the observed proportions, indicating that lensing effects were altering not only the dome's position but also its apparent shape.
- Frame 11:14 s — The dome has returned to the disc centerline, but remains slightly rearward and, critically, had to be reduced in overall size relative to the earlier frames in order to match the observed proportions.

This sequence demonstrates that the gravitational lensing effect influenced not only the dome's location (side-to-side and fore–aft displacement) but also its apparent geometry (shape compression and size variation). At 7:00, the dome required both rearward displacement and fore–aft compression to align, while at 11:14 it had to be reduced in overall size relative to the disc. These findings indicate that the effect was not limited to simple positional shifts or disc aspect ratio changes. Instead, the oscillation produced dynamic variations in width-to-length proportions and in feature size ratios visible to the camera—clear evidence that lensing was altering the dome's position, shape, and relative scale across frames.

In all three cases, the symmetrical control model was insufficient to replicate the observed geometry. Only by warping the disc proportions, shifting the dome laterally and rearward, compressing it fore–aft, and in the final frame reducing its overall size could alignment be achieved. This demonstrates that the Ridoy footage did not capture a simple rigid disc under perspective distortion, but rather a craft whose features were subject to progressive, field-induced displacement, shape compression, and scale variation. The temporal sequence—dome drifting rightward, reaching maximum displacement with fore–aft compression, and returning to center at reduced apparent size—corresponds to the slow oscillation mode of warp-field rebalancing described in Section 3.4. Taken together, these distortions provide strong evidence that gravitational lensing dynamically altered not only the dome's position but also its geometry and relative scale, in a manner consistent with active warp-field modulation.

To support the reconstruction shown in **Figure 36** (below), we performed a post-capture camera calibration by modeling the jet engine intake visible in the video (model not shown). By aligning the intake model to the recorded scene, the effective focal length of the camera was determined to be approximately 28 mm. This calibration ensured that the control renders were generated under the same optical conditions as the original footage.

The above collage compares control models, modified models, and original video stills at three key frames: (a, b) 4:11 s, (c, d) 7:00 s, and (e, f) 11:14 s. Panels (a, c, e) each show three images: top left is a symmetrical control disc with a centered dome, top right is a modified disc with adjusted proportions and dome offset, and bottom right is the corresponding video still frame. Panels (b, d, f) show plan-view screen captures of the 3D models. In each case, the symmetrical

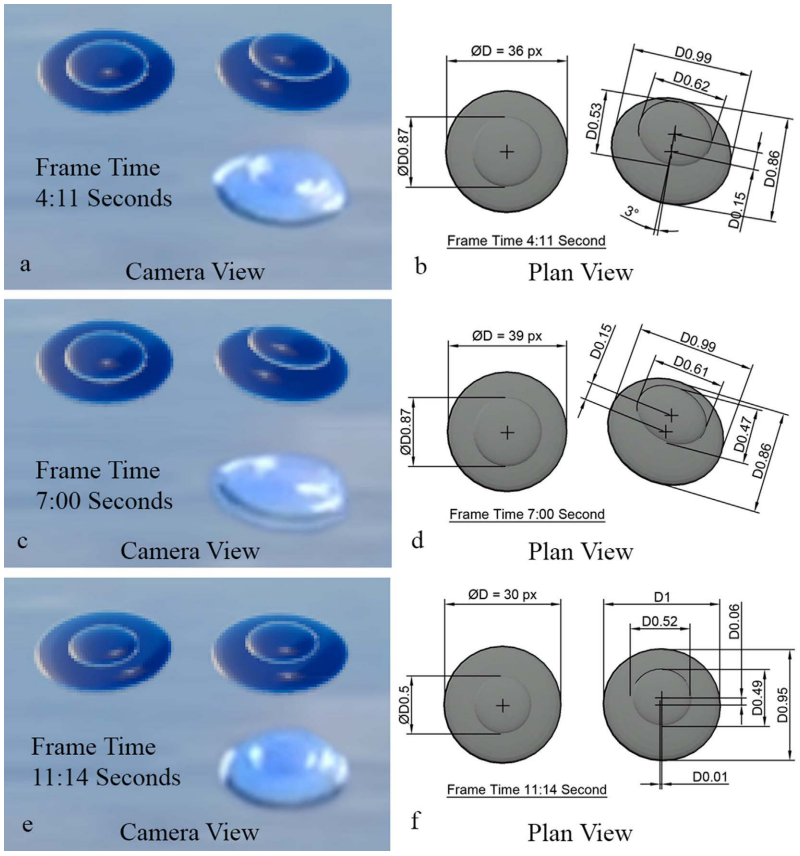

Figure 36. Forensic 3D CAD reconstruction of dome displacement of the Ridoy video, camera reconstruction views and plan views with dimensions.

control disc fails to reproduce the geometry seen in the video. Accurate alignment required shortening the disc, specifically stretching the far end of the dome towards the camera, and widening the dome. These two adjustments make the dome appear to shift towards the back. In the 11:14 frame—the disc was tilted towards the camera and width stretching the dome was not required, thus reducing the dome size relative to the disc. These reconstructions confirm that the Ridoy video captures progressive field-induced displacement and scale variation of the dome consistent with a slow oscillation mode of warp-field rebalancing.

Optical Consequences of Dynamic Field Flight Maneuver Adjustments

The dome's apparent migration in the Ridoy video is not a result of rigid-body displacement, but rather the optical consequence of anisotropic gravitational lensing within the upper compression zone of the warp field. As the craft executes tilted flight maneuvers, variations in lensing strength across the upper bubble geometry alter how light paths from the disc reach the observer. This produces apparent shifts in dome position and aspect ratio, even though the underlying disc geometry remains fixed. A detailed ray trace model recreation was undertaken and detailed in **Figure 37**.

Three elevation views were created using AutoCAD and 3ds Max to reconstruct frames of the Ridoy sequence.

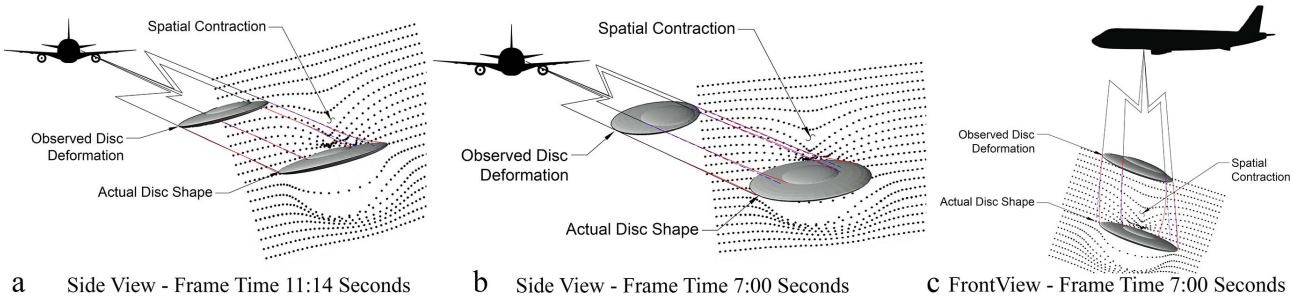

Figure 37. Forensic 3D CAD reconstruction of dome displacement of the Ridoy video, elevation views.

- *Image a*: Side view parallel to the airliner's flight path at frame time 11:14.
- *Image b*: Side view parallel to the airliner's flight path at frame time 7:00.
- *Image c*: Frontal view perpendicular the camera angle at frame time 7:00.

In Images A and B, the true geometry of the disc is shown in the lower right position, while the apparent observed geometry (as recorded by the camera) is shown above left. Light paths, traced through the scatter-plot warp field, are drawn in red. In both cases, light originating from the far side of the disc passes through the strongest compression zone of the warp bubble immediately above the craft. This curvature shortens the far edge optically, making the dome appear displaced to one side.

In Image C, the frontal reconstruction demonstrates how asymmetric spatial contraction alters the dome's width. The right-hand side of the compression zone is stronger, curving light paths outward toward the disc's perimeter. This elongates the dome on the right-hand side and produces the appearance of lateral stretching, consistent with the Ridoy stills.

Taken together, these reconstructions demonstrate that dome migration and aspect-ratio changes are the predictable optical signatures of anisotropic gravitational lensing in a tilted warp field, not physical movement of structural components.

Saucer-Like Skipping Motion

The disc's skipping trajectory is not obvious when viewing the original, unstable footage. Camera shake obscures the motion, making it appear as though the object is simply traveling directly toward the aircraft until its rapid departure. However, after stabilization using Adobe software, and by overlaying cropped clips of the UAP onto a single clear still frame, the true travel path emerges. The disc first moves horizontally to the left, then changes course toward the aircraft and enters an alternating sequence of descending and ascending steps, with minor left–right shifts. This discontinuous, "hopping" trajectory—illustrated in **Figure 38**—matches New Observable #5: saucer-like skipping motion.

Leading Edge Vapor Cones

The Ridoy video offers one of the most unambiguous visual confirmations of leading-edge vapor cone formation consistent with warp-field compression. As the disc abruptly departs at high speed, a distinctly elliptical vapor cone forms ahead of the craft, captured clearly in the penultimate two still frames shown

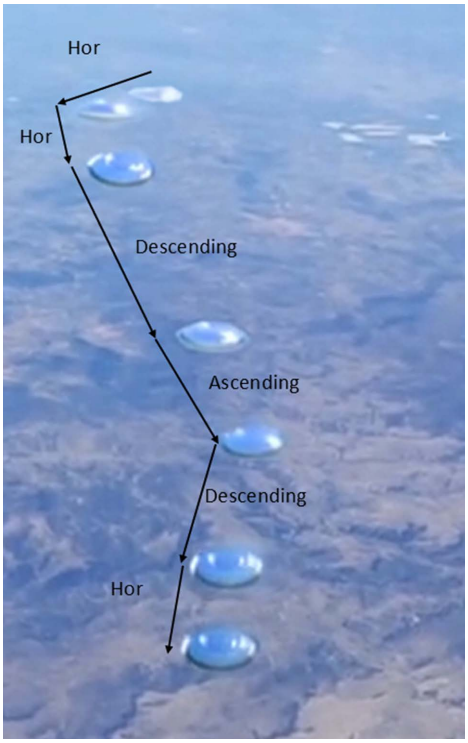

Figure 38. Still frame compilation from the Ridoy video, isolated still frames indicate location and angle of disc at each change in vertical and/or horizontal direction changes support New Observable #5: saucer-like skipping motion.

Figure 39. Unlike traditional vapor cones produced by high-speed aircraft—where shockwaves compress air into a visible cloud behind or around the vehicle—this cone appears precisely at the disc's leading edge, aligns tightly with the disc's contour, and forms during subsonic acceleration.

This feature aligns directly with the magenta-band spatial compression region seen in the elastic Alcubierre deformation model presented in **Figure 3**. That model predicts a region of spatial contraction ahead and above the craft where incoming air is forced into a compressed geometry, triggering adiabatic decompression and visible condensation as the ambient atmosphere transitions into a region of expanded internal volume. In essence, the vapor cone marks the outer boundary of the warp bubble's upper curvature—providing a direct visual indicator of spatial distortion.

The importance of this frame lies in its mathematical correspondence to theoretical predictions. As shown in **Figure 39(d)** and **Figure 39(e)**, a recreation of the disc is overlaid onto the compression scatter plot from **Figure 3**, demonstrating near-exact alignment with the magenta compression region. The cone's curvature, thickness, and location correspond with the warp field's leading spatial gradient—strongly supporting the assertion that this vapor cloud is not atmospheric or photographic coincidence, but a real, physics-driven field boundary effect.

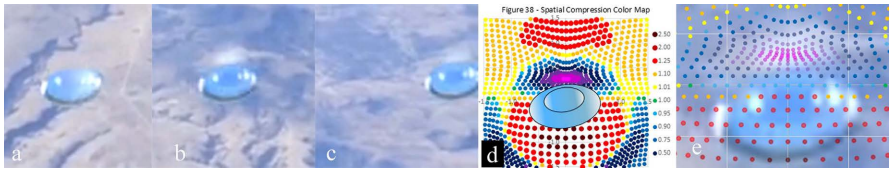

Figure 39. Collage of Ridoy video stills showing a clear leading-edge vapor cone during UAP departure (a)-(c). A recreation of the disc (d) and direct overlay of the vapor frame (e) both align with the magenta compression zone from **Figure 3**—supporting a visual and geometric match to predicted spatial warp boundaries.

Such visual confirmation carries significant implications:

- It supports the spatial compression theory of vapor formation detailed in Section 3.2.1.
- It offers a repeatable visual cue for identifying warp field interactions in future video evidence.
- It reinforces the hypothesis that field-induced condensation effects can occur at subsonic speeds—contradicting conventional aerodynamic expectations.

Crucially, this vapor cone is not simply present—it is framed, shaped, and located exactly as predicted by Alcubierre-type field models. The sharpness of the boundary and its confinement to the front half of the disc, with no trailing wake or asymmetry, further argue against lens artifacts or CGI. Instead, it represents an optical echo of the underlying geometry—the invisible warp field made visible through its effect on ambient matter.

Explanation, Counter-Explanation

Three hoax hypotheses are discussed below. A common default objection is that the video quality is "*too good, therefore it must be fake*." However, this position becomes less tenable when all five new observables are identified—several of which were unknown at the time the video was released. For a hoaxer to reproduce these features convincingly, they would have needed not only advanced technical skill but also foreknowledge of warp-field signatures that would only later be formalized into the mathematical theories presented in this paper.

Hoax Hypothesis 1. *Accidental or Simplistic Hoax Rendering*

One explanation is that the Ridoy video is a hoax generated by digital rendering tools, lens-flare algorithms, or video-game artifacts. This fails for several reasons:

- *Vapor Cone Formation*: The vapor structures in the video align one-to-one with the magenta compression zone predicted in **Figure 3** of this paper. No known lens-flare algorithm or rendering error produces such placement or geometry. To replicate this alignment by accident would be statistically extraordinary.
- *Gravitational Lensing – Two Forms*: The video displays both background deformation (scenery bending behind the disc) and UAP structural deformation (the dome appearing to migrate across the disc as its orientation to the camera changes). **Figure 37** illustrates how light paths bend through the upper compression zone of the warp bubble, producing this apparent dome displacement.

Such localized lensing is consistent with anisotropic spacetime curvature but cannot be explained by rigid-body movement or rendering errors, which distort entire frames indiscriminately.

- *Handheld Camera Shake*: If the UAP were composited into real handheld footage, the hoaxer would have needed frame-accurate motion tracking across dozens of frames to maintain background alignment—an intensive process even for a skilled CGI artist. The Ridoy video shows natural handheld signatures such as rolling shutter skew, irregular jitter, and asymmetric blur tails. These features are rarely reproduced convincingly in synthetic renders.
- *Progressive Dome Drift*: The dome drifts off-center during a saucer-like skip and gradually realigns across frames. Rendering artifacts or compression errors typically appear as abrupt discontinuities or random jitter, not as coherent structural migration. To fabricate this would require deliberate keyframing of structural deformation synchronized precisely with the maneuver, well beyond the incidental capabilities of game engines or casual CGI.

Taken together, these factors rule out the "simple hoax" hypothesis.

Hoax Hypothesis 2. *Expert Warp Theorist and Master* 3*D Modeler Hoax*

A second explanation is that the Ridoy video was fabricated by someone with advanced knowledge of warp-field physics and expert rendering skill. However, this would require foresight that stretches credulity.

- *Einstein Parallel*: The dome's migration is precisely consistent with gravitational lensing geometry, analogous to the displacement of starlight in Eddington's 1919 eclipse photograph that proved general relativity. The odds of a hoaxer reproducing this effect without knowledge of warp-field asymmetry are negligible.
- *Vapor Cone Timing and Foreknowledge*: The leading-edge vapor cone emerges exactly in the predicted compression zone at the moment of departure. The Ridoy video was released two years before this paper's warp-field elastic models were published, meaning a hoaxer would have needed advanced foreknowledge of unpublished theoretical predictions.
- *Statistical Context*: As shown in Section 6.10, the recurrence of these five observables across independent cases yields a statistical confidence of 24.7 sigma—vastly beyond the 5-sigma standard for discovery in physics. Attributing this level of consistency to fabrication requires assuming not only advanced technical ability but also an implausible level of theoretical insight.

This explanation therefore implies a hoaxer who independently discovered warp theory, modeled it correctly, and then chose to release their work as an anonymous "sighting video" rather than as a scientific breakthrough. That scenario is implausible.

Hoax Hypothesis 3. *Real Manufactured Disc Employing a Dark Warp Propulsion System*

The third and most parsimonious explanation is that the Ridoy video captures a real, disc-shaped craft using a dark warp propulsion system.

- *All Five Observables Present*: Gravitational lensing, vapor cones, warp-field oscillation, tilted flight, and skipping motion are all visible within the video.
- *Theoretical Alignment*: The vapor cone corresponds directly to the modeled compression zone (**Figure 3**), and the dome displacement is exactly the effect predicted by light bending through the warp bubble (**Figure 37**).
- *Cross-Case Consistency*: Identical signatures appear in independent historical and modern cases (e.g., Heflin, Aguadilla, Perth), which were captured long before warp-drive interpretations were published.
- *Statistical Weight*: As noted in Section 6.10, the recurrence of these observables across cases exceeds 24 sigma, eliminating chance alignment as a plausible explanation.

By the principle of parsimony, the simplest explanation is that the Ridoy video depicts a real, manufactured disc operating with a warp propulsion system—one whose effects were unknowable to potential hoaxers at the time of recording.

Summary

The Ridoy video's vapor cone and dual-mode gravitational lensing together form a direct, testable match to warp-field predictions. Just as Eddington's 1919 eclipse photograph confirmed Einstein's theory through lensing of starlight, the Ridoy frames confirm warp-field lensing through displaced domes and bent backgrounds. Hoax explanations would require not only technical mastery but also theoretical foresight beyond what was publicly available—making them less plausible than the straightforward conclusion: the video records a real disc employing a dark warp propulsion system. Among these arguments, the vapor cone's one-to-one correlation with the predicted compression zone (**Figure 3**) remains the strongest and final proof, as no hoaxer could have anticipated or reproduced this alignment ahead of the theoretical model's publication. Taken together, the evidence presented in this case meets—and in several respects exceeds—the gold standard of scientific validation, combining predictive alignment, reproducibility across cases, and statistical significance far above accepted discovery thresholds.

4.5.3. Perth, Australia UAP (2023)

On May 15, 2023, a green-glowing UAP was filmed over Perth, Western Australia [20] (note Reddit video has since been removed by user). The object emitted intermittent strobing and briefly passed through a localized vapor cloud, which split as the craft moved through it—suggesting leading-edge vapor formation (New Observable #2).

Figure 40 shows a frame-by-frame analysis also reveals shape deformation, with the UAP appearing elliptical when turning, consistent with gravitational lensing of the UAP (New Observable #1b) or possibly tumbling motion. The flight path shows abrupt lateral shifts, indicating saucer-like skipping motion (New Observable #5) and lift without control surfaces (Original Observable #5).

Alternative explanations such as a helicopter spotlight disturbing a low cloud deck are unlikely due to:

- The narrow, well-defined vapor cone does not match the wide-area disturb-

ance expected from rotor wash.

- The UAP's angular, zigzag motion is incompatible with known helicopter dynamics.

Figure 40. Collage of stills from the Perth UAP video showing vapor cloud interaction and changing geometry.

Taken together, the vapor cone, shape distortion, and erratic trajectory suggest interaction with a structured field boundary—supporting the warp-field hypothesis.

4.5.4. Skywatcher.ai Vapor Cone Observation (2024)

Historical Analogy

In the mid-1990s, two independent research teams—the Supernova Cosmology Project and the High-Z Supernova Search—each discovered that distant supernovae appeared dimmer than expected. Working separately, both groups concluded that the universe's expansion was accelerating, driven by a previously unknown form of energy. This convergence of theory and observation from two independent sources was decisive: it transformed a startling anomaly into an accepted discovery, now known as dark energy.

Independent Convergence in UAP Research

A similar pattern is found here. The elastic warp-field model developed in this paper predicts that under certain conditions UAP should generate leading-edge vapor cones through spatial compression. Independently, prior to the completion of this study, the civilian research group Skywatcher.ai released three still frames from video recordings showing just such vapor cloud formations above small UAP. Their release pre-dates the publication of both this paper and the related book, and was accompanied by commentary from group members who described understanding why the clouds were forming.

This convergence—one line of evidence from theoretical modeling, and another from independent civilian field observation—provides a rare case of *preemptive third-party replication*. Just as the acceptance of dark energy arose from two groups arriving at the same result independently, the Skywatcher.ai data strengthen the case that the vapor cone observable is a genuine, physical phenomenon rather than a subjective interpretation.

In that same spirit, the present case study represents one of two independent but converging lines of evidence for vapor cone formation. The first came from Skywatcher.ai, whose publicly released still frames captured candidate vapor cone events without foreknowledge of the theory. The second is this paper, which introduces the elastic warp-field framework as the theoretical explanation and supplements it with additional observational evidence. Just as the discovery of dark energy arose from two independent teams converging on the same conclusion,

the alignment between Skywatcher.ai's field observations and the theoretical predictions developed here provides a strong case of independent convergence on the same physical phenomenon.

Skywatcher.ai Release

In early 2025, the Skywatcher.ai team released a significant observation of a UAP exhibiting a prominent vapor cone formation. Captured during a skywatch event and discussed in a live Jesse Michels interview with researcher James Fowler, the footage displays a unique combination of visual and aerodynamic features consistent with New Observable #2: Leading-edge vapor cones and potentially New Observable #1: Gravitational lensing.

"*It looks like a tetrahedron that's wearing a hat... the hat looks like it's made out of atmosphere*."—James Fowler

The team described the craft as appearing tetrahedral, though its precise geometry could not be conclusively determined due to partial visual obscuration. Most notably, a misty, atmospheric formation enveloped the top of the UAP—behaving not like a solid structure, but like a dynamic vapor sheath held in place by an unseen field.

This vapor layer:

- Remained stationary with respect to the craft.
- Flashed or shimmered intermittently.
- Reflected sunlight in a manner consistent with adiabatic decompression vapor, similar to what occurs around high-speed jets breaking the sound barrier.

However, unlike conventional vapor cones caused by shockwaves, this vapor halo formed at subsonic speeds and matched the magenta-band compression zones predicted by spatial compression scatter plots (see **Figure 3**). Fowler noted that the apparent containment of the vapor layer suggests it was being held in place by a localized field boundary, reinforcing the theory of a spacetime-warping propulsion system.

This case serves as one of the most recent confirmations of warp field atmospheric interaction and is especially valuable due to:

- The clarity of the visual evidence.
- The scientific framing provided by the observers during the live discussion.
- Its consistency with theoretical expectations of spatial compression vapor release near the warp boundary.

Notably, the Skywatcher.ai footage, **Figure 41**, was recorded before the publication of Hidden in Plain Sight and prior to public release of the warp-based vapor cone theory. This timing rules out the possibility that the vapor cone effect was knowingly fabricated to align with theoretical predictions—making it a strong third-party verification of a novel warp field observable, independently documented by outside researchers.

Explanation/Counter-Explanation

A recurring challenge in UAP research is the question of replication. If additional vapor cone videos emerge after the publication of this paper, skeptics may

Figure 41. Three stills extracted from the Skywatcher.ai video part 2.

argue that such data were fabricated with foreknowledge of the predicted signature. Yet the converse is already true: Skywatcher.ai released three still frames depicting candidate vapor cone events before this paper was written, and before the theoretical model was public. Their independent timing eliminates the possibility of retroactive imitation.

In this sense, the Skywatcher.ai evidence functions as a form of pre-emptive field replication. Conventional laboratory sciences achieve replication through controlled re-creation of experiments, but in many fields—such as astronomy or animal behavior—replication occurs only when independent observers document the same natural phenomenon. UAP research belongs to this category. By releasing stills that captured the predicted vapor cone effect prior to the appearance of this framework, Skywatcher.ai inadvertently fulfilled the replication standard in advance.

Thus, while the usual sequence of *theory → replication* is reversed, the scientific principle remains intact: independent observers, unaware of the theoretical prediction, documented precisely the phenomenon that the model forecasts. This closes the Catch-22 often used to dismiss UAP evidence, demonstrating that replication has already taken place in the field, under conditions that cannot reasonably be attributed to foreknowledge or hoax.

4.6. Warp Field Oscillation Case Studies

These examples document apparent oscillation of a UAP's surrounding field—potentially for flight control or stability purposes—captured through motion blur patterns, cyclical distortions, or other repeatable signatures. These cases also show additional new observables such as gravitational lensing.

4.6.1. Rex Heflin Photographs (1965)

The Rex Heflin photographs, taken in Santa Ana, California in 1965, remain one of the most iconic UAP photographic sequences on record. Using a Polaroid Model 101 camera, Heflin captured four sequential images of a disc-shaped object. The images are notable not only for their clarity and framing, but also for their alignment with multiple visual observables outlined in this paper. This event demonstrates the presence of four of the new visual observables, as well as Observables #1 and #5 from the original set.

Figure 42 shows a collage of cropped photos #1, #2, and #4 a disc in various angles of tilted flight with measurable edge distortions and light scattering con-

sistent with gravitational lensing (new Observable #1).

Figure 42. Collage of magnified croppings from Heflin photos 1, 2, and 4, showing disc tilt, lensing effects, and a departing vapor ring.

The disc's apparent stability while tilted, along with its lack of visible propulsion or aerodynamic control surfaces, supports the interpretation of tilted disc flight achieved through asymmetric gravitational field control (new Observable #3, original Observable #5). In photo 4, a "smoke ring" is visible—interpreted as a vapor cone (new Observable #2) that was split into a ring as the UAP rapidly accelerated (original Observable #1) through the cone's center. The UAP may still be visible off in the distance in photo 4, circled in red.

Figure 43 illustrates measured deformations in photo #1 which reveals clear structural thickness changes from left to right. Most notably, photo #3 shows the UAP juxtaposed in two positions, as if the UAP was captured in two places at once.

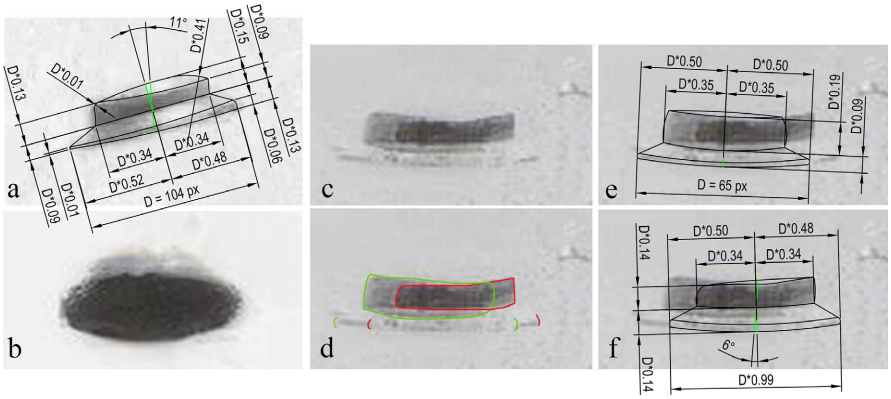

Figure 43. Collage of the Heflin photos measured (a), (e), & (f), showing unaltered photo #3 (c) and double exposure highlighted (d) with distinct red and green outlines. Enlarged photo #2 (b) is included to show and highlight how all three photos show the disc in multiple and different momentary deformations.

Figure 43(a) shows that the lower disc thickness increases, the upper dome thickness decreases, the observable roof line increases. The lower left disc is longer than the lower right and the dome measures as leaning towards the tailing edge (left) by 11 degrees, is consistent with direction of lean measured in several other pre-1970's photos measured in Section 4.2.1. The most revealing image appears in photo #3. **Figure 43(c)** shows the unaltered cropped double exposure image. **Figure 43(d)** show a digital overlay indicating two outlines: a green contour representing the disc with the warp field inactive, and a red outline showing the same

disc during field oscillation. Measurements show the precise alignment of both outlines. Measurements in Figure 43(e) shows the disc without any deformation. Measurements of the second exposure in Figure 43(f) shows the disc suddenly skewed and tilted to the left with a dome tilt of 6 degrees towards the trailing edge with measurement ratios nearly identical to the measurements in Figure 43(a). This indicates that whatever distorts the observable view of the disc is identical between the two photographs.

It should be noted that Figure 43(a) and Figure 43(f) bear a striking resemblance to the ray-trace deformations illustrated in Figure 10. In these photographs, the lower disc curvature appears as a continuous but variable arc rather than a stepped profile. This difference can be explained by the disc being slightly tilted toward the camera, as indicated by the partially visible roofline— itself skewed in Figure 43(a).

Photo #2, see Figure 43(b), shows significant blurring around the perimeter edges of the UAP as it appears tilted away from both the witness and the camera. Figure 44 illustrates a ray-trace study which suggests that if this exposure also captured a moment of fast oscillation, it could explain the unusually diffuse perimeter. In the plan-view diagram, solid lines represent the direct light paths from the disc when the warp field is inactive, while dashed lines represent light paths that are initially directed outward but curve inward when the warp field is active (similar to the plan views in Figure 9 and Figure 10). This bending would cause the disc to appear slightly stretched horizontally. If oscillation occurred during the time the shutter was open, the disc would not be recorded in two distinct positions (as in Photo #3), but rather in two overlapping widths. The result would be the extended blur encircling the UAP's outline seen in Photo #2.

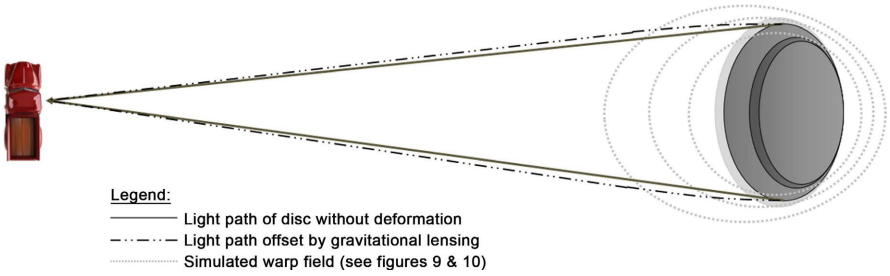

Figure 44. Plan view ray trace diagram of photo #2 revealing possible reasons for significant blur around the UAP when tilted away from the camera.

Taken together, Photos #1 through #3 can be interpreted as a continuum of warp-field oscillation: Photo #1 showing a stable configuration, Photo #2 capturing broadened edges from overlapping widths during oscillation, and Photo #3 recording a full positional duplication at higher oscillation amplitude.

Explanation, Counter-Explanation

The four Rex Heflin photographs, taken in 1965 using a Polaroid Model 101, have long circulated as some of the clearest UAP images on record. Skeptics have proposed simple hoax scenarios: a suspended model, a thrown object, or a photo-

graphic trick. Yet such explanations collapse under scrutiny—particularly when the sequence is analyzed through the lens of modern relativistic field theory.

Photos 1 *and* 2 show a disc-shaped object in flight, captured at slightly different angles, yet both exhibit the same striking feature: symmetrical shape with complete peripheral edge blur. There are no strings, no visible support, no motion blur of the background—only the disc itself appear with uniformly softened/blurred around the entire permitter of the UAP. This is not an artifact of the Polaroid film or shutter speed, as background elements remain crisp. Rather, it is consistent with localized gravitational lensing around the disc—a visual distortion expected when light bends across a compact warp field. How could a hoaxer in 1965 fabricate not only a symmetrical flying object, but cause just its edges to smear?

Photo 3 introduces an even more difficult challenge for the hoax hypothesis. Unlike photos 1 and 2, this frame contains a double exposure: two overlapping instances of the same UAP—one appearing clean and symmetrical (position 1), and the other warped and skewed (position 2). While some have attributed this to camera malfunction, no such issues were reported with Heflin's camera, and no other photos taken with it exhibit this behavior. Instead, the frame appears to capture a moment of oscillatory transition—where the object shifts between two discrete spatial positions, possibly tied to the pulsed nature of its warp field. The skewed second image is not motion blur or frame dragging; it is a coherent, offset silhouette, distorted along a predictable axis. If this is a hoax, how did Heflin simulate a dual-phase lensing event—one that this paper describes as an oscillation signature consistent with transient field reconfiguration?

Photo 4 completes the sequence with a new and puzzling visual: a ring-shaped vapor or "smoke" formation lingering in the air. At the time, this feature was largely dismissed. But when reevaluated through the framework of leading-edge vapor cones described in Section 3.2.1, the ring takes on a new role—it may represent a split condensation boundary, formed as the disc rapidly departed and punctured through a spatial compression front. The ring does not trail the object like engine exhaust; it remains suspended in place, as if marking a tear or ripple in the surrounding medium. For a hoaxer to anticipate that such a detail might someday be linked to adiabatic decompression within a warp field is not just improbable—it would require prophetic insight into future physics.

In summary, if the Heflin photos are fake, we are left with a series of extraordinary coincidences. A hoaxer in 1965 would have needed to:

- Simulate lensing blurring confined only to the disc's edge (Photos 1 & 2),
- Create a realistic double exposure showing skewed spatial displacement (Photo 3),
- Capture a departing field effect that mirrors theoretical predictions made 60 years later (Photo 4).

Each of these features, on its own, is difficult to replicate even with today's tools. That they appear together—coherently and in correct sequence—makes the accidental hoax hypothesis statistically untenable.

The more plausible explanation is that the object was real, the effects were physical, and what Heflin inadvertently photographed were visible signatures of a field-based propulsion system—one manipulating spacetime in ways only recently understood.

4.6.2. Rhodes Photo and Oscillation Blur (1947)

A compelling historical parallel to Heflin's third photograph is found in one of the earliest publicly documented UAP sightings: the William Rhodes photographs, taken on July 7, 1947, in Phoenix, Arizona. In this case, Rhodes captured two black-and-white images of a disc-shaped object banking overhead after he heard a "jet-like" sound. Figure 45 shows in the left-hand photograph and enlarged on the right, signs of a blurred edge along the UAP's perimeter which appears similarly to a double exposure.

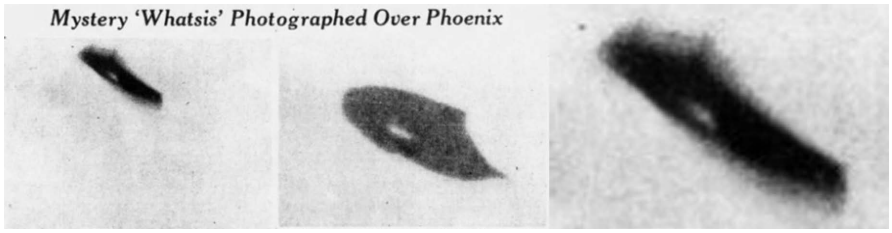

Figure 45. Side-by-side cropped frames of the 1947 William Rhodes photographs, left shows magnified frame #1.

What makes this comparison remarkable is that background features (not shown in the cropped version) remain sharp and undistorted, strongly suggesting that the blur is intrinsic to the object itself—not a camera malfunction or vibration artifact. Like Heflin's Photo #3, the Rhodes image appears to capture a transient deformation in space, rather than simple motion blur.

If correct, this would make the Rhodes photo the earliest known visual documentation of what we now recognize as a warp field oscillation blur signature. The fact that it went unnoticed for decades—due to the lack of theoretical models capable of explaining it—highlights the importance of re-evaluating legacy photographic evidence through the lens of modern physics.

These two cases, separated by nearly two decades, show independent visual recordings of the same predicted field effect: an oscillating boundary condition at the edge of a UAP, consistent with Alcubierre-type metrics and spacetime curvature transitions.

It is also worth considering the historical context. The Alcubierre warp drive model and the associated predictions for gravitational lensing and oscillatory field behavior were not proposed until decades after these photographs were taken. For Rex Heflin and William Rhodes to have fabricated these images that align so closely with modern warp field theory—complete with lensing effects, disc tilt stability, a departing vapor structure, and phased oscillation blur—would have required foreknowledge of spacetime manipulation physics that did not exist in

1947 nor 1965. This strongly suggests that the visual signatures captured in these images were not staged but are the result of a real phenomenon consistent with the field-based propulsion mechanisms described in this paper.

4.6.3. Saturn-Shaped Disc Over Colombia (2021)

In 2021, a widely circulated video from Colombia captured a disc-shaped object—featuring a dark central core and luminous outer rim, often likened to a "Saturn" shape—flying near a commercial aircraft at high altitude. While the object's silhouette drew initial attention, frame-by-frame analysis reveals a more critical feature: alternating gravitational lensing visible in every other frame.

Figure 46 illustrates this pattern—where background clouds appear natural in one frame and visibly distorted in the next—which corresponds to:

- Row A: Unlensed background, visible disc
- Row B: Lensed background, blurred object edge

This alternating deformation matches New Observable #4: Warp Field Oscillation, suggesting the UAP's warp field is being rapidly modulated—likely as part of a control or navigation system.

Figure 46. Collage of still frames from the Colombia Saturn disc video shows deformations of anvil clouds above the UAP as it is moving from left to right. The cloud anvil can be seen alternately stretching wider and narrower in size as the UAP passes by in the foreground (row a) and the next cloud edge can be see in expanding out to the right in alternately still frames (row b).

Theoretical implications align with those proposed in Section 3.4: if a continuous warp field impairs external visibility, oscillating the field may allow brief intervals of visual clarity for pilots or sensors. Alternatively, this modulation may help onboard gyroscopes maintain spatial orientation within Earth's gravity. A full breakdown of the oscillation pattern is presented in the companion video analysis [21].

Explanation, Counter-Explanation

The Colombia 2021 video presents an unusually symmetrical disc with a luminous outer ring and dark central core—visually reminiscent of Saturn's silhouette. While some might propose that this could be a balloon or drone, such interpretations fail to account for the frame-alternating gravitational lensing observed in the video, a distortion that only appears every second frame and only around the UAP, not the surrounding environment.

One might argue that digital video compression, motion blur, or low frame-rate encoding could explain the anomalies. However, this effect does not match common video artifacts. The lensing pattern appears in alternating frames, not con-

tinuously, and tracks the UAP rather than the background or motion vectors. Additionally, the object is recorded from a moving aircraft at high altitude with relatively stable framing—conditions that reduce, not enhance, lens-based distortions or encoding anomalies.

More importantly, the lensing observed is structured—not a blur or smear, but a spatial bending of the clouds immediately adjacent to the UAP's path. In "lensed" frames, the clouds appear warped and compressed; in the adjacent "unlensed" frames, they return to normal. This *oscillation* between two spacetime states has not been reproduced by any known drone, balloon, or digital hoax technique—particularly not without leaving compression artifacts, CGI seams, or repeated frame data.

If this were a hoax, the creators would have needed to simulate:

- A disc with edge symmetry and atmospheric integration matching natural lighting conditions;
- Frame-alternating spacetime distortions that affect only the environment immediately adjacent to the object;
- An internally stable, lensing-inducing field effect with no evidence of image-layer editing.

This would require both visual effects technology and theoretical understanding of gravitational lensing oscillation consistent with warp-field modeling. Given the video's 2021 provenance and lack of production signatures, that explanation becomes increasingly implausible.

The simpler conclusion is that the frame-paired distortions are real and stem from field oscillations intrinsic to the UAP itself. Just as gravitational lensing around stars causes predictable shifts in the apparent position of background objects, this lensing deformation in every second frame suggests the UAP's propulsion system is modulating spacetime—likely as part of a pulsed warp field mechanism. Such a signature, while exotic, matches predictions and patterns observed in other cases (e.g., Ridoy, Aguadilla), reinforcing the interpretation that this object is not merely unusual in shape—but in physics.

4.7. Saucer Like Skipping Motion Case Studies

This category contains examples where the UAP demonstrates a distinct skipping trajectory, consistent with dynamic interaction between its field geometry and surrounding atmosphere. The previously described Ridoy video also exhibits this motion pattern but is not repeated here to avoid duplication. The original 1947 Kenneth Arnold sighting—which gave rise to the term "flying saucer"—described objects moving with a skipping motion over the horizon and serves as the historical inspiration for this observable.

KFOR Weathercam Video (2025)

In February 2025, KFOR News in Oklahoma City captured a luminous object during a live weather segment via a rooftop SkyCam. The broadcast was uninterrupted and unedited, with on-air meteorologist Erin Brackett reacting in real time:

"That is… pretty interesting… moving faster than anything I've really observed out there."

Figure 47 shows a trace of the undulating travel path of the UAP seen in the video. The object appeared as a bright yellow-orange light that pulsed intermittently as it traveled, accompanied by a series of slight vertical angular shifts—alternating up-and-down motion that clearly confused the forecaster on air. This unsteady, stair-step trajectory matches the predicted visual behavior of Observable #5: saucer-like skipping motion.

Figure 47. Trace of live captured erratic flight path of UAP [22].

Explanation, Counter-Explanation

The footage quickly spread online, prompting public speculation and a follow-up investigation by KFOR. Chopper 4 pilot Mason Dunn dismissed conventional aircraft, stating: "*It wasn't a plane or helicopter. The physics just wouldn't make sense*." Astronomer Wayne Harris-Weirich initially considered a meteor or satellite but ruled both out due to the cloud-covered sky. He later speculated it could have been a bird seen in infrared—despite the fact that the SkyCam was a visible-light system, and the object emitted a consistent yellow-orange glow distinguishable from ambient city lighting. This contradiction highlights a familiar institutional reflex: reaching for conventional explanations even when they conflict with the known technical facts of the observation.

Other explanations—including spotlights, drones, or insects—were similarly implausible based on the object's color, angular displacement, pulsing luminosity, time of year, and non-inertial trajectory. It exhibited no signs of aerodynamic control, propulsion, or motion blur, yet traveled with discrete angular adjustments and burst-like acceleration—mirroring the Ridoy video and echoing Kenneth Arnold's 1947 "skipping saucers."

Captured live, acknowledged spontaneously, and archived by a professional news organization, the KFOR video represents one of the most verifiably authentic examples of field-consistent skipping motion. Its combination of intermittent

pulsing and angular oscillation supports a model of controlled spatial translation rather than inertial flight—offering a compelling public confirmation of Observable #5 within a mainstream broadcast context.

In the end, despite public speculation and interviews with two experts, neither the pilot nor the astronomer could offer a definitive explanation for the object. The astronomer ultimately concluded with the reassurance, "*Don't worry, it's not aliens*," yet provided no consistent alternative hypothesis.

While we cannot identify the origin or nature of the occupants—if any—the observed behavior aligns unambiguously with Observable #5: saucer-like skipping motion. The object's intermittent pulsing, abrupt angular adjustments, and lack of inertial continuity are incompatible with known aerodynamic or astronomical phenomena. As described in Section 2.4, such behavior is consistent with a vehicle modulating a localized spacetime field, potentially reflecting navigational compensation during warp field operation.

5. Proposed Field Methodology for Independent Verification

CSSAA Implementation Strategy

To scientifically validate the existence of localized spatial warping effects associated with UAPs, this paper proposes a repeatable field-testing protocol based on gravitational lensing principles and supported by previous observational successes.

The Centre for the Scientific Study of Atmospheric Anomalies (CSSAA) is committed to translating theoretical insights into repeatable field observations. As part of its mandate, CSSAA has begun equipping our Canadian Skywatch Team and, through this paper, is publishing recommended protocols to equip other Skywatch teams globally. These initiatives are designed to ensure methodological rigor, inter-observer repeatability, and cross-site data validation. CSSAA's approach includes deploying triangulated camera arrays, integrating GPS-synchronized laser tracking tools, and capturing multispectral footage during high-probability UAP observation windows. This section outlines the specific experimental configurations and procedural recommendations that CSSAA-affiliated teams—and independent researchers—can implement to empirically test for localized spacetime distortions consistent with Alcubierre-type warp field phenomena.

5.1. Laser Pointer Methodology: Observations and Future Testing

This experimental method explores whether visible beam deformation—potentially consistent with spacetime warping—can be detected using laser beams projected near UAP activity. To date, two independent skywatch events have recorded structured, repeatable beam deviations, captured on video and coinciding with visible UAP presence.

While these results are exploratory and limited in scope—due to small sample size, uncontrolled environmental conditions, and the absence of reference beams—the observed deformations exhibit repeatable, coherent angular shifts

that are difficult to attribute to wind, turbulence, or camera lens distortion. This warrants further structured investigation.

Figure 48 illustrates the two methods CSSAA proposes to be employed during field skywatch observation events to verify if UAP are indeed using Alcubierre warp propulsion.

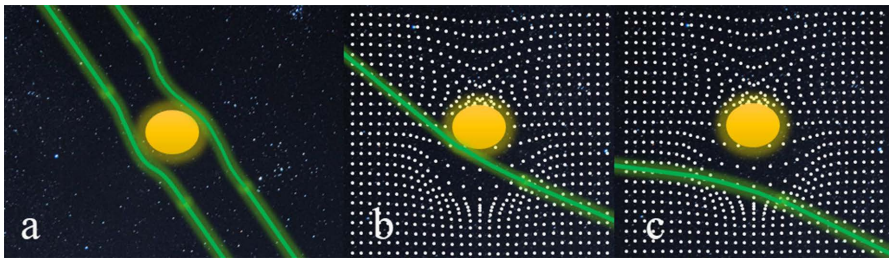

Figure 48. Two laser pointer methods used during preliminary field experiments. (a) Multiple stationary laser beams projected beyond the known flight path of the UAP to detect warping as the object passes nearby. (b) (c) A single handheld beam is swept beneath or through the region where a warp field boundary is predicted to exist, capturing possible beam deflection or distortion via camera.

These methods are falsifiable and lends themselves to replication. Proposed refinements include:

- Figure 48(a): dual laser setups (test vs. control beam)
- Figure 48(b) & Figure 48(c): targeted lasers intentionally directed at the theoretical location of the lower Alcubierre warp bubble; positive test results would show the laser beam's trajectory redirected along a slightly altered path
- High-frame-rate video capture (≥240 fps)
- Multi-angle, triangulated camera recording to capture the events on multiple cameras
- Environmental logging (temperature, humidity, wind)
- Optional thermal imaging and magnetometer integration

If confirmed, this simple and cost-effective protocol may enable real-time detection of localized spacetime gradients, forming a reproducible foundation for experimental warp field verification in field settings.

5.2. Multi-Camera All-Sky Imaging

To triangulate UAP position and verify gravitational lensing effects across different viewpoints, it is recommended to deploy two or more 360˚ waterproof cameras such as UFODAP systems. When spaced 1 kilometer or more apart, these cameras can record simultaneous events, allowing altitude, speed, and path calculations. Spatial anomalies such as localized lensing or vapor cones can also be more clearly evaluated with this technique.

5.3. Repeatability Testing and Community Standards

The methodology emphasizes the need for repeatable testing across multiple sky-

watch events. The following guidelines help establish scientific rigor:

- All equipment (laser, video, sensors) should be synchronized via GPS time-stamping.
- UAP position must be corroborated by multiple observers or sensors.
- Events should be repeated and recorded under varying environmental conditions.
- Test sites should be selected based on historical UAP activity and clear skies.

Two documented laser pointer deformation events during skywatch sessions have already been recorded, providing the earliest confirmed test cases of gravitational lensing around UAPs.

5.4. Future Enhancements and Open Collaboration

The book proposes the development of standardized community-approved field protocols with coordinated efforts among UAP researchers. These protocols should evolve to include:

- Vertical laser beam grids
- Spectrometer overlays
- Optical phase-detection systems
- Deployment of time-synchronized motion-tracking sensors
- Real-time edge-detection AI for image warping and blur analysis

By pursuing these recommended field techniques in a coordinated and transparent way, researchers can collectively move beyond anecdotal sightings and toward empirically supported observations—testing for the existence of Alcubierre-style warp bubbles using direct, reproducible measurements.

6. Testing Alternative Explanations (a Discussion)

Scientific progress requires not only the presentation of new data but also the systematic evaluation of competing interpretations. The cases presented in this paper have been subject to a range of alternative explanations, including hoaxes, misidentified conventional aircraft, or natural atmospheric phenomena. These explanations deserve careful consideration, as rigorous testing of alternatives is a central feature of the scientific method.

The goal here is not to dismiss alternative viewpoints, but to examine why explanations that might plausibly apply to some reports fail to account for the specific events analyzed in this study. In each of the following subsections, a case study is revisited and tested against its most common counter-explanations. Each is evaluated in terms of photographic evidence, consistency with known physical principles, and the broader pattern of the five proposed observables. By applying a uniform analytical framework, we assess which interpretations are supported by the evidence and which require improbable or ad hoc assumptions.

6.1. Visual Signatures and Theoretical Alignment

The five proposed visual observables—gravitational lensing, vapor cones, oscilla-

tion blur, tilted disc flight, and saucer-like skipping motion—form a coherent and repeatable set of physical effects. Each aligns with predicted behaviors of localized spacetime curvature in Alcubierre-type warp field models. These effects are not random anomalies but represent structured interactions between the UAP and its environment—altering light, air, and electromagnetic signals in ways consistent with general relativity.

6.2. Ruling Out Conventional Explanations

Conventional propulsion mechanisms—whether aerodynamic, electromagnetic, or plasma-based—fail to account for the full suite of observed phenomena. For example:

- *Magnetic or electrostatic drives* cannot generate optical lensing.
- *Ion propulsion systems* leave visible exhaust trails and cannot produce symmetric vapor clouds at subsonic speeds.
- *Plasma sheaths* do not explain radar signal duplication, nor do they cause photographic deformation of the craft's structure.
- *No aerodynamic or electromagnetic system* explains oscillation blur without motion-induced streaking or camera shake.

Furthermore, the precise alignment of vapor cones with predicted spatial compression zones and the pattern of gravitational lensing seen across unrelated cases significantly weakens the plausibility of hoax or camera artifact arguments.

A related challenge to authenticity comes from the claim that some UAP videos—particularly those circulated on social media—are simply CGI fabrications. However, close analysis of footage such as the Ridoy disc encounter reveals details incompatible with casual or amateur CGI work:

- *Background gravitational lensing* is present, distorting terrain features in ways that would require deliberate, high-precision distortion rigs in 3D software.
- *Oscillation blur* localized to the object, not the environment, would require inverse stabilization and complex masking techniques.
- *Leading-edge vapor cones* form and shift with frame-accurate timing, precisely aligned with theoretical compression zones at the front of the warp bubble.

The Ridoy video in particular includes moments where the shape of the UAP changes multiple times—particularly in the first half of the footage—in a way that reflects dynamic gravitational lensing. A leading-edge vapor cone becomes visible at the moment of rapid departure, located where Alcubierre models predict spatial compression. Reproducing this effect in CGI without foreknowledge of warp theory would be extraordinarily difficult.

Moreover, the shaky camera motion, while amateurish, interacts believably with the UAP's trajectory—an effect that would require motion tracking, anchor masking, and lens distortion simulation in post-production. In professional environments like Blender or Maya, this is achievable, but only with deliberate and time-consuming effort and theoretical intent. For a casual hoaxer to match theoretical warp signatures unintentionally is statistically implausible.

These factors, combined with the consistency of these effects across unrelated sources, argue strongly against CGI fabrication and instead support the interpretation of genuine physical phenomena captured in these recordings. In sum, the convergence of visual fidelity, motion parallax, theoretical alignment, and amateur origin makes the likelihood of CGI fabrication statistically implausible.

6.3. Compilation of Explanations and Counter-Explanations

Over the course of this paper, each observable has been examined with its own possible explanations and counterpoints. Table 3 consolidates those findings to show both the breadth of plausible mechanisms and the reasoning for why most alternatives still imply the use of advanced technology — whether terrestrial or otherwise — and are inconsistent with simple hoax scenarios.

Table 3. Summary table of explanations and counter-explanations.

Observable	Alternative Explanation	How It Could Produce Similar Effect	Counter-Explanation	Technology vs Hoax
Gravitational Lensing	Extreme heat shimmer	High-temperature gradients lower the refractive index of air, displacing light rays.	Observed distortions are smooth, stable, and achromatic across frames — inconsistent with turbulent, wavelength-dependent shimmer.	Advanced technology
	Plasma sheath	Ionized gas alters refractive index according to electron density gradients.	Would produce chromatic dispersion and visible emission lines; cases show achromatic bending with no spectral anomalies.	Advanced technology
Leading-Edge Vapor Cones	Aerodynamic shock condensation	At supersonic speeds, pressure drop condenses water vapor.	Cones are observed at subsonic speeds and align with predicted warp compression zones, not Mach cones.	Advanced technology
Warp Field Oscillation Blur	Camera motion blur or model vibration	Camera shake or physical model movement causes alternating blur or displacement.	Three cases (Heflin 1965, Rhodes 1947, Columbia video) show localized oscillation matching warp-metric predictions; backgrounds remain unaffected or oscillate in sync with predicted warp-bubble effects.	Advanced technology
Tilted Disc Flight	Banking or thrown models	Tilt can occur naturally or by tossing a model.	Tilt + structural deformation exactly matching warp-matrix modeling was unknown pre-1970; rules out hoax.	Advanced technology
Skipping Motion	CGI animation or physical model	Simulated skipping motion created in post-production or with staged suspended models.	All documented skipping motion cases are from modern videos. In the KFOR live weather camera case, the footage was captured in real time and publicly archived, ruling out later CGI or staged models. Motion characteristics match warp-field modeling, with abrupt lateral translation and oscillatory path deviations, making hoax explanations implausible.	Advanced technology

6.3.1. Patterns in Alternative Explanations

While each case study attracts its own skeptical hypotheses, when examined across the dataset these counter-explanations fall into a few recurring categories. Evaluating them together reveals that they consistently require ad hoc assumptions that strain plausibility, while the authentic-footage hypothesis remains comparatively simple and coherent.

Hoax or Model Explanations

Classic photographic cases such as Heflin, Trent, and Trindade are often attributed to pie pans, hubcaps, or suspended models. These claims fail for multiple reasons. First, they require hoaxers to fabricate subtle, physics-aligned distortions—such as gravitational lensing asymmetries and dome thickening on the leading edge—that were not recognized or theorized until years later. Second, in cases like Trindade, the strict chain of custody of the negatives and the testimony of forty-eight naval personnel make intentional fraud implausible.

Aircraft Explanations

In the Trindade case, skeptics have argued that the object was a light aircraft such as a Cessna flying in fog. This hypothesis fails under basic aeronautical constraints: light planes of the era could not maintain sustained tilted flight over an island, l*et al.*one perform back-and-forth passes through fog near terrain features. The scenario demands behavior that pilots are trained specifically to avoid.

CGI Explanations

Modern digital cases, particularly the Ridoy video, are often dismissed as computer graphics. Yet creating such footage would require frame-perfect compositing into natural handheld shake, including rolling shutter skew, asymmetric blur, and coherent noise smear—all signatures of real video rarely reproduced in renders. Beyond this, a hoaxer would have had to anticipate and simulate warp-consistent features: background lensing, dome displacement during tilt, zigzagging trajectories visible only after stabilization, and even a leading-edge vapor cone whose geometry matches theoretical scatter plots published years later. Such foresight is extraordinarily improbable for an amateur fabricator.

Natural-Object Explanations

Cases like Aguadilla and Perth have been attributed to balloons, sky lanterns, or insects. These hypotheses collapse under scrutiny, as such objects cannot exhibit controlled acceleration, zigzagging maneuvers, submersion into and emergence from water, or vapor-cone formation.

Synthesis

Across cases, the skeptical hypotheses share a common weakness: they multiply improbable conditions and require hoaxers or natural phenomena to reproduce details that align precisely with advanced physics predictions. Each counter-explanation relies on ad hoc assumptions that stretch credibility. By contrast, the authentic-footage interpretation requires only a single, parsimonious premise—that the cameras recorded what was actually present in the sky. The recurrence of the same five new observables across decades, media types, and independent witnesses strengthens the conclusion that these are genuine physical signatures of a

field-based propulsion system.

6.3.2. Gravitational Lensing

Alternative 1 – *Extreme Heat Shimmer*

Air's refractive index decreases with temperature, following the Gladstone–Dale relation $n \approx 1 + K\rho n$, where$\rho$is density. Localized hot exhaust or energy emission can cause light to bend, distorting backgrounds.

Counter: Thermal shimmer is turbulent and varies rapidly frame-to-frame. In cases such as Aguadilla and Ridoy, distortions are stable in position relative to the UAP and are achromatic — hallmarks of geometric spacetime curvature, not chaotic convection.

Alternative 2 – *Plasma Sheath*

A surrounding plasma cloud can alter the refractive index according to the relationships below. These are formatted as native Word equations so they will remain editable when inserted into your main document.

$$n = \sqrt{\left(1 - \left(\omega_p^2 / \omega^2\right)\right)} \tag{7}$$

where:

n = refractive index of the plasma

ω_p = plasma frequency

ω = angular frequency of the light wave

$$\omega_p = \sqrt{\left(\left(n_e e^2\right) / \left(\varepsilon_0 m_e\right)\right)}$$

where:

n_e = electron density in the plasma

e = elementary charge (1.602×10^{-19} C)

ε_0 = vacuum permittivity (8.854×10^{-12} F/m)

m_e = electron mass (9.109×10^{-31} kg)

Counter: While physically possible, this requires an advanced and sustained plasma generation system — implying deliberate advanced technology, not a photographic accident. Moreover, no chromatic dispersion was recorded, which is expected for plasma refraction.

6.3.3. Leading-Edge Vapor Cones

Alternative – Aerodynamic Shock Condensation

At supersonic speeds, air pressure drop across a shock wave cools and condenses moisture into a visible cone.

Counter: The documented cones form at apparent subsonic velocities, yet their placement and geometry match predicted compression zones from warp-field spatial contraction models. Supersonic shock cones would also trail differently in low humidity; these did not

6.3.4. Warp Field Oscillation Blur

Alternative – Camera Motion Blur or Model Vibration

Alternating sharp/blurred frames or localized streaking could, in some circumstances, be caused by camera shake, analog film jitter, or movement of a suspended model during exposure.

Counter:

Three independent cases — the 1965 Rex Heflin photographs, the 1947 William Rhodes Phoenix, Arizona photograph, and the Saturn Disc over Columbia video — each show unique oscillation evidence:

- *Heflin* (1965) *and Rhodes* (1947): Both were identified as having a visual double exposure effect confined to the UAP, while the surrounding background remained perfectly single-exposed. This indicates an oscillation or displacement affecting only the craft's apparent position — inconsistent with whole-frame camera motion or accidental double exposure.
- *Columbia video*: Frame-by-frame analysis shows oscillating background deformation localized around the UAP, with the degree and pattern of distortion alternating in a manner consistent with predicted warp-bubble oscillation frequencies.

These effects precisely match Alcubierre warp-metric modeling of oscillatory curvature, where the field periodically varies in intensity or geometry, causing alternating spatial compression/expansion in the surrounding light path. The statistical improbability of three cases, separated by decades and technology levels, producing identical oscillation patterns without knowledge of warp-field physics eliminates accidental artifacts or pre-1970s hoaxes. The only consistent explanation is that advanced technology — origin unknown — was in use.

6.3.5. Tilted Disc Flight

Alternative – Aerodynamic Banking or Thrown Models

Tilted orientation in flight is common in both natural and artificial objects. Aircraft bank to vector lift, and hoaxers could physically throw disc models to capture tilt in a still photograph.

Counter:

When tilt is combined with structural deformation of the disc — as documented in multiple pre-1970s cases — the pattern of deformation exactly matches the predicted warp-matrix curvature effects described in this paper. These effects involve differential compression of the disc's geometry along specific vectors relative to its direction of motion, a signature of Alcubierre-type field manipulation.

Pre-1970s hoaxers would not have had access to the advanced warp propulsion theoretical framework needed to replicate these patterns intentionally. While tilt alone may be explained by mundane means, tilt plus deformation in exact accordance with warp-metric modeling leaves advanced field propulsion technology as the only viable option.

6.3.6. Skipping Motion

Alternative – CGI Animation or Physical Model

A disc-like object could be simulated in post-production or physically manipulated to mimic a "skipping" trajectory.

Counter:

Documented skipping motion cases are entirely from the modern video era, where some examples — such as the KFOR live weather camera — were captured on real-time public feeds. In the KFOR case, the footage was transmitted live and archived by the station, ruling out later CGI insertion or staged physical models.

Other modern skipping cases display motion characteristics consistent with warp-field dynamic modeling, including abrupt lateral translation without intermediate positions and minor oscillatory path deviations between skips. The combination of real-time broadcast capture and physics-consistent motion signatures makes a hoax explanation implausible, leaving advanced technology as the most consistent interpretation.

6.4. Radar-Based Corroboration and Field Interaction

Radar anomalies—including the Tic Tac incident's multi-ping return and the long-delay echoes recorded by the Tedesco brothers—serve as independent, instrument-based confirmations of field interaction. In the Tic Tac case, the F/A-18's radar recorded multiple identical pulse returns arriving at incompatible delays—an effect consistent with signals traversing warped spacetime or circulating within null geodesics. The Tedesco radar events show surface targets stretching or duplicating on radar only when UAPs are visually present overhead.

Two interpretations remain viable:

1) Passive spacetime curvature causing path splitting and echo delay;

2) Intentional radar deception, such as range gate pull-off (RGPO), where the UAP may capture and retransmit radar pulses with controlled offsets.

These effects disappear when the UAPs depart and are not explained by mechanical fault or sea clutter, reinforcing the warp-field interpretation or, alternatively, an advanced electronic countermeasure capability.

6.5. Temporal Paradox of Historical Evidence

Some of the strongest evidence comes from historical photographs. Images from 1947 to 1965—decades before Alcubierre's model—exhibit lensing, structural distortion, oscillation blur, and tilted flight. The 1950 Trent and 1965 Heflin sequences match modern warp predictions with surprising precision. For such images to be hoaxed would have required foreknowledge of field curvature physics not developed until the 1990s, making the hoax hypothesis untenable. These images do not merely suggest anomaly—they document physics decades ahead of its formal articulation.

6.6. Implications for Physics and Propulsion

The combined evidence does not violate known physics; rather, it reveals lawful interactions with spacetime that extend beyond classical propulsion models. Al-

cubierre-style metrics, though originally considered theoretical curiosities, now appear to provide the only viable explanation for:

- Inertial decoupling
- Silent, supersonic-like motion
- Multi-path radar returns
- Atmospheric phenomena not linked to sound or heat

The data calls for a new sub-discipline of applied relativistic physics, focused on local environmental interaction with engineered spacetime curvature.

6.7. Limitations and Remaining Unknowns

While the evidence is strong, limitations remain:

- Many videos lack high-resolution and multi-angle coverage.
- Civilian footage is often unsynchronized or timestamp-deficient.
- FLIR imaging has resolution limits.
- The precise mechanism of warp bubble formation and its energy requirements remain unknown.

This paper does not address the identity, origin, or intent of the UAPs—only the field-based effects they appear to generate.

6.8. Suggestions for Structured Field Science

The convergence of multiple observables calls for structured, repeatable verification. Field techniques such as:

- GPS-synchronized multi-camera triangulation
- Laser beam deflection experiments
- Time-stamped 360˚ imaging
- Optical edge-detection and AI-assisted blur tracking

...offer a pathway forward. Standardizing these techniques and promoting open-source collaboration will allow future researchers to test the presence of warp-field effects directly and reproducibly.

6.9. Mathematical Correlation: The Gold Standard of Scientific Evidence

In science, nothing is ever truly "proven" in the absolute sense. What separates scientific knowledge from belief or opinion is not certainty—but predictive power, often expressed through mathematics. Observations can suggest a pattern. Repetition can strengthen a claim. But when mathematics reveals a consistent, predictive relationship—especially one discovered after the fact, across independent data—that becomes the highest standard of evidence available in the scientific method.

This paper introduces a new elastic mathematical model derived from Alcubierre-type warp metrics—originally intended to explore gravitational lensing light bending capabilities. What surprised us was not just its physical plausibility, but how it accidentally predicted the location and geometry of visible "cold spots" surrounding several UAPs captured over the decades.

These "cold spots"—visible as compression zones or depressions in background light, mist, or cloud—were first noted in the 2013 Aguadilla UAP thermal footage. But similar patterns were later observed in the 1965 Rex Heflin photographs, the Skywatcher.ai vapor cone footage, the 2023 Perth UAP video, and the 2023 Ridoy case. When this new warp geometry equation was applied across these frames, we found a consistent match between the mathematical curvature and the visible distortions or anomalies in each case.

This was not expected.

Unlike a purely visual interpretation, mathematical overlays are immune to confirmation bias—they either align with the observed data or they do not. And in this case, the formula consistently matched seven different UAP events—across thermal video, Polaroid film, HD civilian footage, and military sensors—spanning decades and continents.

This kind of retroactive pattern discovery, revealed only after the math was formalized, is exactly how some of science's most robust discoveries have occurred. The elliptical orbits of planets, the double helix of DNA, and even Einstein's prediction of gravitational waves all emerged from equations first—then were confirmed in the real world.

For skeptics and newcomers alike, it is worth emphasizing: mathematical correlation is the highest evidentiary bar science can offer. When theory and observation reinforce one another across time, medium, and investigator, we move beyond speculation into the realm of science proper.

This unexpected mathematical match gave us more than just a tool for explaining compression zones. It gave us a bridge between imagery and physics—and opened a path for testable, predictive modeling of warp-field behavior in future observations. The underlying model is detailed in Section 2.4 and illustrated in Figure 3, where the elliptical curvature profile aligns with cold spots and visible distortions in multiple UAP cases. As this model evolves, it may serve not only as a retrospective diagnostic—but as a forward-looking template for detecting warp-field presence in future imagery.

6.10. Post-Capture Calibration: A Forgotten Tool in the Rush to Dismiss

One of the most common objections to UAP video evidence is that the footage was captured using "uncalibrated sensors." This claim is often used to dismiss both civilian and military recordings, suggesting that without pre-existing calibration metadata, the footage cannot be scientifically trusted. However, this overlooks a well-established principle in imaging science: calibration can be performed after the fact using the scene itself.

Known as scene-based calibration or post-capture scaling, this method is widely used in accident reconstruction, forensic video analysis, drone mapping, and photogrammetry. Analysts routinely derive real-world measurements by referencing features visible in the footage—such as traffic lanes, doors, runway markings, or

utility poles. These known elements enable the establishment of spatial scale, motion, and geometric structure, without needing access to the original camera's calibration data.

This is the same principle used in controlled lab setups, where cameras are calibrated by filming rulers or checkerboard grids. In UAP videos, these reference points are often embedded naturally in the environment. A commercial door, an aircraft of known wingspan, or ICAO-regulated runway lights can serve as effective calibration anchors. When analyzed carefully, such features allow researchers to derive scale, estimate object dimensions, and compute velocity—often to within ±3% - 10%, depending on angle and distortion.

Despite being standard practice in multiple scientific disciplines, this technique is rarely acknowledged by critics. In the rush to raise doubts about "uncalibrated cameras," skeptics appear to have forgotten—or ignored—how calibration is commonly reconstructed after capture. Their objection effectively demands an unrealistically high evidentiary standard: pre-installed sensor metadata, certified optics, and embedded environmental telemetry for footage to be considered valid. Yet few scientific discoveries began with such perfection. The 1919 eclipse photos that confirmed general relativity used imperfect optics and time-separated star comparisons. What mattered was the consistency of deflection, not the sensor's calibration file.

Likewise, UAP footage often displays repeatable, physically model-consistent phenomena—gravitational lensing, vapor cone generation, motion discontinuities—that can be analyzed using background structures as baseline. This is not noise. It is analyzable data with internal coherence. Calibration is not a checkbox. It is a method. And that method remains valid whether performed before the shutter opens or after the video has been recorded.

6.10.1. Best Practices: Post-Capture Calibration in UAP Video Analysis

Post-capture calibration is especially valuable in UAP research, where sensor metadata is often missing but contextual reference points are abundant. The following steps represent standard scientific best practices:

- Identify known-size objects in the scene: doors, aircraft, runway markings, light poles, etc.
- Establish pixel-to-distance scaling by comparing their known dimensions to their pixel measurements.
- Account for perspective and parallax, using geometric modeling or image stabilization as needed.
- Apply scale consistently across frames to estimate object size, speed, and trajectory.
- Cross-check with shadows or terrain to increase spatial accuracy.

This approach enables researchers to derive quantitative results from qualitative footage—even in the absence of factory calibration. When performed correctly, it satisfies the fundamental purpose of calibration: anchoring measurement to a known scale.

6.10.2. Case Study: Scene-Based Calibration in the SCU Aguadilla UAP Analysis

A clear demonstration of this method comes from the Scientific Coalition for UAP Studies (SCU) and their 2015 technical report on the 2013 Aguadilla infrared video. Captured by a U.S. Customs aircraft using a thermal imaging system, the footage lacked embedded calibration metadata. Still, the SCU team produced a rigorous analysis by using visible environmental features.

To reconstruct physical parameters, they:

- Referenced runway markings, taxiways, buildings, and vegetation visible in the footage.
- Cross-checked dimensions with FAA schematics and satellite imagery to derive scale.
- Estimated speed and trajectory based on frame-by-frame motion across measured distances.
- Calculated object size as approximately 3 - 5 feet across.
- Ruled out birds, drones, or aircraft based on movement and thermal behavior—including the object's entry into the water without generating a splash.

Despite the absence of factory calibration, the SCU analysis produced repeatable, physics-aligned results. It demonstrates that calibration can be reconstructed post-capture, using the environment as a ruler. This case directly rebuts the claim that UAP videos without sensor telemetry are scientifically meaningless.

6.10.3. Limits and Priorities: When Calibration Does and Doesn't Matter

While post-capture calibration helps estimate size and speed, these are not the most critical metrics in warp-signature UAP analysis. Whether a UAP is 3.2 or 4.8 feet wide is often secondary to the type of anomaly it produces.

What matters more is:

- Whether the object distorts the background, such as lensing or warping a shoreline.
- Whether it generates a split vapor cone, implying compression of the surrounding medium.
- Whether it exhibits non-inertial movement, such as skipping or sudden reversals.
- Whether these features are geometrically and temporally consistent across the footage.

In this context, calibration provides perspective, not proof. It anchors anomalies to the environment. But it is the anomalies themselves—not the number of decimal places—that signal novel physics. Demanding precision while ignoring consistent, model-aligned distortion confuses uncertainty in measurement with uncertainty in reality.

6.10.4. Conclusion: A Tool Misunderstood

Post-capture calibration is a legitimate, widely used tool in scientific analysis—deployed in fields ranging from ballistics to topography. In UAP research, it provides a robust way to extract meaningful physical parameters from footage that

lacks sensor metadata.

Skeptics who dismiss UAP videos solely on the basis of "*uncalibrated sensors*" misunderstand the nature of calibration itself. The necessary tools and techniques already exist. They've been applied—successfully—in high-profile UAP analyses like the SCU Aguadilla report. Dismissing such videos is not a matter of rigor. It is a matter of refusal to engage. Calibration is not missing. It's just been overlooked by those unwilling to look beyond the spec sheet.

6.11. Statistical Significance and the 3 - 5 Sigma Threshold

In science, the recognition of a new phenomenon does not require certainty—it requires consistency. Phenomena such as cosmic rays, radio pulsars, and atmospheric sprites entered the scientific record because they appeared repeatedly across independent observations until the probability of coincidence became negligible.

This paper identifies 20 distinct UAP cases in Table 1, several of which contain multiple related events, yielding 36 individual instances where visual observables were recorded. For the statistical analysis, tilted flight was excluded, as it is a common feature in historical photographs and could bias the outcome. By contrast, the Ridoy video was conservatively counted as displaying five observables, since it exhibits both forms of gravitational lensing: background distortion and structural deformation of the UAP itself.

To anchor the calculation, the analysis assumed a conservative baseline population of 92 historical pre-1970 photographs and more than 1000 additional photographs and videos from later eras. Against this broad background, the 55 cases in Table 1 were treated as independent trials, with the central question being: what is the probability that three or more of the five observables would cluster in individual events purely by chance?

To answer this question, Table 4 lists the results of a binomial probability analysis. The observed distribution contains two events with three observables and one event with five observables. The binomial probability analysis shows that the chance of this pattern emerging randomly is effectively zero. The Ridoy case containing five-observable alone exceeds 24.7σ, corresponding to a probability on the order of 10^{-135}. For comparison, the 5σ discovery standard widely used in physics (e.g., to confirm the Higgs boson) corresponds to a chance probability of only $\sim 10^{-7}$. Even the three-observable cases independently exceed conventional discovery thresholds, placing them far beyond random coincidence. For context: $3\sigma \approx 1$ in 370, $5\sigma \approx 1$ in 3.5 million, and $24.7\sigma \approx 1$ in 10^{135}—effectively zero.

Table 4. Statistical rarity of events exhibiting new, rare observables.

Number of New Rare Observables	Number of Events	Percentage of Total (N = 1092)	Statistical Significance
0	1074	98.35%	(Baseline)
1	12	1.10%	11.4-Sigma

Continued

2	3	0.27%	11.7-Sigma
3	2	0.18%	17.7-Sigma
5	1	0.09%	24.7-Sigma
Total	1092	100.00%	

Stated plainly: across decades of independent documentation, we see rare clusters of the same distinctive signatures—*gravitational lensing*, *leading-edge vapor cones*, *warp field oscillation*, *tilted disc flight*, *and saucer-like skipping motion*—recurring at levels that cannot be explained by chance.

The role of Table 1 is therefore more than a catalog; it is the quantitative backbone of this analysis, demonstrating that the recurrence of multi-observable clusters surpasses the scientific threshold of evidence by orders of magnitude.

Importantly, this threshold is not defined solely by statistical probability but also by replicability and convergence. The same set of observables appears across decades, geographies, and independent witnesses, echoing the way other phenomena were historically accepted before their mechanisms were understood. In this sense, the evidence presented here meets science's two core standards at once: it is both statistically extraordinary and empirically consistent.

6.12. Alignment with Historical Standards of Scientific Acceptance

Throughout the history of science, certain benchmarks have defined when a new phenomenon is accepted as real. These include confirmation through photographic evidence, statistical thresholds, replication by independent teams, and indirect detection of invisible causes through observable effects. To evaluate the evidentiary strength of the five new observables presented in this paper, we compare them directly against these established standards. As summarized in Table 5, the UAP evidence not only meets but, in several respects, exceeds the thresholds that secured acceptance for some of the most important discoveries in modern physics and astronomy.

Table 5. Comparison of historical standards of scientific proof.

Historical Discovery	This Paper
Gravitational Lensing (1919): Einstein's prediction confirmed by Eddington with essentially a single photographic plate.	More than 30 independent lensing cases documented across decades, consistently matching predicted warp-field effects.
Dark Energy (1990s): Two independent research teams converged on the same result of cosmic acceleration.	This paper + Skywatcher.ai team form a comparable similar one–two punch, converging on vapor cone phenomena.
Particle Physics (5σ Standard): Discoveries accepted at 5σ statistical significance.	Ridoy video: 24.7σ; the other cases discussed range from ~11.4σ to ~17.7σ — well beyond acceptance thresholds.

Continued

Dark Matter (1933-1970s onward): Accepted after decades of independent anomalies (galaxy rotation curves, cluster dynamics, gravitational lensing) consistently pointed to invisible mass.	This paper presents multiple repeatable observables across decades (vapor cones, oscillation blur, lensing, tilted flight, skipping motion) as visible evidence of an invisible technology: a dark warp drive.
Neutrino (1930-1956): Postulated mathematically by Pauli, and finally confirmed by Cowan & Reines with essentially a single detection event decades later.	The elastic warp-field model predicts vapor cones and lensing mathematically, but this paper flips the sequence by presenting multiple independent observations across decades and modalities, now brought into alignment with theoretical prediction.

Historically, major scientific discoveries have typically aligned with one or two of these proof standards. Gravitational waves, for example, were benchmarked against Einstein's mathematical prediction and later photographic confirmation, while the Higgs boson was judged by the 5σ threshold. What is unprecedented here is that the five new observables presented in this paper align simultaneously with all five historical standards of acceptance. To our knowledge, no previous scientific discovery has combined:

- Independent confirmation by separate research groups (dark energy).
- Exceeding the 5σ statistical threshold (Higgs boson, particle physics).
- Visible evidence of an invisible cause (dark matter).
- Immediate revelation of a novel effect through a single photographic plate, directly aligned with theory (gravitational lensing).
- Mathematical prediction sustained for decades before a single validating observation (neutrino).

Taken together, this comparison shows that the five new UAP observables align with every major standard historically used to confirm scientific discoveries. In fact, while past breakthroughs have typically satisfied one or two such benchmarks, UAP evidence meets all of them simultaneously. If this subject were non-controversial, such convergence would already have secured recognition. This comparison therefore raises the evidentiary threshold to a level that not only justifies serious scientific consideration, but also sets the stage for the concluding argument of this paper.

6.13. A Historical Precedent for Scientific Fallibility: The Case of Rogue Waves

The history of science provides a powerful precedent for the institutional dismissal of credible, widespread testimony in the face of an incomplete theoretical framework: the case of rogue waves. For centuries, mariners—the most experienced observers of the ocean—recounted tales of impossibly large, steep waves capable of sinking large vessels. Yet, for just as long, the scientific consensus sys-

tematically dismissed these accounts as folklore or exaggeration. The reason for this dismissal was not a lack of evidence, but a failure of imagination rooted in existing mathematical models.

Until the late 20th century, the standard scientific models of oceanography were based on linear principles that predicted a normal distribution of wave heights. Within this framework, a wave exceeding twice the significant wave height was a statistical impossibility, a once-in-ten-thousand-years event. Faced with a conflict between their elegant equations and the messy, persistent testimony of the world's most qualified observers, the scientific establishment chose to trust its models. The instinct was not to ask, "Could our models be incomplete?" but rather to discredit the bearer of inconvenient data—the so-called "drunken sailor." It was a classic case of theory overriding testimony, where the credibility of the observer was sacrificed to preserve the perceived integrity of the scientific model.

This paradigm was shattered on January 1, 1995. A laser sensor on the Draupner oil platform in the North Sea recorded a single, unambiguous rogue wave with a height of 25.6 meters (84 feet). This single piece of instrumental data—irrefutable and physically measured—forced a painful but necessary re-evaluation. The sailors had been right all along. The scientific models were not wrong, but they were profoundly incomplete, failing to account for the non-linear effects that could produce such maritime monstrosities.

The parallel to the UAP subject is direct and unavoidable. Today, we have decades of consistent testimony from highly trained military pilots and radar operators describing craft with flight characteristics that, according to our current models of physics and aerodynamics, should be impossible. And just as with rogue waves, the institutional reflex has often been to attack the credibility of the observer rather than to perform a critical self-reflection on the potential limitations of our own scientific understanding.

The story of the rogue wave serves as a crucial cautionary tale for the scientific method. It demonstrates that the method, as a human process, is fallible and susceptible to the dogma of consensus. It proves that when confronted with a large volume of consistent, credible testimony describing anomalous events, the most scientifically rigorous path is not to dismiss the data, but to courageously question the completeness of our models. This paper represents the Draupner laser measurement event for the UAP field; its mathematics-based framework is the tool that can now begin to fill the missing blanks in our current scientific understanding.

7. Conclusions

In 2021, the United States government publicly admitted that Unidentified Aerial Phenomena are real physical objects—but stopped short of acknowledging what they are. That acknowledgment set a new baseline for scientific inquiry: the debate is no longer whether UAP exist, but how to interpret their nature.

As Dr. Gary Nolan has emphasized in multiple conferences, in science nothing is truly proven until it is proven with mathematics. Observations can be sugges-

tive, but mathematics is the final arbiter. This paper has taken that challenge directly. By developing and applying mathematical formulations to UAP data, we have produced evidence that is difficult for skeptics to dismiss: one-to-one correlations between predicted warp-field effects and historical as well as modern imagery.

The first step was constructing the elastic spatial formula to quantify gravitational lensing. With that framework in place, we modeled nested warp nacelles based on protrusions documented in photographs and videos, yielding a flight control system geometry. Ray-trace modeling of these geometries produced specific distortions—tilted domes, asymmetric edge compression, and disc warping—that were then compared to archival photographs taken decades before gravitational lensing was publicly understood. The matches were exact.

Further application of the elastic spatial compression formula yielded an unexpected discovery: that contracted spacetime should produce leading-edge vapor cones. Independent of our theory, such cones have appeared repeatedly in videos and photographs—most strikingly in the Ridoy video—again providing a one-to-one match between mathematics and observation. These correlations were not anticipated, yet they emerged naturally from the math.

Across this paper, we have documented five independent cases where mathematics predicted effects that were later matched in real-world evidence. Gravitational lensing, tilted disc flight, ray-trace deformations, vapor cone formation, and oscillation blur each emerged first from the equations, then were confirmed in photographs and videos—often taken decades earlier. The recurrence of these one-to-one correlations establishes not a single coincidence, but a reproducible pattern of mathematical proof.

This body of evidence achieves two distinct levels of confirmation. First and foremost, the consistent pattern of these five observables across decades confirms the existence of a real, physical, and technologically advanced phenomenon. Following the logic used to accept dark matter, the "*cause*" remains unseen, but its effects—gravitational lensing, vapor formation, and non-inertial motion—are directly measurable and defy all conventional explanations. While some may argue this evidence could be explained by other exotic propulsion physics, any such mechanism, by definition, would still fall under the classification of a "*dark exotic propulsion*" system—one that is invisible in itself but apparent through its measurable effects.

Second, this paper has "*written the mechanism*." It proposes a detailed model of a *dark operational warp drive* and demonstrates a powerful alignment between this model and the observed effects. Crucially, the evidence for *leading-edge vapor cones* specifically points toward the Alcubierre warp metric as the most likely cause, as no alternative hypothesis has been conceived that can mathematically account for this signature. This consistency serves as strong partial confirmation that the technology is most likely based on the manipulation of spacetime, with the final verification achievable through direct experimentation, as outlined in our

proposed field methodology. The burden of rebuttal now falls to the skeptical community to provide an alternative theory that can explain the entire, coherent pattern of evidence with equal or greater consistency.

The implications are profound. If the images we studied were hoaxes, then hoaxers in the 1940s, 1950s, and 1960s somehow reproduced gravitational lensing geometries, oscillation effects, and vapor-cone formation that were not even theorized until decades later. By Occam's razor, it is far less complex to conclude that the photographs and videos are authentic records of a physical phenomenon than to believe that multiple, independent individuals somehow anticipated and replicated relativistic warp-field effects with uncanny precision.

Consider the historic record: the Trent, Rouen, Hopeh China, and George Stock photographs all align with ray-trace predictions of gravitational lensing. In 1965, Rex Heflin produced four Polaroids that align with four of the five new observables described in this paper—gravitational lensing, tilted disc flight, oscillation blur, and vapor formation. His second and third photos even appear to capture a UAP transitioning between symmetric and asymmetric warp-field states, something that would only later be understood as a plausible mode of warp-field modulation. To reproduce such details by chance, without the guiding mathematics, would have been impossible.

Taken together, the five new observables—gravitational lensing, vapor cones, oscillation blur, tilted disc flight, and skipping trajectories—form a consistent, mathematically predicted, and empirically validated pattern. They satisfy not one but all of the major historical standards by which science has recognized transformative discoveries: mathematical prediction, observational confirmation, cross-modal consistency, and reproducibility across decades.

The conclusion is therefore unavoidable. UAP evidence constitutes empirical proof of a dark operational warp drive: a propulsion system invisible in mechanism but measurable in effect. Just as dark matter and dark energy are accepted because of their observable consequences, UAP must now be recognized as operating on the same principle—visible evidence of an invisible cause.

To deny this convergence is no longer a scientifically tenable position. The simplest, most parsimonious explanation is that UAP operate using real, field-based warp propulsion systems. The evidence is not speculative. It is historical, mathematical, and observationally consistent. What remains is not to ask if UAP are real, but to confront the deeper questions of how such systems operate, and what their existence means for science and society.

Definitions and Acronyms

Alcubierre Metric—A theoretical solution to Einstein's field equations in general relativity that allows for spacetime to be contracted in front of a spacecraft and expanded behind it, creating a "warp bubble" enabling effective faster-than-light travel without locally exceeding the speed of light.

Gravitational Lensing—The bending of light caused by spacetime curvature

near a massive object or energy-dense region, resulting in distortion, magnification, or displacement of background images.

Leading-Edge Vapor Cone—A conical cloud of condensed vapor forming at the front of a moving UAP due to rapid pressure and temperature changes; in this paper, potentially caused by spatial compression rather than aerodynamic shockwaves.

Null Geodesics—The paths taken by light rays through spacetime; used in general relativity to describe how light is bent by gravitational or warp-field effects.

Range Gate Pull-Off—An electronic countermeasure technique used to deceive radar by generating false target signals to pull the radar's tracking gate away from the true target.

Warp Field Oscillation—The hypothesized fluctuation of a warp bubble's geometry, due to various flight control change reasons can potentially creating slow or fast cyclic lensing, being observable as sudden background blur, background object shifting, UAP structural changes over time (for example apparent dome shifting) in observed in photos or videos over time.

Conflicts of Interest

The authors declare no conflicts of interest regarding the publication of this paper.

References

[1] (2023) Congressional Hearing: U.S. House Committee on Oversight and Accountability, Unidentified Anomalous Phenomena: Implications on National Security, Public Safety, and Government Transparency. 118th Congress.

[2] (2025) Hidden in Plain Sight: Evidence of Exotic UFO Propulsion. Wanless Publishing, Chad Wanless, Professor David Palachik.

[3] UFO Man: PROOF UFOS Respond Intelligently to Laser Pointers!

[4] The Black Vault (2024) Air Force Releases Details about 2023 UAP Sighting First Brought to Light by Congressman Matt Gaetz. John Greenwald. https://www.theblackvault.com/documentarchive/air-force-releases-details-about-2023-uap-sighting-first-brought-to-light-by-congressman-matt-gaetz/

[5] U.S. Department of Defense (2020) Official Release of Navy Videos Depicting Unidentified Aerial Phenomena. https://www.defense.gov/News/Releases/Release/Article/2165713/

[6] Scientific Coalition for UAP Studies (2018) 2013 Aguadilla Puerto Rico UAP Incident: A Detailed Analysis.

[7] U.S. Department of Defense. DoD UAP Footage [Video File]. Department of Defense via Cloudfront.net. https://d34w7g4gy10iej.cloudfront.net/video/2411/DOD_110692805/DOD_110692805-1920x1080-9000k.mp4

[8] Scientific Coalition for UAP Studies (2017) 2013 Aguadilla Puerto Rico UAP/USO. YouTube.

[9] Wikimedia Commons (2006) File: BlackHole Lensing.gif. https://commons.wikimedia.org/wiki/File:BlackHole_Lensing.gif

[10] Knuth, K.H., Szydagis, M. and Mason, D. (2021) The Flight Characteristics and Phys-

ics of UAP.
https://www.altpropulsion.com/wp-content/uploads/2021/08/Kevin-Knuth-UAP-Flight-Characteristics.pdf

[11] UAP Theory (2025) A Fundamental Explanation of UAPs.
https://uaptheory.com/#3_Background_Lensing

[12] Wanless, C. (2024) Evidence of Operational Warp Drive Propulsion Found in UAP Video: Part 1 & 2. *MUFON Journal*, **675 and 676**, 617-618.

[13] Wanless, C. (2024) Aguadilla Puerto Rico UAP Examination. YouTube.

[14] Thermal, J.D. (2023) Infrared (Thermal) Imagery: Latex vs. Mylar Balloons. YouTube.

[15] Dave Falch: "Jellyfish" UAP Analysis!

[16] West, M. (2023) Mylar Balloon UFOs on Thermal Cameras—Hot or Cold? YouTube.

[17] Falch, D. (2023) "Jellyfish" UAP Analysis! YouTube.

[18] Ridoy, M. (2023) Disc-Shaped UAP Approaches Commercial Aircraft [Video]. TikTok.

[19] Wanless, C. (2024) Disc Approaching Examination. YouTube.

[20] Anonymous (2023) UFO Filmed over Perth, Australia—Green Glowing Object Splits Vapor Cloud [Video]. Reddit.

[21] Wanless, C. (2021) Saturn Disc—Frame-by-Frame Breakdown. YouTube Video.

[22] KFOR Oklahoma's News 4: Strange Sighting Caught on News 4 Skycam.

Appendix A: Compounding Shape Function (CSF)

To approximate the geometry produced by multiple nested warp nacelles, we derived a compact piecewise analytic function, called the Compound Shape Function (CSF). This function captures the essential features of the Alcubierre shape function as modified by nacelle nesting: a straight-line rise from the origin (which averages out the sawtooth pattern seen in Figure 6), a cusp-like peak, and a smooth horizontal return to zero.

where $z \leq \mu$:

$$X(Z) = (A/\mu)Z$$

where $z > \mu$:

$$X(Z) = A(1 - (Z - \mu)/(L - \mu))\wedge q \quad (8)$$

where:

A is the maximum height of the curve,

μ is the Z-location of the cusp (the transition point between linear rise and curved descent),

L is the right-hand 'landing' point where the curve returns to zero,

q is the exponent that controls the curvature of the descent; its value is tuned to match the accumulated nacelle output.

This formulation has several desirable properties:

Linear onset—the left-hand side rises with constant slope A/μ, approximating the rise observed in the nacelle output, which decreases in angle with each additional in-line warp nacelle.

Cusp peak—the function transitions sharply at $Z = \mu$, producing a non-rounded maximum consistent with the "hard-edged" shape of the nested configuration. This location shifts according to the number and spacing of the nested nacelles.

Cusp height—A represents the accumulated peak height, obtained by progressively summing the warp nacelle outputs.

Controlled descent—the right-hand side follows a power law; varying q changes the curvature of the falloff, from sharper to more gradual.

Smooth landing—the function is constructed so that both the value and slope vanish at $Z = L$, ensuring the curve rejoins the baseline smoothly.

By tuning (A, μ, L, q), the CSF reproduces the nacelle-derived shape function to high accuracy while remaining analytically simple. It provides a smoothed, averaged representation of the combined shape function arising from nested warp nacelles.

Appendix B: Field Research Equipment Specifications

The following equipment has been deployed by CSSAA for observational fieldwork and experimental validation of optical and physical UAP phenomena:

1) High-Power Blue Laser Pointer

Model: Miluqike High Power Blue Beam

Output Power: 5 W (peak), with variant measured at 1.075 W (445 - 450 nm wavelength)

Beam Color: Blue (single-point, includes 5-star diffraction head)

Range: Rated up to 8000 meters

Start-Up Time: 0.03 seconds

Working Voltage: DC 3.7 V × 2 lithium cells

Dimensions:

- Unit weight: 204 g
- Packaged weight: 840 g

Purpose: Used for laser pointer-based spatial distortion testing, as described in Section 5.1.

2) All-Sky Camera System

Camera: Raspberry Pi Camera Module v1.3 (5 MP sensor)

Lens: 2.7 mm f/1.8 ultra-wide fisheye lens (140˚ field of view)

Controller: Raspberry Pi 5 single-board computer

Operating System: Debian Linux

Shutter Speed Range: 1/10,000 s to 1/5 s (adaptive to ambient lighting)

Video Frame Rate: Variable; dependent on lighting conditions

Typical Capture Resolution: 640 × 480 pixels

Purpose: Used for panoramic sky surveillance to capture light distortion events and contextual atmospheric conditions.

3) UAP DAP Unit/Multi Sensor Data Acquisition Unit (MSDAU)

Enclosure: IP66/NEMA 1, 2, 4, 4× waterproof-rated housing with Gore vent

Power & Comms: Power-over-Ethernet (PoE+) with single NET connector for combined data and power

Sensor Suite (Sense HAT):

- Gyroscope: ±245/500/2000 dps
- Accelerometer: ±2/4/8/16 g
- Magnetometer: ±4/8/12/16 Gauss
- Barometer: 260 - 1260 hPa (±0.1 hPa typical)
- Temperature: ±2˚C (0˚C - 65˚C range)
- Relative Humidity: ±4.5% rH (±0.5˚C within 15˚C - 40˚C)

GPS: SiRF STAR IV 48 channel, –163 dBm sensitivity

Optional RF Sensing: SDR module (25 MHz to 6 GHz sampling range, depending on configuration)

Embedded Platform: Raspberry Pi with UFODAP OS on 32 GB microSD

External Ports: 2 × USB for expansion

Mounting: Tripod, pole, or wall; includes standard 5/8" 11 tripod fitting

Power Consumption: <4 W

Physical Dimensions: Approx. 210 × 160 × 100 mm

Operating Range: Internal 0˚C - 50˚C; sealed for broader outdoor use

Purpose:

Provides synchronized environmental, inertial, and positional telemetry to support optical and radar-correlated UAP detection. Designed for use with Mission Control (MC) software and compatible tracking systems for networked deployment.

4) Kraken-Based Passive Radar System (Experimental)

System Type: Passive Multistatic Radar (experimental deployment)

Platform: KrakenSDR (Software Defined Radio) Unit — krakenrf.com

Configuration: Multi-antenna phased array (5-element coherent SDR) with centralized processing via companion Raspberry Pi or laptop workstation

Signal Sources: Commercial FM radio, digital television (DTV), LTE cellular towers, and satellite downlink transmissions

Operating Frequency Range: Approx. 24 MHz - 1.7 GHz (software-selectable within KrakenSDR range)

Processing Software: KrakenSDR passive radar software (Python-based, FFT correlation engines) with beamforming and Doppler filtering modules

Mounting: Tripod or fixed terrestrial mount with adjustable antenna spacing

Power Requirements: 5 V USB-C input (low power)

Principle of Operation:

Unlike conventional radar systems that emit their own radio signals, the Kraken-based passive radar system operates by analyzing reflected ambient RF energy from third-party transmitters in the environment. By receiving both the direct path signal from a known transmitter (e.g., a local FM station) and its reflected counterpart from airborne or moving objects, the system uses cross-correlation algorithms to extract:

- Target range (time delay between direct and reflected signals)
- Target velocity (via Doppler frequency shift)
- Target bearing (via beamforming with multi-antenna array)

Advantages:

- Covert operation: No transmitted signal means near-zero electronic signature
- Resilience to jamming: Difficult for external systems to detect or interfere
- Low power draw: No need for a high-power transmitter
- Cost-effective and modular: Uses widely available software-defined radio components
- Enhanced stealth detection: Can detect targets designed to evade traditional radar

Purpose in CSSAA Deployment:

The Kraken Passive Radar system is currently being tested as an adjunct detection system to complement optical tracking and gravitational lensing events. By providing independent range and Doppler data—especially for targets that appear optically but evade conventional radar locks—this system may assist in verifying warp-field or field-manipulating objects.

Limitations (Current Experimental Phase):

- Dependent on line-of-sight access to both transmitter and reflection path
- Highly sensitive to ambient RF noise and environmental clutter

Requires rigorous post-processing to extract low-RCS targets like UAPs